Development of a mutation-independent approach to treat merosin-deficient congenital muscular dystrophy type 1A (MDC1A)

by

Annie Infancia Arockiaraj

BSc, Madurai Kamaraj University, 2010

MSc, Madras University, 2012

MS, University of Pittsburgh, 2019

Submitted to the Graduate Faculty of the

School of Public Health in partial fulfillment

of the requirements for the degree of

Doctor of Philosophy

University of Pittsburgh

2023

UNIVERSITY OF PITTSBURGH

SCHOOL OF PUBLIC HEALTH

This dissertation was presented

by

Annie Infancia Arockiaraj

It was defended on

April 12, 2023

and approved by

Dr. Quasar S. Padiath, Associate Professor, Human Genetics and Neurobiology

Dr. Yvette Conley, Professor, Nursing and Human Genetics

Dr. Zsolt Urban, Associate Professor, Human Genetics

Dissertation Director: Dr. Dwi U. Kemaladewi, Assistant Professor, Pediatrics and Human Genetics

Development of a mutation-independent approach to treat merosin-deficient congenital muscular dystrophy type 1A (MDC1A)

Annie Infancia Arockiaraj, PhD

University of Pittsburgh, 2023

Merosin-deficient congenital muscular dystrophy (MDC1A) is an autosomal recessive disorder caused by mutations in the *LAMA2* gene, resulting in a defective form of the extracellular matrix protein laminin-α2 (LAMA2). Individuals diagnosed with MDC1A exhibit progressive muscle wasting and declining neuromuscular functions. No treatments for this disorder are currently available. Our group previously showed that postnatal *Lama1* upregulation, achieved through CRISPR activation (CRISPRa), compensates for *Lama2* deficiency and prevents neuromuscular pathophysiology in a mouse model of MDC1A. In this study, I assessed the feasibility of upregulating human *LAMA1* as a potential therapeutic strategy for individuals with MDC1A, regardless of their mutations. I hypothesized that CRISPRa-mediated upregulation of human *LAMA1* would compensate for the lack of *LAMA2* and rescue cellular abnormalities in MDC1A fibroblasts. Global transcriptomic and pathway enrichment analyses of fibroblasts collected from individuals carrying pathogenic *LAMA2* mutations, compared with healthy controls, indicated higher expression of transcripts encoding proteins that contribute to wound healing, including Transforming Growth Factor-β (TGF-β) and Fibroblast Growth Factor (FGF). These findings were supported by wound-healing assays indicating that MDC1A fibroblasts migrated significantly more rapidly than the controls. Subsequently, the MDC1A fibroblasts were treated with *Sa*dCas9-2XVP64 and sgRNAs targeting the *LAMA1* promoter. Robust *LAMA1* expression was observed, which was accompanied by significant decreases in cell migration and

expression of *FGFR2, TGF-β2,* and *ACTA2*, which are involved in the wound-healing mechanism in MDC1A fibroblasts.

Collectively, our data suggest that CRISPRa-mediated *LAMA1* upregulation may be a feasible mutation-independent therapeutic approach for MDC1A. This strategy might be adapted to address other neuromuscular diseases and inherited conditions in which strong compensatory mechanisms have been identified.

Table of Contents

List of Tables

List of Figures

Preface

First and foremost, I would like to thank my PhD mentor, Dr. Dwi Kemaladewi, for her mentorship and for helping me grow as a researcher. She provided all the resources and all the help I needed to complete my dissertation work. Above all, I am truly grateful for her moral support throughout my pregnancy and early days as a new mother, juggling lab work and a baby. This work would not have been possible without her mentorship.

I want to extend my warmest gratitude to Marie Johnson, our lab manager, for her contribution to the study and encouragement throughout my time in the lab. I thank all the members in the Dr. Kemaladewi lab, Anushe Munir, Dr. Oluwaseun Akinyele, Jia Qi Cheng Zhang, Dr. John Wang, Dr. Yonne Menezes, and Caleb Kim for their thought-provoking discussions and guidance in the lab.

I sincerely thank my committee members, Dr. Yvette Conley, Dr. Quasar Padiath, and Dr. Zsolt Urban, for their generous time in every committee meeting and for providing insightful suggestions and feedback on my project, ensuring it's always on the right track.

The core facilities, Health Science Sequencing Core at the Children's Hospital of Pittsburgh and Health Sciences Library System at the University of Pittsburgh have been resourceful for my PhD work. I thank Dr. McAllister-Lucas, Dr. Lucas, and Dr. Ekambaram for lending me with the IncuCyte instrument for my study.

I express my deepest gratitude to my beloved father, Arockiaraj. Even though he is not with me now, his unconditional love and encouragement have sculpted me to into who I am. I am grateful to my mother, Amelia, for her everlasting support and constant source of energy for me. I

thank my grandparents, Rajakannu and Samadanam, for their love and blessings. I thank my sister, Jennie Rosaline, for all her help and companionship.

I would like to thank my husband, Remigious Mano, and my son, Ryan Andrew, for giving me joy and happiness and the warmth of the family. They have kept me grounded, always pushed me out of my comfort zone and routed me on all occasions like no other. I always love them and thank them so much.

1.0 Introduction

1.1 MDC1A pathogenesis

Merosin-deficient congenital muscular dystrophy type 1A (MDC1A) accounts for 1/3 of congenital muscular dystrophy cases [1]. Studies done in UK and Italy provide a prevalence rate of 1:150,000 [2-4]. Lake et al. estimated a prevalence of 8.3 per million across all populations based on the population allele frequencies available in the genome aggregation database (gnomAD) [5].

The age of onset is at birth or within six months of life [6]. Some symptoms at birth include weak cries, hypotonia, and feeding difficulties. Nearly 2/3 of the kids are diagnosed at birth. In the months following birth, the patients do not attain sufficient control of the trunk and neck muscles and exhibit a delay in reaching all the developmental milestones, such as sitting, crawling, walking, and jumping, and individuals rarely achieve independent ambulation [7-10]. The patients experience progressive joint contractures, scoliosis, and elevated creatine kinase levels (>1000 IU/L) [11, 12]. In addition, white matter abnormalities in the brain on magnetic resonance imaging (MRI) [13-15] and sensorimotor demyelinating neuropathy are commonly observed in MDC1A patients [16, 17]. Mild intellectual disabilities are also reported in a small proportion of individuals [18, 19].

The less common findings of MDC1A involve cardiac involvement and epilepsy. Generally, MDC1A does not interfere with cardiac function [20]. However, some studies reported cardiac disorders involving the right bundle branch block and left ventricular dysfunction [21, 22].

Seizures comprising simple or complex partial episodes have also been reported in up to 30% of the patients [7, 23, 24].

1.2 Management of MDC1A

Despite considerable advances in our understanding of the pathophysiology of the disease, there is currently no cure for MDC1A. Treatment involves managing the disease symptoms that affect various functions of the body. For example, facial weakness leading to feeding and swallowing difficulties are addressed by providing gastronomy tube inserts. To prevent chest infections caused by aspiration and other infectious agents, assisted ventilation and tracheotomy are provided to patients to reduce respiratory disorders [25]. Similarly, ambulatory services help patients to cope with mobility difficulties. Other procedures, such as arthrodesis and physiotherapy, are provided to patients to reduce deformations and contractures [26].

The leading cause of mortality involves respiratory failure. A study by Tan et al. on 24 patients in the Chinese population, reported that 78.3% of the patients died due to respiratory failure after pneumonia. Likewise, Zambon et al. reported respiratory failure as the leading cause of mortality in a natural cohort study of 42 patients. MDC1A Patients have no long-term survival rate, and median life expectancy ranges from 12 to 15 years [9, 10].

1.3 Skeletal muscle basement membrane

The basement membrane resembles a sheet-like structure separating the extra-cellular matrix from the plasma membrane of the skeletal muscle. It was originally identified in the skeletal muscle by Bowman in 1840 [27]. In addition to skeletal muscle, the basement membrane underlies epithelial cells, muscle cells, endothelial cells, fat cells, and peripheral nerve axons [28]. The skeletal muscle basement membrane comprises proteins and carbohydrates, devoid of lipid and nucleic acid. Type IV collagen and laminins exist in multiple isoforms, forming triple helical structures. The most abundant isoforms of type IV collagen and laminin are $(\alpha1(IV))_2$ $(\alpha2(IV))_1$ and $\alpha_2\beta_1\gamma_1$, respectively [29]. Both have the ability to self-polymerize to form distinct networks. Nidogen (entactin) binds to the laminin γ chain via its carboxy-terminal and to the type IV collagen via its second and third globular domain [30, 31]. This leads to the formation of a non-covalent bridge between the laminin and the collagen network. Collectively, these networks render stability to the basement membrane and protect the muscle cells from mechanical stress and damage [32]. Further, another component, agrin, provides collateral linkage by binding to the laminin γ chain and α-dystroglycan. This stabilizes the interaction in the cell surfaces [33, 34]. In addition to providing structural integrity, the basement membrane components also help in the cell-communication process by interacting with the transmembrane receptors, such as dystrogylcans and integrins. The α-dystrogylcan binds to sarcoglycan, and the β-dystrogylcan binds to the dystrophin, which in turn binds to the actin in the cytoskeleton. Together, these proteins constitute a connecting link from the basement membrane to the plasma membrane and to the cytoskeleton [29, 35].

1.4 Role of laminin-α2 in MDC1A

MDC1A is caused by mutations in the *LAMA2* gene, located in 6q22-q23 in the human genome [36, 37] and is expressed in skeletal muscle, Schwan cells and placental trophoblast [38, 39]. The *LAMA2* gene is large, spanning 260 kb, and comprises 65 exons. It encodes for an mRNA transcript of around 9.5 kb that produces a 380 kDa protein, laminin-α2 chain, also called merosin (Figure 1A).

The laminin-α2 chain combines with β1 and γ1 chains to form the laminin-211 protein complex, a cruciform-shaped heterotrimeric molecule and is the main component of the skeletal muscle and supports various muscle functions [40, 41]. First and foremost, the N-terminal globular domain (LN) facilitates self-polymerization to form laminin networks and associates with collagen iv and heparan sulfate proteoglycans in the muscle basal lamina. The C-terminal laminin globular (LG) domain binds to major cell-surface receptors such as dystroglycans and integrin α7β1 (Figure 1B) [42] [43-47]. Secondly, they help in basement-membrane assembly, adhesion, and downstream signaling events [48, 49]. Thirdly, they aid in myotube stability and muscle cell survival[50]. In addition to their role in muscle functions, the laminin protein complex also helps in neurite growth and migration of Schwann cells in the nervous system [42] [51]. Owing to its pivotal role in muscle function, the lack of the laminin-α2 chain contributes to loss of muscle integrity and stability in affected MDC1A individuals [50, 52, 53].

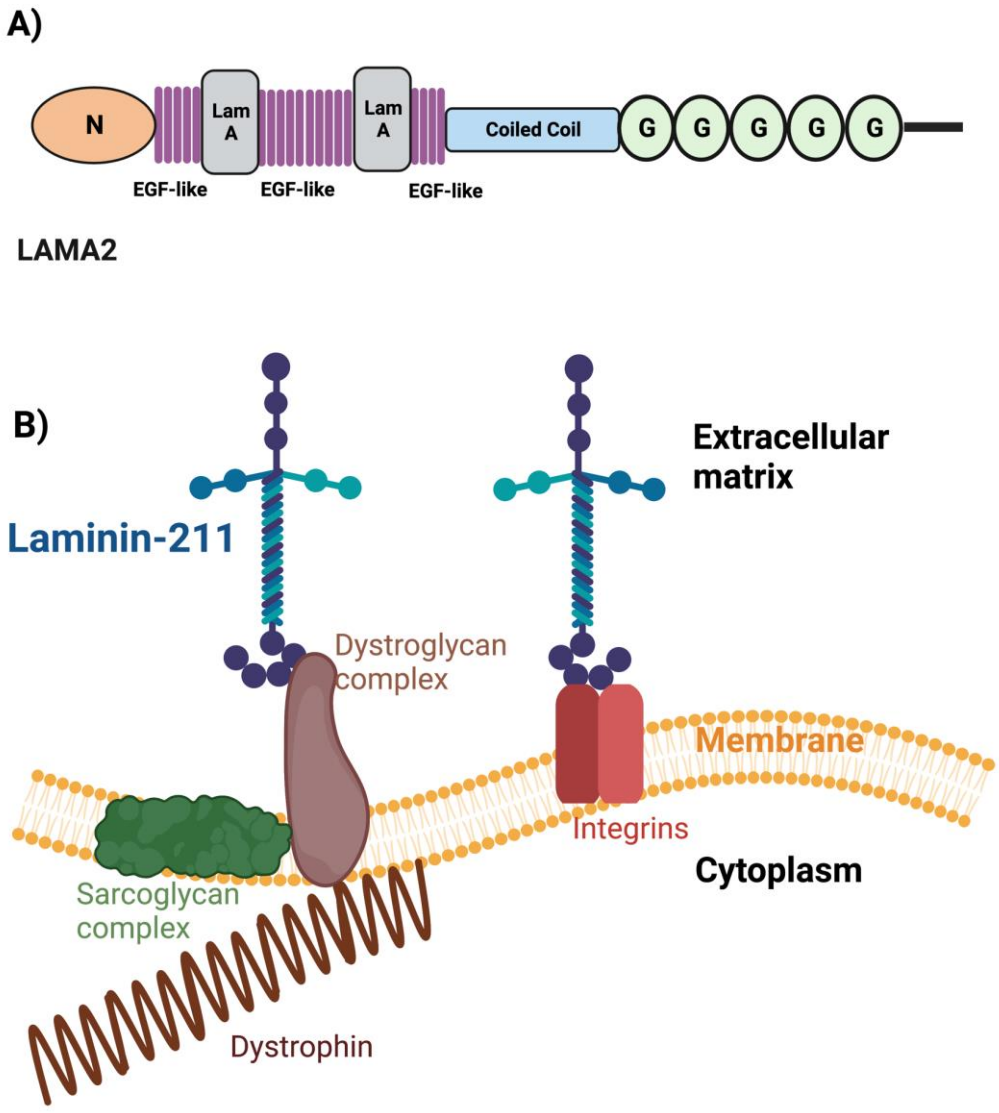

Figure 1. Laminin-211 in skeletal muscle

The upper panel illustrates the different domains in LAMA2: Laminin N-terminal domain (N), laminin-type-epidermal growth factor-like domain (EGF), laminin type IV A domain (Lam A), coiled-coil domain, and Laminin type globular domains (G). The bottom panel shows the heterotrimeric protein, the laminin-211 protein complex (blue). It binds to the cell surface receptors integrin α7β1(red) and dystroglycan (brown) through its globular domains, facilitating a connection between the basement membrane and cytoskeleton. (The figure was created with BioRender.com).

1.5 Diagnosis in MDC1A patient populations

Diagnosis for MDC1A is aided by clinical evaluation of the aforementioned symptoms, muscle biopsy, muscle imaging, and genetic testing. Muscle biopsy examination will reveal the partial or absence of merosin expression, as well as the extent of muscle damage, including heterogeneity of fiber size and fibrosis [54, 55]. Genetic testing, primarily gene panel sequencing, is the standard in diagnosing MDC1A. However, if copy number variants or intronic variants lead to abnormal splicing, such can be identified by whole genome sequencing or RNA sequencing [56, 57]. In addition to the above two main aspects, brain MRI imaging for white matter abnormalities and elevated serum kinase levels will provide additional support for MDC1A diagnosis. Currently, neonatal screening is unavailable for MDC1A, and the diagnosis is usually made after birth. However, laminin-211 is expressed in the placental trophoblast after the 9^{th} week of gestation. Therefore, if a child has MDC1A with two pathogenic variants, then prenatal testing involving chorionic villus sampling could be offered to the mother for the subsequent pregnancies [58].

1.6 Heterogeneity of mutations in MDC1A patient population

Owing to the genetic nature of the disease, correction of mutations would be a promising treatment for MDC1A. Based on the Leiden open variant database (LOVD there are more than 300 pathogenic variants in the *LAMA2* gene involving missense, splice site, nonsense, and deletion mutations that have been documented [59]. The mutations spread throughout the entire *LAMA2* gene without specific mutational hotspots (Figure 2).

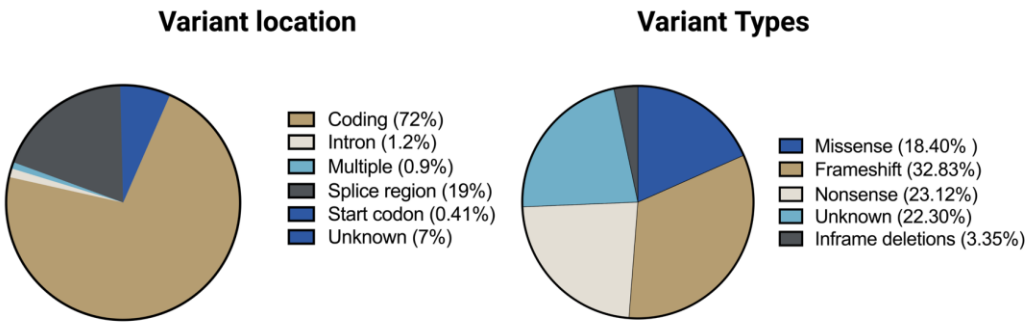

Figure 2. Heterogeneity of mutations in *LAMA2*

Schematic illustration of location and types of variants occurring in the MDC1A patient population. The pie charts were constructed based on the Leiden Open Variant Database.

Generally, patients with a complete absence of LAMA2 exhibit severe phenotypes, and patients with partial expression of LAMA2 exhibit milder phenotypes [25, 60, 61]. However, it is difficult to determine the severity of the clinical presentations based on the type of mutations. For instance, in some cases, the mutations involving the N-terminal region with a preserved C-terminal expression resulted in a mild expression of LAMA2 with mild clinical representation [55, 62, 63]. Likewise, intrafamilial clinical variability also exists in the patient population. For instance, a study by Prandini et al. reported that two sisters carried the same homozygous loss-of-function mutation in the *LAMA2*. However, one had a severe presentation of the disease while the other had a milder presentation of MDC1A, suggesting that varied clinical presentation might be due to the role of disease modifiers in patients [23].

Collectively, the high degree of mutation heterogeneity reported in patients would pose a significant challenge for developing a therapeutic strategy based on mutation correction in *LAMA2*. An alternative approach, such as the upregulation of compensatory proteins, would enable universal treatment of more patients, irrespective of their mutation types.

1.7 LAMA1 can compensate for the lack of LAMA2

The laminin-α1 chain is one of the early laminin isoforms to be expressed in mammalian embryos and plays a vital role in early embryogenesis[50, 64]. Albeit, around the 9th week of gestation, it is replaced by the laminin-α2 chain in skeletal muscle [58, 65] and is found in the basement membrane of the kidney [66].

Laminin-α1 chain shares many similar traits as laminin-α2. Structurally, like the laminin-α2 chain, the laminin-α1 chain combines with β1 and γ1 to form a heterotrimeric complex laminin-211. The structural similarity is very similar between LAMA1 and LAMA2 (Figure 3). The laminin-α1 chain/LAMA1 protein interacts with similar cell surface receptors as LAMA2. It binds to integrin α7β1 [67] and dystroglycan like LAMA2[46]. This is of utmost importance because it establishes a connection between the basement membrane and cytoskeleton and helps in the downstream signaling process in the cell. Collectively, these suggests that LAMA1 could act as a strong compensatory disease modifier and a therapeutic target for MDC1A. Further, research done on LAMA1 is covered in the below sections 1.10.6 to 1.10.7

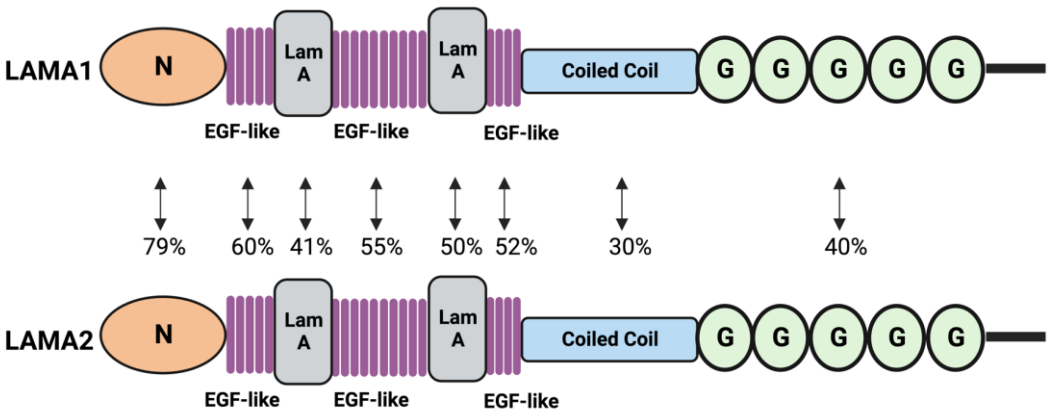

Figure 3. Structural similarity between LAMA1 and LAMA2

The figure illustrates the structural similarity in the protein sequences between each domain in human LAMA2 and LAMA1, and sequential similarity is represented in percentages. N; Laminin N-terminal domain, EGF; laminin-type-epidermal growth factor-like domain, Lam A; laminin type IV A domain, G; Laminin type globular domains. (The figure was created with BioRender.com).

1.8 The use of animal and cellular models in MDC1A

The LAMA2 expression and disease severity is recapitulated in mouse models of MDC1A. The three most commonly used models are dy^{3K}/dy^{3K}, dy^{W}/dy^{W}, and dy^{2J}/dy^{2J} [68, 69] (Table 1) The dy^{3K}/dy^{3K} knock-out mouse model completely lacks the expression of LAMA2, which results in severe muscular dystrophy, peripheral neuropathy, hind limb paralysis, and a shorter lifespan of 3-5 weeks [70]. The dy^{W}/dy^{W} knock-out mouse model expresses a very low level of LAMA2 and has severe muscular dystrophic and peripheral neuropathic features and a lifespan of 5 to 16 weeks [71-73]. The dy^{2J}/dy^{2J} mouse model has a spontaneous splice site mutation in the *Lama2* gene, resulting in a slightly reduced expression of LAMA2. They exhibit mild dystrophic and peripheral

neuropathic features with a normal lifespan [74-76]. These mouse models are valuable tools for studying disease pathophysiology and therapeutic development in MDC1A.

Table 1. Mouse models to study MDC1A

Mouse model	Mutation	Laminin production	Life span (weeks)	Dystrophic features
dy^{3K}/dy^{3K}	Targeted knock out	Absent	3-5	Severe
dy^{W}/dy^{W}	Targeted knock out	Very low level	5-16	Severe
dy^{2J}/dy^{2J}	Splice site mutation	Reduced level	Normal	Mild

Besides the mouse models, two zebrafish models closely resemble the muscular dystrophic features in humans. (i) The *candyfloss* zebrafish model comprising of homozygous mutations in the *lama2* gene resulting in loss of lama2 protein expression and a degenerating muscle phenotype [77, 78]. (ii) The *lama2*^{c1501} zebrafish model carries a mutation in the coiled-coil α-helical domain, resulting in loss of lama2 protein expression. The model is similar to the *candyfloss* model, but these mutants also exhibit brain defects[79].

In addition to the mouse and zebrafish models, cellular models involving myoblasts, myotubes, and fibroblasts are used in MDC1A research. First, they are helpful in identifying the *LAMA2* mutation in an MDC1A patient. The LOVD database documents the different types of mutation and the consequence of these mutations in protein expression and the phenotype. As of now, there have been more than 300 mutations documented in the *LAMA2* gene. Second, they retain the genetic background of the individual. This would enable the researchers to identify the genetic differences that cause variations in severity of the disease. Third, they mimic the characteristics of the MDC1A disease, allowing the researchers to test the efficacy of the developed treatment strategy. Moreover, some cell-model systems, such as fibroblasts, are non-

invasive, and are easier on the affected patients. Albeit the advantages of the cellular models, they do not fully mimic the *in vivo* behavior and cannot recapitulate the interaction between different systems in the body.

1.9 Pharmacological approaches to ameliorate MDC1A pathogenesis

1.9.1 Targeting the apoptotic pathway

Many different groups have worked towards targeting the potential disease mechanism in MDC1A. In 2004, Girgenrath et al. demonstrated that either by increasing the transgenic expression of the apoptosis inhibitor, *Bcl-2* or by inactivating the proapoptosis protein *Bax*, dy^W/dy^W mouse model had a prolonged survival rate and decreased fixtured contractures [80]. Based on this research, preclinical studies were done on dy^W/dy^W and dy^{2J}/dy^{2J} and mouse models using the drug omigapil [N-(dibenz(b,f)oxepin-10-ylmethyl)-N-methyl-N-prop-2-ynylamine]. Omigapil binds to GAPDH and inhibits the activation of GAPDH-Siah1-mediated apoptosis[81]. This led to improved locomotor activity and decreased fibrosis in skeletal muscles and diaphragm of the mice [82, 83]. This led to the foundation of the phase I of the clinical trial of Omigapil in MDC1A patient population (Clinicaltrials.gov Identifier NCT01805024). In addition to MDC1A subset, the study also included individuals from collagen VI-related dystrophy (COL6-RD) [84]. This phase I clinical trial, termed CALLISTO, included 20 participants and was conducted for 12 weeks with doses ranging from 0.02-0.08 mg/kg/day. Overall, omigapil was established as a safe drug with a favorable pharmacokinetic profile in these disease populations. The study concluded that it requires more in vivo experiments for COL6-RD, and biomarkers are needed to study the

drug's impact on the disease without needing muscle biopsies. Santhera pharmaceuticals have discontinued the development of omigapil based on their internal pipeline review, resulting in a shift in their priority [85, 86].

1.9.2 Targeting the proteasome degradation and autophagy pathways

Carmignac et al. showed that the ubiquitin-proteasome pathway was upregulated in an MDC1A mouse model. To further understand the implication of the proteasome pathway, they administered a proteasome inhibitor MG-132 systemically to the dy^{3K}/dy^{3K} mouse model. The study results showed reduced fibrosis, apoptosis, and improved life span in dy^{3K}/dy^{3K}, suggesting that the proteasome pathway could be targeted for developing a drug to mitigate MDC1A [87].

Further, the same group, in 2011, also investigated additional pathways/mechanisms that are affected in MDC1A and showed that the autophagy-lysosome pathway is also overactivated in the dy^{3K}/dy^{3K} mouse model. Therefore, they administered an autophagy inhibitor 3-methyladenine (3-MA) and observed a reduction in muscle fibrosis, apoptosis, increased muscle regeneration, and muscle mass in the dy^{3K}/dy^{3K}mice [88]. Based on these findings, a commercially available proteasome inhibitor Bortezomib, currently used for multiple myeloma, was administered in the MDC1A mouse model. They observed improved locomotion, survival, and increased body weight [89].

1.9.3 Targeting the inhibition of fibrosis

MDC1A leads to the deposition of fibrotic tissue in the skeletal muscle, and marked fibrosis is one of the characteristic features of the disease. In 2010, Nevo et al. group studied the

implications of Halofuginone in dy^{2J}/dy^{2J} mouse model. This drug inhibits the TGF-mediated collagen synthesis, reducing collagen deposition, infiltrated fibroblasts, and degenerated areas in the skeletal muscle [90]. Based on these findings, losartan, a commercially available drug for hypertension, was administered in dy^{2J}/dy^{2J} mouse model. Losartan inhibits the TGF-β signaling pathway, and there was a decrease in the downstream pSmad2/3 protein and a reduction in fibrosis in the mice [91].

1.10 Gene therapies in MDC1A

All the aforementioned therapies involving the drugs omigapil, bortezomib, losartan involve in inhibiting apoptosis/proteasome/autophagy pathways, respectively, have some challenges. First, they do not rectify the underlying disease condition but act upon the pathways that are affected downstream, and thus they don't provide complete recovery. Second, these therapies are systemic and therefore affect the entire body which might cause complications in the other organ systems. To circumvent these challenges, an alternate solution would be to focus on therapies that restore/compensate the function of laminin-211 protein complex in the skeletal muscle.

1.10.1 Transgenic expression of *LAMA2*: Rationale for *LAMA2* restoration

Kuang et al. transgenically expressed human *LAMA2* using muscle-specific creatine kinase promoter in two MDC1A mouse models. The dy^{W}/dy^{W} has a severe phenotype with complete loss of laminin- α2, while the dy^{2J}/dy^{2J} has a mild phenotype with partial expression of laminin- α2.

Overall, the mice showed improvement in muscle morphology, integrity, lifespan, and reduction of dystrophic features of the mice [71]. However, the mice had visible hindlimb paralysis indicating a nerve defect since the transgene was not expressed in the peripheral nerve. These results suggest that the expression of LAMA2 is crucial in skeletal muscle and peripheral nerves for overall well-being. Despite the success in the mitigation of dystrophic features, this approach cannot be translated to clinical trials in humans due to the large size (9.5kb) of LAMA2 that exceeds the packaging capacity of adeno-associated viral vectors (AAVs)[92, 93].

1.10.2 Micro-laminin gene therapy

To circumvent the problem of packaging the entire *LAMA2* gene, Packer et al. developed a micro-laminin gene therapy that consists of a shortened version of *LAMA2*. AAV9 carrying shortened *LAMA2* encoding only the five globular domains (G1-G5) of the protein was introduced intravenously in dy^W/dy^W mouse model. The results showed partial restoration of the phenotypes in mice, indicating that such truncated protein was inadequate to achieve proper function owing to the lack of functionally redundant domains of the LAMA2 protein [94].

1.10.3 Miniaturized agrin (mag)

In patients with MDC1A, the other isoform of laminin-α2, laminin-α4, is upregulated. The laminin-α4 combines with β1 and γ1 subunits to form a laminin-411 protein complex. However, unlike laminin-211, laminin-411 cannot self-polymerize and cannot bind with the cell surface receptor, α-dystroglycan. This is essential as one of the chief functions of laminin-211 is to link the basement membrane and cytoskeleton.

An approach involving a miniaturized version of the protein agrin, miniagrin (mag) was developed, connecting Laminin-411 to the α-dystroglycan. This would establish a connection to the cell-surface receptors and compensate for lacking laminin-211. This approach involving the transgenic miniagrin expression was tested in dy^{W}/dy^{W}, dy^{3K}/dy^{3K} mice, and both the models showed improved muscle histology [34, 95]. However, even though this strategy improved laminin-411 binding affinity to α-dystroglycan, it did not improve the capacity of laminin-411's self-polymerization.

1.10.4 αLNND and mini-agrin

To circumvent the polymerization problem, Mckee et al. designed a chimeric protein consisting of laminin-α1 N-terminal, and EGFa domains (LN-LEa) fused with a C-terminal region of nidogen-1 fragment. This fusion protein, termed αLNND, would facilitate the self-polymerization of laminin. The group tested this strategy in a dy^{2J}/dy^{2J} mouse model with minimal expression of laminin-211. The dy^{2J}/dy^{2J} mice have a splice site mutation resulting in a deletion of part of the laminin-α2 LN domain. This deletion impairs the polymerization ability of the laminin-211 in dy^{2J}/dy^{2J} mice. Transgenic expression of αLNND in dy^{2J}/dy^{2J} mice served as a linker protein and enhanced laminin polymerization, further reducing fibrosis and improving grip strength in the mice[96].

Collectively, miniagrin facilitates binding to the α-dystroglycan, and αLNND protein promotes self-polymerization. Reinhard et al. used both these strategies to enhance the function of laminin-411. The group transgenically expressed both minagrin and αLNND in dy^{W}/dy^{W} in a mouse model. The linker proteins, αLNND and minagrin, enhanced the polymerization and binding capacity of laminin-411 to α-dystroglycan, respectively. This improved basement

membrane stability, survival and body weight of the dy^W/dy^W mice. Therefore, the results establish that with the help of the two linker proteins, the performance of laminin-411 can be significantly improved and could compensate for the functions of laminin-211[97].

1.10.5 CRISPR gene editing

The approach of re-introducing *LAMA2* gene is not feasible due to the large size and an effort to miniaturize the *LAMA2* gene is hampered by the lack of functionally redundant domains of the LAMA2 protein. Finally, the use of linker proteins relies on the upregulation of laminin-411. To circumvent all these challenges, Kemaladewi et al. used the CRISPR gene editing tool to successfully correct the *Lama2* mutation within the dy^{2J}/dy^{2J} mouse model. This model has a splice donor site mutation in intron 2 of the *Lama2* gene, c.417+g → a. This mutation results in the skipping of exon 2, with 57 amino acid deletions (residues 34-90). The expressed LAMA2 protein has a truncated N-terminal protein domain that disrupts the laminin polymerization to form a laminin network [76]. Kemaladewi et al. used CRISPR-Cas9 and two sgRNAs to create double-strand breaks and excised the region containing the mutation, which was then repaired by non-homologous end joining (NHEJ). After excision, exon 2 was joined with a 'gt' dinucleotide and thus reconstituting a functional donor splice site. This strategy resulted in the inclusion of exon 2 in *Lama2* and the production of a functional LAMA2 protein in the mice. This improved muscle histopathology and function and mitigated the dystrophic features in MDC1A mice [98]. This successful strategy might be translationally challenging due to the heterogeneity of mutations in MDC1A patient populations [2, 99-104].

1.10.6 Transgenic expression of *LAMA1*: Rationale for *LAMA1* restoration

As an alternative, several groups have performed experiments focused on the upregulation of LAMA1, a disease modifier in MDC1A. Previously, Gawlik et al. demonstrated that transgenic overexpression of *Lama1* in an MDC1A model showed reduced dystrophic features. In addition, since the transgene is expressed ubiquitously, the mice were protected from hindlimb paralysis. The mice also showed reduced muscular fibrosis and near normal life span [105-109]. Thus, it bolsters the potential of *LAMA1* as a disease modifier gene.

1.10.7 LAMA1 upregulation using CRISPR/dCas9 system

The postnatal expression of LAMA1 may not be feasible in human subjects primarily because the large size of the LAMA1 transcript exceeds the AAV packaging capacity. To circumvent this problem, Kemaladewi et al. induced endogenous expression of *Lama1* in the MDC1A mouse model using the CRISPR activation (CRISPRa) system, which features deactivated Cas9 (dCas9) devoid of endonuclease activity, transcriptional activators VP64, and three sgRNA targeting the proximal promoter of *Lama1*. Kemaladewi et al. showed that dy^{2J}/dy^{2J} mice, treated with AAV9 carrying the CRISPRa components, exhibited robust expression of *Lama1*, which led to an overall reduction in dystrophic features, including reduced fibrosis and hindlimb paralysis [110]. A detailed explanation of CRISPR activation system is covered in the section 1.12.

1.11 Evolution of CRISPR-Cas9 as a gene-editing technology

Clustered regularly interspaced short palindromic repeats (CRISPR) was initially identified in bacteria as a part of its defense mechanism from bacteriophages. The prokaryote genome contains sequences homology to the invading pathogen, termed CRISPR array, which is transcribed as CRISPR RNA (crRNA). It combines with trans-activating CRISPR RNA (tracrRNA) and CRISPR-associated (Cas) protein to form a ribonucleoprotein (RNP) complex. It scans and binds to the phage's genome that complements with the sequence encoded by the crRNA. The Cas9, being an endonuclease, causes double-stranded breaks and thereby destroying the phage's life cycle [111-113].

There are many Cas9 proteins available (Table 2) but the two most used Cas9 are those derived from *Streptococcus pyogenes* (*Sp*Cas9) and *Staphylococcus aureus* (*Sa*Cas9). Each Cas9 protein requires a specific recognition sequence near the target site for binding and initiating DNA melting in the target region. These short DNA sequences, termed Protospacer adjacent motif (PAM) are not encoded in the crRNA but should be available in the host genome near the user-defined target site. The PAM sequence for *Sa*Cas9 is NNGRRT, and for *Sp*Cas9 is NGG [114, 115]. Albeit *Sp*Cas9 PAM sequences are short and more frequently available in the genome, the Cas9 protein is larger (4.1 kb) than *Sa*Cas9 (3.2 kb) protein and is more favorable for packaging in AAVs which has a packaging limitation capacity of ~ 4.7 kb [92, 93]. Notably, there are Cas9 proteins shorter than *Sa*Cas9, such as the Cas9 derived from *Campylobacter jejuni* comprising 984 aa but it requires a complex PAM sequence for recognition.

Table 2. Major CRISPR-Cas proteins

Name	Origin	Size	PAM sequence
*sp*Cas9	*Streptococccus pyogenes*	1368	NGG
*sa*Cas9	*Staphylococcus aureus*	1053	NNGRRT
*Fn*Cas9	*Francisella novicida*	1629	NGG
*Nm*Cas9	*Neisseria meningitidis*	1082	NNNNGATT
*St1*Cas9	*Streptococccus thermophilus*	1121	NNAGAAW
*St3*Cas9	*Streptococccus thermophilus*	1409	NGGNG
*Cj*Cas9	*Campylobacter jejuni*	984	NNNNACAC
*As*CPf1	*Acidaminococcus sp*	1307	TTTV
*Lb*Cpf1	*Lachnospiraceae bacterium*	1228	TTTV

This original system comprising of crRNA, tracrRNA and Cas9 used to defend the bacteriophage was adapted to evolve as a precise-gene editing tool. Jinek et al. fused the crRNA and tracrRNA into a single chimeric RNA called single guide RNA (sgRNA) [113]. Therefore, the CRISPR system has two components: the sgRNAs that guide the Cas9 to bind to a user-defined genomic site and a Cas9 protein that causes a double-strand break in the genome. The double-strand breaks are eventually repaired by non-homologous end-joining or homology-directed repair (HDR). The end-joining could be classical non-homologous end-joining (C-NHEJ) or microhomology-mediated end-joining/alternate end-joining (MMEJ or Alt-NJ). It usually results in random insertions/deletions. Additionally, direct insertion of exogenous DNA at the break site is also feasible with NHEJ based on recent studies [116-119]. The HDR requires the presence of an additional DNA template and is feasible only in dividing cells (Figure 4) [113] [120-123].

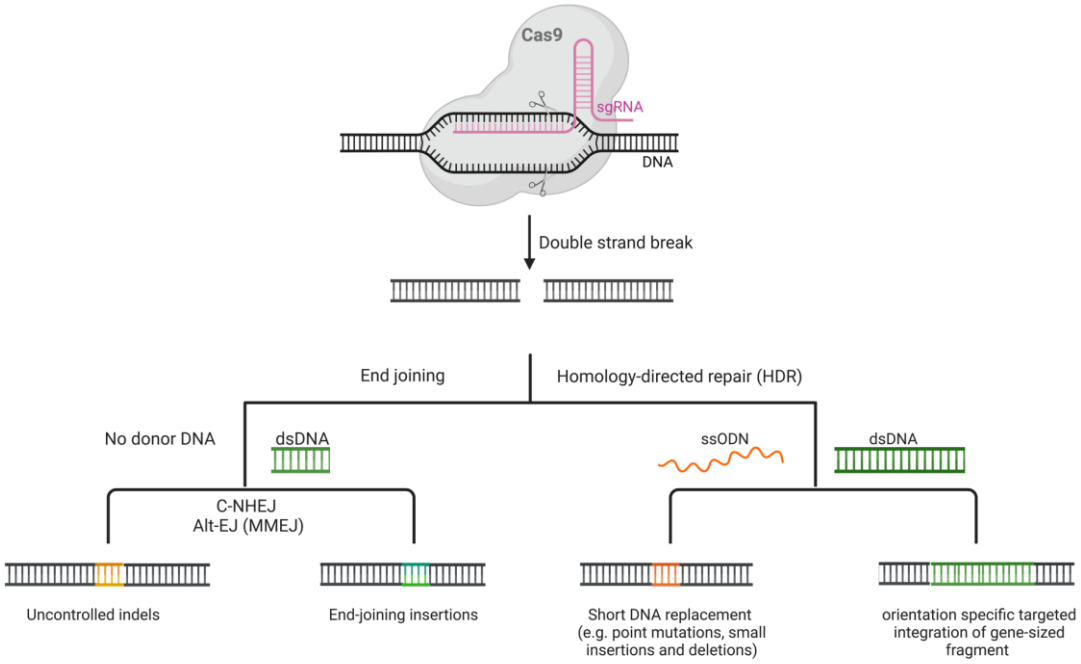

Figure 4. CRISPR/Cas9 System

Schematic representation of CRISPR/Cas9 mechanism in gene-editing. The single guide RNAs guide the CRISPR/Cas9 system to the desired target site and causes double-strand breaks which is repaired by classical non-homologous end-joining (C-NHEJ) or alternate end-joining (A-EJ). Homology directed repair occurs in dividing cells when single-strand oligonucleotide donors (ssODNs) or double-strand DNA templates are provided. (The figure was created with BioRender.com).

In addition to excising the gene fragments, CRISPR-Cas9 systems are modified to perform base editing and prime editing roles. The Cas9 is engineered by mutating the catalytic domain, RUVC domain (D10A) resulting in a nickase Cas9 that produces a single-strand break [120]. The nickase Cas9 is combined with base editors to convert the nucleotide bases at the target site resulting in CRISPR base-editing system. Komor et al. demonstrated the fusion of nickase Cas9 with APOBEC1 cytosine deaminase converts cytosine to thymine [124]. Similarly, Gaudelli et.al employed adenosine deaminase with the nickase Cas9 to convert adenine to guanine [125].

Notably, this approach was used in sickle cell disease (SCD), caused by mutations in the β-globin gene (*HBB*). The sixth amino acid codon 'GAG' mutates to 'GTG', resulting in SCD. Using a CRISPR-base editing strategy, the researchers converted thymine base to cytosine resulting in 'GCG', a non-pathogenic variant. This successful approach led to phase I of the clinical trial[126].

Prime editing comprises a nickase Cas9 fused with a reverse transcriptase enzyme. The prime editing guide RNA (pegRNA) guides the Cas9 to the target site and encodes the desired gene sequence for editing. The reverse transcriptase transcribes based on the genetic information carried by the pegRNA. The technology is useful for correcting point mutations, primarily because prime editing work where base-editing is not applicable, such as transversion [127]. Zhi et al. used this strategy to cause the transversion guanine to thymine in the DNA methyltransferase 1 (*Dnmt1)* gene in a mouse model [128].

1.12 Engineering CRISPR-Cas9 to mediate gene expression and regulation

Mutations in the RUVC domain (D10A) and in the HNH domain (H840A for *Sp*Cas9) will result in a deactivated/dead Cas9 that lacks the ability to cleave the DNA [129]. The engineered/modified Cas9 protein can be fused with a transcriptional regulator resulting in a wide range of genome editing possibilities.

In the CRISPR activation system (CRISPRa), the dCas9 is fused with transactivation domains to increase the endogenous expression of the desired target gene [130]. In my study, I have used CRISPRa; therefore, this subsection is elaborated. The commonly used transcriptional activator is VP64 which consists of four copies of the 16-amino acids long transactivation domain (VP16) of the Herpes simplex Virus (HSV). In addition, the transcriptional activator VP160,

consisting of 10 copies of VP-16, is also used in CRISPRa. Several next-generation activation systems – VPR, SAM, SunTag- have evolved. VPR system consists of VP64, P65, and Rta, where P65 is a transcription activation domain of the mammalian NF-kB transcription factor and Rta is an R trans activator from the Epstein-Barr-virus [131, 132]. The synergistic activation mediator (SAM) complex is also a next-generation activation system, which consists of bacteriophage MS2-coat protein (MCP) complex and heat shock transactivation complex P65-HSF1 [133]. SunTag is a repeating peptide array fused with dCas9 and can be used to recruit multiple copies of the protein to the target site enabling an increase in endogenous gene expression [134]. Any of these transcription activators can be connected to the dCas9. The sgRNA will guide the Cas9 system to the target site, which is usually a proximal promoter region of the gene. Thereafter, the transcriptional activators will interact with the transcription factors to increase the endogenous expression of the target gene (Figure 5) [130, 135].

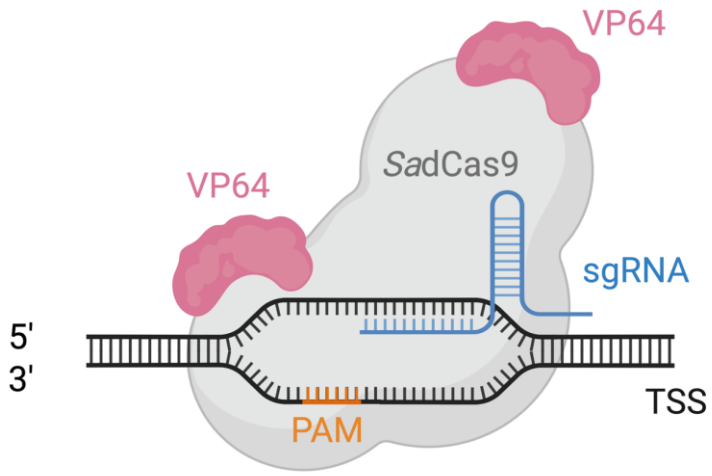

Figure 5. CRISPR activation system

Schematic representation of CRISPR activation system. The sgRNA (blue) guides the *Sa*dCas9 (grey) to the proximal promoter region of gene. The PAM sequence (orange) is recognized by the Cas9 for binding. The VP64 transcriptional

regulators (pink) interacts with transcription factors to increase the expression of the target gene. (The figure was created with BioRender.com).

The CRISPR interference system (CRISPRi) comprises a dCas9 fused with a transrepression domain such as a Kruppel-associated box (KRAB). The sgRNAs guide the Cas9 complex to the desired target site, and transrepressors induce local gene repression [136]. This strategy was applied to reduce the expression of Na_v.17, sodium ion channel protein in a mouse model. The-loss-of function mutation in the Na_v.17 (*SCN9A*) leads to pain insensitivity, a rare genetic disorder [137]. Therefore, reducing the expression of sodium ion channel protein led to a reduction in pain sensitivity [138].

Likewise, targeted DNA methylation can be enabled by fusing the dCas9 to DNA methyltransferases such as DNMT3. In contrast, to remove the methyl groups, dCas9 is fused with ten-eleven translocation methylcytosine dioxygenases 1 (Tet1) [139-141]. These strategies have been used in many disease, and one such example is its application in fragile X syndrome. It is an intellectual disability caused by silencing the *FMR1* gene encoding for Fragile X mental retardation protein (FMRP). The dCas9-tet1system reversed the extensive hypermethylation in iPSC-derived neurons [142].

Similarly, histone modifications can be done by fusing dCas9 with histone acetyltransferase, which adds an acetyl group to the lysine 27 of histone H3 (H3K27ac). Similarly, the fusion of dCas9 with histone deacetylase removes the acetyl group in the target site [143, 144]. Recently, Liu et al., used this approach to silence an oncogene, *KRAS* encoding for K-Ras protein, that is mutated in many cancers. The suppression of the K-Ras protein resulted in reduced cell proliferation and cell growth [145].

Overall, the advancements in CRISPR systems are developing rapidly. Recent advances led to the development of multiplexed systems that can modify two or more loci in the human genome. These consist of Cas12 protein with short crRNA compared to the Cas9 sgRNA enabling multiplexing [128]. In another approach, Kiani et al. showed that Cas9 possess the nuclease activity when sgRNAs are of usual length (20-21 nt), while they lack the ability to cleave when the sgRNAs are shorter (14-15 nt). The group showed that the Cas9-VPR-sgRNAs (14-15 nt) induced activation in the genome [146]. In addition to this, other approaches not discussed here, such as inducible and logic-gated gene regulation CRISPR systems, have also emerged [147]. We direct the readers to excellent review articles of Adli and Chavez et al. for an overview of the recent trends [148, 149].

1.13 Applications of CRISPR gene-editing for therapeutic developments in neuromuscular disorder

CRISPR-gene editing has been widely used to treat muscular dystrophies primarily because the defective genes are large for many muscular dystrophies. This hinders the delivery of the transgene to substitute for the defective gene owing to the limitation in the packaging capacity of the vector. Due to the enormous volume of work currently being performed using CRISPR-Cas9 on muscular dystrophies, I have highlighted only a few of the research in this section.

1.13.1 Duchenne muscular dystrophy

Duchenne muscular dystrophy is (DMD) caused by mutations in the dystrophin gene (*DMD*) and has an X-linked inheritance. Several studies involving CRISPR gene editing have been performed to develop a therapy for DMD patients. Single-exon deletion or skipping by NHEJ was done in the *mdx* mouse models [150-153] and canine model [154]. Similarly, multi-exon deletions in *Dmd* gene were also done in the mdx mouse model [155, 156]. A base editing strategy was applied in a DMD mouse model consisting of a premature stop codon in exon 20, which halted the dystrophin expression. Conversion of the premature stop codon to glutamine codon restored the dystrophin expression in the mdx mouse model [157]. A study by Kwon et al. used the CRISPR-Cas9 system to excise the exon 23 in the *Dmd* gene in the satellite cells of the DMD mice. The mouse model has a mutation in the exon 23 of the *Dmd* gene, resulting in a premature stop codon and absence of dystrophin production. This resulted in the reconstitution of the reading frame and the production of a dystrophin protein. Further, the CRISPR-edited satellite cells were isolated and transplanted into recipient DMD mice showing increased dystrophin-positive fibers [158].

CRISPR-Cas9 has also been applied to correct duplications in DMD. Wojtal et al. used CRISPR-Cas9 with one sgRNA to bind to two spots in the duplicated region of a *DMD* gene, thereby creating double-strand breaks and removing the intervening sequence in the DMD patient-derived cells, resulting in functional dystrophin [159]. Further, Maino et al. developed a mouse model (Dup18-30) capturing the tandem duplication exhibited by the DMD patient-derived cells. They translated the approach of using one sgRNA to remove the duplicated region. The mice showed full-length dystrophin expression and improved the dystrophic phenotypes [160].

Nearly 60% of the DMD mutations occur in the mutational hotspot region, comprising exons 45-55. Young et al. used the CRISPR-Cas9 system and deleted exons 45-55 in several DMD patient-derived iPSCs, resulting in a shorter yet functional dystrophin [161]. Pickar-Oliver et al. used the homology-independent targeted integration (HITI) strategy and co-delivered CRISPR-Cas9 and the donor sequence in a humanized mouse model of DMD (hDMDΔ52/mdx). The donor sequence consisted of either exon 52 or the last 28 exons downstream of 51. Both scenarios resulted in dystrophin expression in the mice [162]. In another approach, Bengtsson et al. employed muscle-specific CRISPR/Cas9 components and utilized various approaches to correct the mutation in the DMD mouse model. One such approach was excising the exons in 52 and 53, resulting in dystrophin production [163]. Recently, Chemello et al. implemented two strategies to correct a mutation in a DMD mouse model harboring a deletion of exon 51 that results in a premature stop codon at exon 52 and a truncated non-functional protein. In the first strategy, the group delivered adenine base editor (ABE) components using a split-intein trans-splicing system and modified the splice site in exon 50, resulting in the skipping of exon 50-51. This results in joining exon 49 to exon 52 and restoring the reading frame and dystrophin production. In the second strategy, the group used prime editing and precisely introduced a two nt (GT) in the nicked site in exon 52, resulting in exon reframing and, thereby restoring the dystrophin expression [164].

Rather than correcting the mutation, research has been focused on upregulating the disease modifier in DMD, *UTRN* gene encoding for Utrophin. For instance, Wojtal et al. utilized the CRISPR activation system consisting of VP16, targeting the utrophin promoter to upregulate the transcription of utrophin [159]. Alternatively, Sengupta et al. increased the expression of *UTRN* in DMD patient-derived iPSCs by deleting five microRNA (miRNA) binding sites in the *UTRN* 3' UTR using the CRISPR-Cas9 system [165].

1.13.2 Myotonic dystrophy

CRISPR-Cas9 homology-directed repair strategy was implemented in developing a therapy for myotonic dystrophy (DM1). It is an autosomal dominant disorder DM1 caused by an expansion of a trinucleotide repeat (CTG) in the noncoding region of the myotonic dystrophy protein kinase (*DMPK*) gene [166]. In 2018, Wang et al. used CRISPR-Cas9 to delete the extensive CTG repeats in the *DMPK* gene, responsible for causing DM1. The group inserted polyadenylation (polyA) signals upstream of *DMPK* CTG repeats in an *in vitro* model of differentiated neural stem cells. The insertion of PolyA signals resulted in premature termination upstream of the CTG repeats [167]. Scrudato et al. used CRISPR-Cas9 and dual sgRNAs to delete the CTG repeats in the *DMPK* gene in patient-derived muscle cells and a myotonic dystrophy mouse model (DMSXL)[168]. In another approach, Batra et al. employed RNA targeting CRISPR-Cas9 (RCas9) to target the CUG repeat transcripts for degradation. The approach successfully degraded CUG repeats in the *DMPK* transcripts in patient-derived cellular model [169]and CUG repeats in the *HSA* gene in the HSA_{LR} mouse model [170]. Further, Cardinali et al. employed a drug-inducible CRISPR-Cas9 system comprising tetracycline repressor-based guide RNAs and Cas9 to delete the CTG repeat in DM1 patient-derived cells and DM1 mouse model [171].

1.13.3 Facioscapulohumeral muscular dystrophy

Facioscapulohumeral muscular dystrophy (FSHD) is caused either by hypomethylation of the tandem repeat array (3.3kb) D4Z4, which is located in the subtelomeric region of fourth chromosome (4q35). Epigenetic de-repression at the D4Z4 array leads to chromatin relaxation and abnormal expression of D4Z4-related noncoding RNAs in the skeletal muscle. One such

consequence is the aberrant expression of *DUX4* gene (double homeobox 4) and its protein DUX4 protein whose transcriptional targets include germline cells, immune mediators, and apoptosis. CRISPRi consisting of dcas9 and KRAB repressor was employed by Himeda et al. to target the *DUX4* promoter or exon 1 to repress the aberrant gene expression in primary FSHD myocytes [172]. In addition to FSHD myocytes, the research group successfully translated this approach by delivering the CRISPR components using AAVs in a mouse model of FSHD, resulting in *DUX4* repression [173] .

1.13.4 Ulrich Congenital muscular dystrophy

Ulrich Congenital muscular dystrophy (UCMD) stands at the severe end of the collagen type VI-related myopathies spectrum. Mutation in *COL6A1, COL6A2,* and *COL6A3* leads to null or deficient production of collagen type VI resulting in muscle weakness, connective tissue abnormalities, skeletal anomalies (scoliosis, kyphosis, spinal stiffness), and respiratory insufficiency [174-176]. Bolduc et al. used CRISPR-Cas9 and sgRNAs to delete the pseudo exon in *COL6A1* in UCMD, resulting in collagen VI production in patient-derived fibroblast [177].

1.14 Use of CRISPR in generating disease models for neuromuscular disease

In addition to therapeutic developments, CRISPR gene editing technology has also been used to develop animal models recapitulating the disease. For example, Amoasii et al. created a DMD mouse model (ΔEx50) using the CRISPR-Cas9 system by deleting exon 50 of the *Dmd* gene [178]. Likewise, Maino et al. generated a mouse model, *Dup18-30,* with tandem duplication of

exons 18-30 in the *Dmd* gene [160]. In another approach, Wong et al. generated a mouse model, *Dmd* Δ52-54, comprising deletion of exons 52-54, resulting in no dystrophin production [179]. In addition to the mouse models, other animal model systems were also created using CRISPR-Cas9 technology, such as DMD rat, pig, and rabbit model systems. For example, Nakamura et al. generated a rat model by deleting exons 3 and 16 [180], while Yu et al. targeted the deletion of exon 27 to create a DMD pig model system [181]. Finally, Sui et al. produced a DMD knockout rabbit model with mutations in the exon 51 of the dystrophin gene using CRISPR-Cas9 gene editing [182]. Collectively, the studies suggest the efficiency and versatility of CRISPR technology in creating disease model systems.

1.15 Delivery of CRISPR components

CRISPRs are multi-components comprising the large Cas protein and sgRNA, which together poses challenges in packaging and delivery for efficient gene editing. They are delivered as DNA, RNA, or ribonucleoprotein (RNP) complexes using viral or non-viral methods [183, 184].

Lentiviral vectors are used to deliver the CRISPR components owing to their high cloning capacity (< 8Kb) capacity [185]. However, they pose problems due to insertional mutagenesis and low efficiency. Further, if integrating lentiviral vectors are used, they pose the problem of being integrated with the host genome. This mode of delivery is mainly used for in vitro and ex vivo models [186]. The two most non-viral physical methods used are microinjection and electroporation. In microinjection, the CRISPR components are directly delivered to the cells through a microneedle. In electroporation, electric currents create transient pores to absorb the CRISPR components. Both these methods overcome the challenges of the size limitation of the

packaging and provide controlled dosing. However, these technologies are not feasible for *in vivo* applications [187, 188].

The most used method to deliver CRISPR components in the field of gene therapy, both in vivo and ex vivo, is AAV [189]. The CRISPR components could be delivered as one vector or split into two vectors [190]. They have several advantages as they are replication defective and unable to integrate with the host genome. The main disadvantage of AAVs is the limitation in their packaging capacity (4.7 kb). Using a small Cas protein derived from *Staphylococcus aureus*, some space could be obtained in the vector [114]. However, 4.7 kb may not be enough if many sgRNAs or transcriptional regulators need to be packed. Another approach to circumvent the problem is the use of intein-mediated protein splicing. The Cas9 is split into two halves and packed in each AAV resulting in an AAV with an N-terminal lobe of 2.5 kb and a C-terminal lobe of 2.2 kb. This provides nearly an extra 2kb in each AAV [191, 192]. Similar to splitting the Cas9, base editors such as ABE have also been split and delivered by intein-mediated splicing successfully in a DMD mouse model[164]. However, there are still challenges of immunogenicity and toxicity which will be discussed in the Chapter 5.

In addition to these methods, several others exist, including the delivery of lipid and gold nanoparticles. In lipid nanoparticles, the CRISPR components could be delivered as DNA, RNA, or protein, while gold nanoparticles deliver as Cas9-Ribonucleoprotein [193, 194]. Both of these methods are safe as they are viral-free and do not elicit an immune response, but they solely rely upon the endosomal pathway for intake in the cells, and therefore efficiency is low compared to the viral vectors or physical methods such as electroporation [184].

Virus-like particles (VLPs) have recently been used to deliver the CRISPR components. VLPs are vehicles comprising viral envelopes and structural proteins but do not contain viral

genomes. Therefore, they possess the ability to infect cells but are unable to integrate into the host genome. The CRISPR RNA or RNP is fused to the retroviral Gag polyprotein (Gag-pol) and packed inside the viral vector. The CRISPR components are released along with the Gap polyprotein during the viral maturation phase. They have several advantages, such as non-integration with the host genome, and packaging capacity can be increased based on the VLP architecture. For instance, retroviruses have a large particle diameter of 100-200 nm that could accommodate the Cas9. Further, by engineering the envelope glycoprotein, they could be reprogrammed to target any cell type. VLPs deliver the CRISPR components as RNA or RNP reducing the off-target effects. VLPs are promising, and it should be noted that since these are derived from viral scaffolds, immunogenicity related to VLPs should be further studied in vivo models [195-198]. Recently Seng et al. developed a system, selective endogenous encapsidation for cellular delivery (SEND), that consists of a modified mammalian retrovirus-like protein PEG10 that could be programmed to deliver CRISPR-Cas9 mRNA components. The SEND platform is less immunogenic than viral vectors and VLPs as it uses an endogenous mammalian viral scaffold [199].

1.16 Public health significance

MDC1A is the most common form of congenital muscular dystrophy. Since the disease manifests at an early age, it affects the quality of life of the MDC1A patients for the rest of their life. Currently, there is no treatment to cure MDC1A owing to heterogeneous mutations in MDC1A patients. Death occurs beginning from the first decade of the patient's life and anytime thereafter based on the severity and repeated occurrences of respiratory tract infection. The disease

poses a significant public health burden. Successful completion of the project will be crucial to move forward with the mutation-independent treatment for all patients with MDC1A and thereby contributing to public health.

1.17 Summary

Merosin-deficient congenital muscular dystrophy (MDC1A) is the most common form of congenital muscular dystrophy, caused by mutations in the *LAMA2* gene. It results in a defective form of the extracellular matrix protein laminin-α2 (LAMA2) [36]. Individuals diagnosed with MDC1A exhibit progressive muscle wasting and declining neuromuscular functions. Currently, there are no treatments for this disorder. There are over 300 mutations in the *LAMA2* gene, and the heterogeneous nature of the mutations makes gene therapy challenging and time-consuming [59].

Rather than targeting the defective gene *(LAMA2)*, a mutation-independent approach aimed to target and upregulate a disease modifier of MDC1A, *LAMA1* (laminin-α1), to compensate for the lack of *LAMA2* might work in MDC1A. However, *LAMA1* cannot be delivered directly to the MDC1A patients owing to its large size and the limited loading capacity of the gene delivery vehicles. Therefore, I employed the CRISPR activation system (CRISPRa) to increase the endogenous expression of *Lama1*, in an MDC1A mouse model[110]. The strategy was successful, resulting in the reduction of dystrophic features in the mice. The next step on a grand scale is to see the feasibility of this strategy in MDC1A patient-derived models.

Thus, my dissertation aims to translate this mutation-independent strategy involving endogenous upregulation of *LAMA1* using CRISPRa in MDC1A patient-derived fibroblasts. Here in Chapter 2 of this dissertation, I describe designing the CRISPR activation system with a Cas9

from *Staphylococcus aureus*, VP64 transactivation domains, and single guide RNAs. Subsequently, I elucidate the efficiency of the CRISPR activation system in human cell lines and MDC1A-derived primary fibroblasts. Chapter 3 of this dissertation builds on the study of transcriptomic profile in MDC1A fibroblasts to identify overall dysregulated biological pathways and pathways directly associated with *LAMA2*. A consecutive goal is to analyze the transcriptomic profile of MDC1A fibroblasts treated with CRISPRa for upregulating *LAMA1* and for pathways associated with *LAMA1*. In chapter 4 of this dissertation, to test the functional consequences of *LAMA1*, I employed a migration assay to observe the wound-healing mechanism in the MDC1A fibroblasts. Ensuring that *LAMA1* can compensate for *LAMA2* in cellular migrations, I developed a model to elucidate the role of LAMA2/LAMA1 in the wound-healing mechanism.

2.0 CRISPR activation system induces LAMA1 upregulation

2.1 Introduction

MDC1A is caused by mutations in the *LAMA2* gene. However, mutations are heterogenous; [100] therefore, developing a gene therapy involving correcting each mutation in a patient is challenging. In this regard, Kemaladewi et al. previously developed an approach to increase the expression of a disease modifier, *LAMA1*, to compensate for the lack of *LAMA2* in an MDC1A mouse model. As a result, the MDC1A mice, treated with AAV9 carrying the CRISPRa components, exhibited robust expression of *Lama1*, which led to an overall reduction in dystrophic features, including reduced fibrosis and hindlimb paralysis [110].

The previous sgRNAs were specific to the mouse genome. To determine efficient upregulation of human *LAMA1*, it is essential to design a CRISPRa system with transcriptional activators VP64 and sgRNAs targeting the proximal promoter region of human *LAMA1*. Therefore, in this study, **I design a CRISPR activation system and validate its efficiency in upregulating human *LAMA1* in fibroblasts from MDC1A individuals.** Thus, this work provides an essential resource for applying CRISPRa in an MDC1A cellular model. Further, it could also be translated to other therapeutic applications, such as diseases involving haploinsufficiency [200] [201].

2.2 Methods

2.2.1 Study population and cell culture conditions

Fibroblasts from de-identified MDC1A donors were obtained under Research Ethics Board-approved protocol 1000052878 at the Hospital for Sick Children, Toronto and University of Pittsburgh Institutional Review Board-approved STUDY220100142. Skin-derived fibroblasts were de-identified, cultured, and banked at Hospital for Sick Children, Toronto and shipped as frozen cultures to the University of Pittsburgh. In addition, healthy human fibroblasts (PCS-201-01-80825173 and PCS-201-01-70004547, PCS-201-01-70005498, referred to as C1, C2 and C3, respectively) were purchased from American Type Culture Collection (ATCC, Manassas, VA, USA).

Fibroblasts were cultured in Dulbecco's Modified Eagle Medium (DMEM) (cat. 10013CM, Corning, VA, USA), supplemented with 15% heat-inactivated fetal bovine serum (FBS) (cat. 10082-147, Gibco, MA, USA), 1% L-glutamine (cat. 15140-122, Gibco, MA, USA), 1% penicillin/streptomycin (cat. 15140-122, Gibco, MA, USA). The culture flasks were incubated at 37°C in a 5% CO_2 atmosphere.

2.2.2 Plasmid for the CRISPR activation system

I used the 3XFLAG-VP64-*Sa*dCas9-NLS-VP64-containing plasmid (Addgene cat # 135338) in which each sgRNA was annealed and inserted by BsaI directional cloning as described previously. The nucleotide sequences and directionality of the inserts were verified by Sanger sequencing.

2.2.3 Transfection of 293T and HeLa cells

Human embryonic Kidney (HEK) 293T and HeLa cell lines were transfected with Lipofectamine™ 3000 (Thermo Fisher, CA, USA) according to the manufacturer's protocol. Cells were seeded at 5 x10^5/well density in a 12-well plate. The concentration of plasmid DNA was 500 ng per transfection. The media was changed 24 hours post-transfection and 72 hours post-transfection, and the cells were harvested for protein analyses.

2.2.4 Transfection of fibroblasts

Electroporation was performed using the Neon™ Transfection system (MPK5000, Thermo Fisher, CA, USA) and Neon™ 100 μl kit (MPK10096, Thermo Fisher, CA, USA). Cells were suspended in Neon Resuspension Buffer R before transfection. Each electroporation included a mixture of 2 x 10^6 cells and 15μg of DNA prepared in a sterile microcentrifuge tube. The vector-alone control cells were electroporated with 15μg of *Sa*dCas9-2XVP64 plasmid. Cells in the treatment group were electroporated with 5μg of *Sa*dCas9-2XVP64-sgRNA10, 5μg of *Sa*dCas9-2XVP64-sgRNA11, and 5μg of *Sa*dCas9-2XVP64-sgRNA12, resulting in 15μg of total DNA. Untreated cells were electroporated without plasmid DNA. The cell-DNA mixture was aspirated without air bubbles using the 100 μl Neon tip and inserted into a Neon tube containing the Neon Electrolytic Buffer E in the Neon Pipette station. Each set of fibroblasts was pulsed under different conditions to achieve high transfection efficiency, i.e., 1400 volts, 30ms, and 1 pulse for control fibroblasts; 1300 volts, 20ms, 2 pulses for M1; 1200 volts, 15ms, and 2 pulses for M2 and 1600 volts, 20ms and 1 pulse for M3 fibroblast. All these electroporation settings were finalized by

several co-transfections of GFP plasmid and the CRISPR constructs to test for transfection efficiency as illustrated in Figure 6.

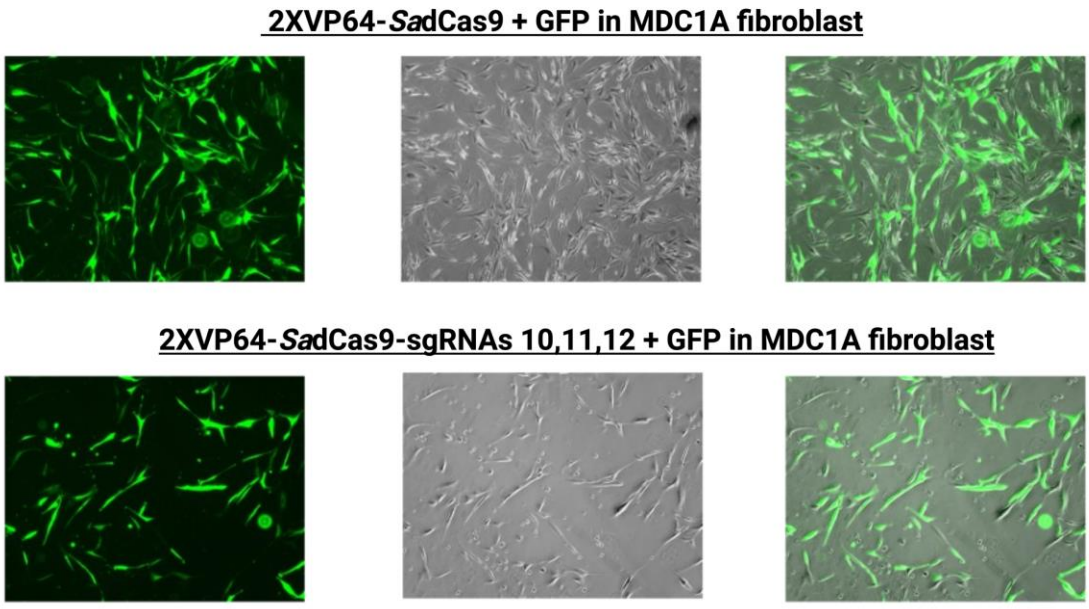

Figure 6. Transfection of CRISPR constructs

The upper panel shows MDC1A fibroblast one-day post transfection with 2XVP64-*Sa*dCas9 and GFP using electroporation. The lower panel shows MDC1A fibroblast one-day post transfection with with 2XVP64-*Sa*dCas9-sgRNAs 10,11,12 and GFP.

2.2.5 RNA isolation and qPCR analysis

A detailed explanation of this methodology and relevant primers used are provided in section 3.2.2 to 3.2.3.

2.2.6 Protein harvesting and quantification

Cells were harvested and extracted in RIPA lysis buffer (cat. 20-188, Millipore, MA, USA) containing Pierce protease inhibitor mini tablets (cat. A32953, Thermo Fisher Scientific, IL, USA) and PhosStop™ tablets (cat. 04906845001, Roche Diagnostics, Manheim, Germany). Cell extracts were centrifuged for 20 minutes at 14,000 x *g* 4°C. The supernatants were collected, and total protein concentration was estimated using Pierce Bicinchoninic Acid (BCA) protein assay kit according to the manufacturer's protocol (cat. 23225, Thermo Fisher Scientific, IL, USA).

2.2.7 Western blot

Twenty μg protein samples were loaded into lanes of a 3-8% Tris-acetate gel (cat. EA0378BOX, NuPAGE™, Invitrogen, Thermo Fisher Scientific, CA, USA) and subjected to electrophoresis. Separated proteins were transferred onto a nitrocellulose membrane using an iBlot™2 Gel transfer device (cat. IB21001, Thermo Fisher Scientific, IL, USA). Non-specific protein binding to the membranes was blocked with 5% non-fat dry milk (cat. M0841, Lab Scientific, MA, USA) for one hour at 4°C. The membranes were then washed four times with Tris-buffered saline containing 0.1 % Tween 20 (TBST; cat. J77500-K2, Thermo Fisher Scientific, NJ, USA) for 5 minutes and then incubated with primary antibodies, including anti-LAMA2 (1:300 dilution, cat. MA524656, Invitrogen), anti-LAMA1 (1:500 dilution, cat. MA531381, Invitrogen), anti-FLAG (1:1000 dilution, cat. F1804, Sigma-Aldrich), anti-Beta-tubulin (1:2000 dilution, cat. ab108342, Abcam) or anti-Vinculin (1:10,000, cat. ab129002, Abcam) on a shaker at 4°C overnight.

After four washes with TBST, the membranes were then incubated with secondary antibodies, including HRP conjugated goat anti-mouse IgG (cat. 1706516, BioRad) at 1:1000, 1:2000, and 1:4000 dilutions to detect bound anti-LAMA2, anti-LAMA1, and anti-FLAG, respectively, and HRP conjugated goat anti-rabbit IgG (cat. 1706515, BioRad) at 1:4000, and 1:5000 dilutions to detect bound anti-beta-tubulin, and anti-Vinculin, respectively. Signals were detected by chemiluminescence using SuperSignal^{TM} west Femto maximum sensitivity substrate (cat. 34095, Thermo Scientific, CA, USA). The blot was imaged using a ChemiDoc Touch Imaging System (BioRad Laboratories, Hercules, CA, USA).

2.2.8 Statistical analyses

Statistical analyses were performed using GraphPad Prism 9 (GraphPad, San Diego, CA, USA). For the comparison of two groups, student's t-test was utilized and for the comparison of multiple groups, one-way ANOVA followed by Dunnett's multiple comparison test was used. For all the analysis, statistical significance defined as $P \leq 0.05$.

2.3 Results

2.3.1 Design of the CRISPR activation system

I designed CRISPRa system comprising of single guide RNAs (sgRNAs) designed to target the proximal promoter region of *LAMA1*, two VP64 transcriptional activators, and dCas9 derived from *Staphylococcus aureus* (Figure 7A). The Transcription start site (TSS) was located using the FANTOM5 database. Nucleotide sequence of 600 bp (chr18:6,941,742-7,118,397) (RefSeq NM_005559) upstream of the start codon of the human *LAMA1* gene was retrieved from the UCSC Genome Browser build hg38. I screened for the presence of *Sa*dCas9 protospacer adjacent motifs (PAM) (NNGRRT) in this region [202]. I identified 17 PAM sequences in this region and sgRNAs of 20-21 nucleotides upstream of the PAM sequences were selected. The target sequences of sgRNA and their locations in the human *LAMA1* promoter region are shown in Table 3 and Figure 7B.

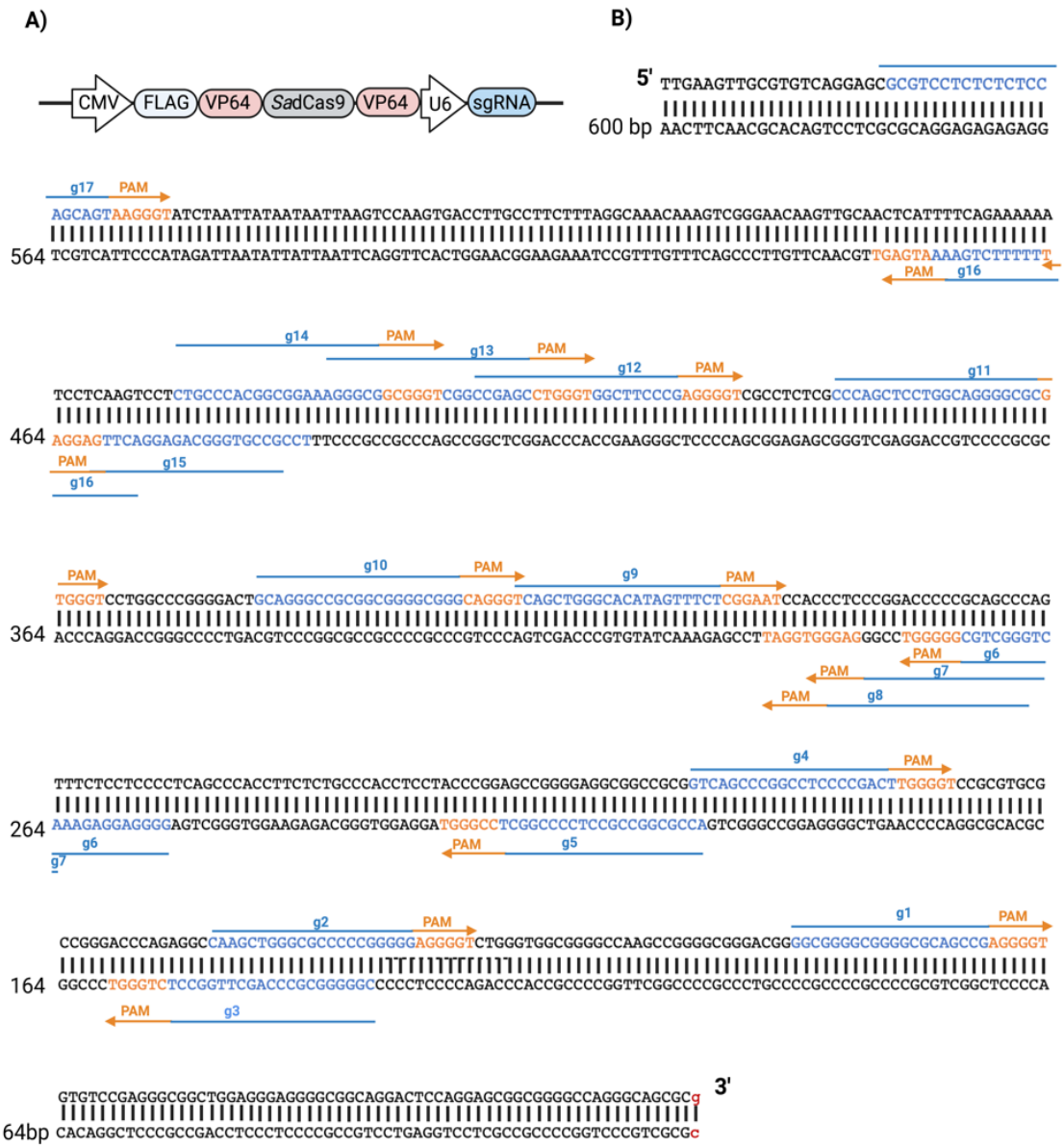

Figure 7. Design and validation of CRISPR activation system

(A) Illustration of sgRNAs in the CRISPR activation construct. The promoters are depicted with an arrowhead. (B) Sequence and location of the 17 sgRNAs (g1-g17) proximal to the human *LAMA1* promoter region. The sgRNAs (blue) is upstream of the PAM (orange) sequences. The arrowhead indicates the direction of the sgRNA. The transcription start site (TSS) is indicated in the red lowercase letter. (The figure was created with BioRender.com).

Table 3. Genetic sequences of designed sgRNAs

sgRNA	Forward sequence (5' to 3')	Reverse sequence (5' to 3')
1	GGCGGGGCGGGGCGCAGCCG	CGGCTGCGCCCCGCCCCGCC
2	CAAGCTGGGCGCCCCCGGGGG	CCCCCGGGGGCGCCCAGCTTG
3	AGGCCAAGCTGGGCGCCCCCG	CGGGGGCGCCCAGCTTGGCCT
4	GTCAGCCCGGCCTCCCCGACT	AGTCGGGGAGGCCGGGCTGAC
5	AGCCGGGGAGGCGGCCGCGGT	ACCGCGGCCGCCTCCCCGGCT
6	GCAGCCCAGTTTCTCCTCCCC	GGGGAGGAGAAACTGGGCTGC
7	CCGGACCCCCGCAGCCCAGTT	AACTGGGCTGCGGGGGTCCGG
8	CCTCCCGGACCCCCGCAGCCC	GGGCTGCGGGGGTCCGGGAGG
9	TCAGCTGGGCACATAGTTTCT	AGAAACTATGTGCCCAGCTGA
10	GCAGGGCCGCGGCGGGGCGGG	CCCGCCCCGCCGCGGCCCTGC
11	CCCAGCTCCTGGCAGGGGCGC	GCGCCCCTGCCAGGAGCTGGG
12	CCGAGCCTGGGTGGCTTCCCG	CGGGAAGCCACCCAGGCTCGG
13	AGGGCGGCGGGTCGGCCGAGC	TCCCGCCGCCCAGCCGGCTCG
14	CTGCCCACGGCGGAAAGGGCG	CGCCCTTTCCGCCGTGGGCAG
15	AAGTCCTCTGCCCACGGCGGA	TCCGCCGTGGGCAGAGGACTT
16	TTTCAGAAAAAATCCTCAAGT	ACTTGAGGATTTTTTCTGAAA
17	GCGTCCTCTCTCTCCAGCAGT	ACTGCTGGAGAGAGAGGACGC

Subsequently, I sought to identify the combinations of sgRNAs that were most effective at upregulating human *LAMA1*. Results from previous studies in which CRISPRa systems were used to activate gene expression revealed that combinations of three to four sgRNAs were typically more effective than one sgRNA alone [110, 131, 203] . Therefore, I combined 17 sgRNAs into six groups of three (i.e., 1+2+3, 4+5+6, 7+8+9, 10+11+12, 13+14+15, and 15+16+17). HEK 293T cells were transfected with 2XVP64-*Sa*dCas9 with either no or three sgRNAs with untransfected cells serving as an additional control.

At 72 hours post-transfection, LAMA1 expression was assessed by western blot (Figure 8A). Higher levels of LAMA1 were detected in response to all combinations tested compared to the groups transfected with 2XVP64-*Sa*dCas9 alone and untransfected controls. The combination of sgRNAs 10+11+12 generated the highest level of LAMA1 expression, relative to any other

combinations tested, and yielded 5.7-fold higher expression than those in the untransfected group. Transfection with the sgRNA triplets 1+2+3 and 4+5+6 resulted in moderate levels of expression at 3.3- and 3.0-fold over the controls, respectively. Transfection with the sgRNA triplets 7+8+9, 13+14+15, and 15+16+17 resulted in comparatively small increases in LAMA1 expression at 1.9-, 2.8-, and 1.5-fold change over controls, respectively (Figure 8B). High expression of LAMA1 when similar combination was used in the HeLa cell lines (Appendix A). Based on these results, I selected sgRNAs 10+11+12 as the combination that was most effective at upregulating human *LAMA1* gene expression in the relevant target cells.

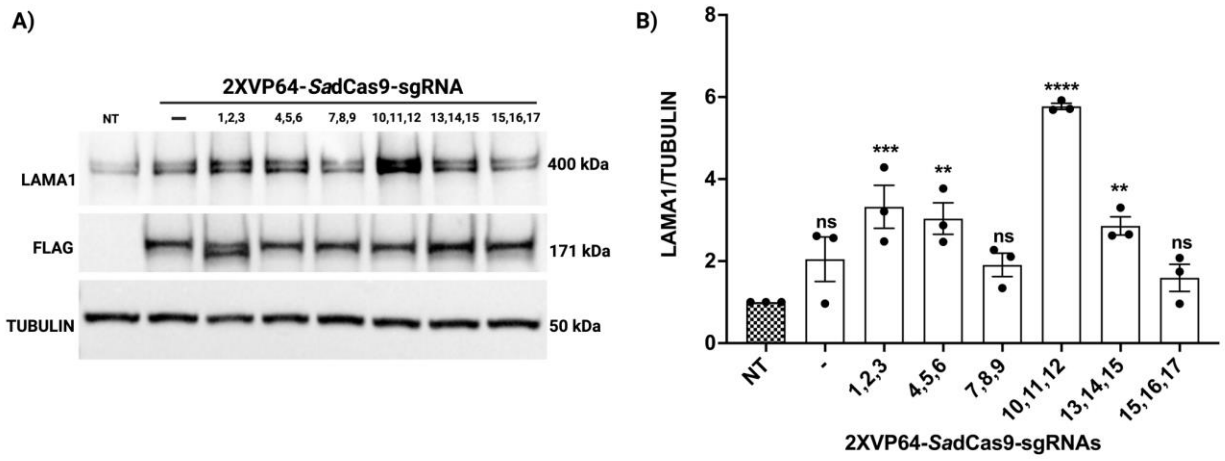

Figure 8. sgRNAs 10,11,12 shows high expression of LAMA1

Western blot analysis of the combination of optimal sgRNAs for LAMA1 expression. NT, non-transfected. '-' 2XVP64-*Sa*dCas9 with no guides. β-TUBULIN is used as the loading control, and quantification was done as a fold change in expression relative to the β-TUBULIN. Data are represented as mean ± s.e from n=3 samples. *$P \leq 0.05$, **$P \leq 0.01$, ***$P \leq 0.001$; one-way ANOVA.

2.3.2 MDC1A study population and LAMA2 expression

Our study's primary fibroblasts were obtained from three independent donors (M1, M2, M3) and three healthy controls (C1, C2, C3). Each of the MDC1A fibroblasts carried a different *LAMA2* gene mutation, as shown in Table 4. The M1 fibroblasts was received from a study that was published by the research group Gonorazky et al. 2019. According to the study, the patient has a mutation in the splice acceptor site of exon 65 that results in abnormal splicing leading to 64^{th} intron retention [56]. The mutation occurs around 3071 amino acid residues for the *LAMA2* gene. Consequently, the affected protein structure falls beyond the globular domains and are identified as "compositional bias; mainly consisting of polar residues" in the UniProt database. At this point, it is unclear about the consequence of this mutation at the structural level. The mutation for the M2 fibroblasts results in a frameshift and a premature stop codon (p.R683fs), corresponding to the Laminin IV type A1 domain in the LAMA2 protein structure. The M3 fibroblasts have a compound heterozygous mutation, and the c.4714_4715delGT affects the 17th Laminin EGF-like domain of the protein structure. Albeit the second mutation's exact consequence is unknown, it could have a role in mRNA stability. Subsequently, the western blot analysis and qPCR analysis also revealed the varied protein expression levels in LAMA2 in MDC1A fibroblasts (Figure 9).

Table 4. Mutations in the MDC1A individuals

MDC1A	cDNA change	Protein change	Region	Consequence
M1	c.9212-1G->A	Intron retention	Intron 64	Mutation occurs at the splice acceptor site, resulting in abnormal splicing
M2	c.2049_2050delAG	p.Arg683Serfs*21	Exon 14	Causes a frameshift and a premature stop codon in exon 15
M3	1st allele: c.4714_4715delGT 2nd allele: 3 bp deletion in 3'UTR	p.Val1572Phefs*5	Exon 32 3' UTR	Causes a frameshift with a premature stop codon in exon 33 Possible mRNA instability

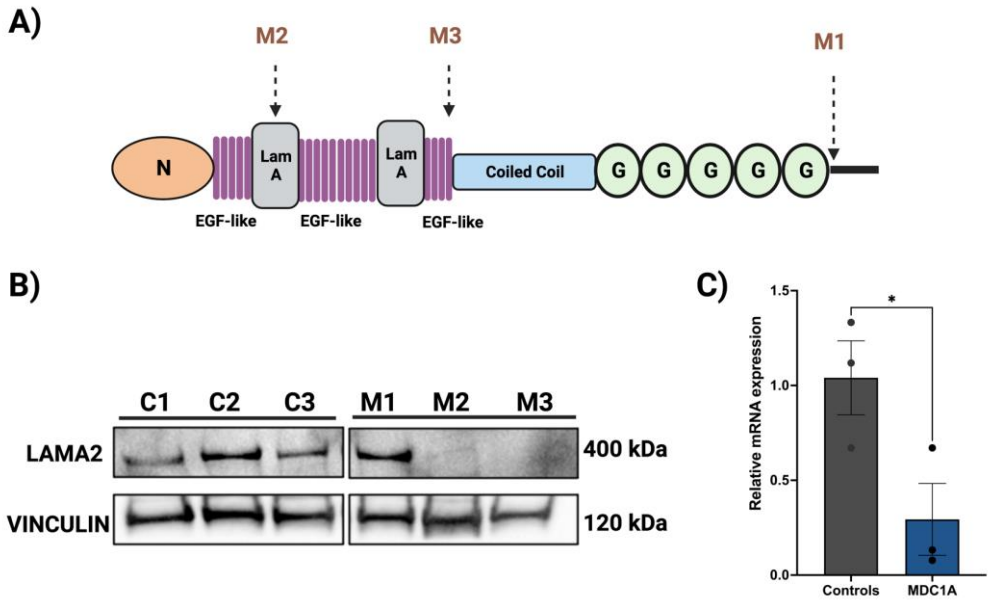

Figure 9. LAMA2 mutations and expressions in MDC1A fibroblasts

(A) Mutations of MDC1A fibroblasts affecting LAMA2 structural domains (B) Western blot analysis of LAMA2 expression in control and MDC1A fibroblasts. Vinculin was included as the loading control. (C) qPCR analysis of LAMA2 in control and MDC1A fibroblasts. Data are presented as fold-change relative to *GAPDH*. The fold change is assessed using the $2^{-\Delta\Delta ct}$ method. The results are expressed as mean $\pm$ s.e. from n = 3 technical replicates; Student's t-test.

2.3.3 CRISPRa drives the endogenous expression of LAMA1

Correction of the mutation for each of these fibroblasts in the LAMA2 gene would be challenging and time-consuming. Therefore, I implemented a CRISPR activation system comprising dCas9, VP64 transcriptional activators, and the sgRNAs 10,11,12 to increase the endogenous expression of LAMA1 in these fibroblasts. As a result, the CRISPRa upregulated LAMA1 in two of the three fibroblasts efficiently and minimal upregulation in M3, as shown in Figure 10.

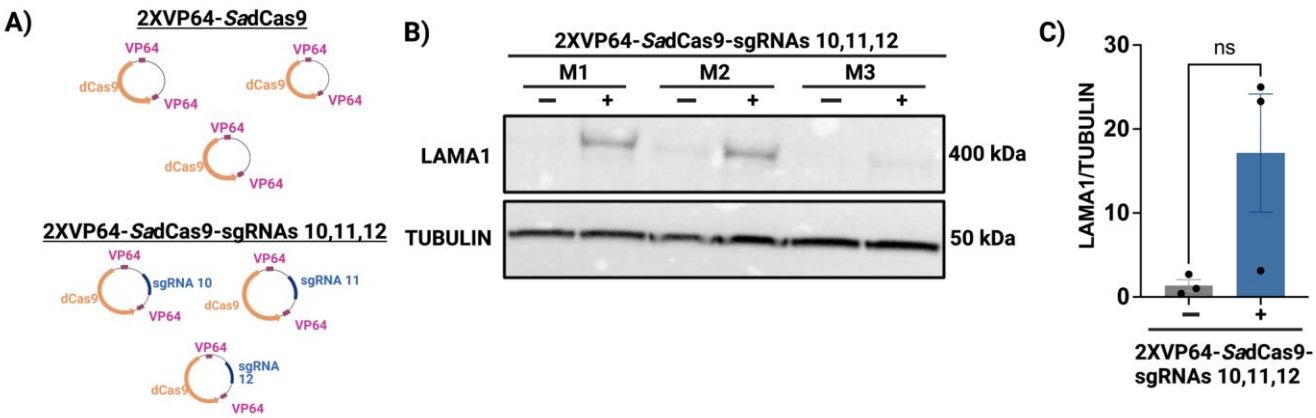

Figure 10. LAMA1 expression in MDC1A fibroblasts

A). The CRISPR construct categorized with and without sgRNAs. B) Western blot analysis of LAMA1 in MDC1A fibroblasts. C). β-TUBULIN is used as the loading control, and quantification was done as a fold change in expression relative to the β-TUBULIN. Data are represented as mean ± s.e from n=3 samples. (The figure 10A was created with BioRender.com).

2.4 Discussion

MDC1A can result from any one of several heterogenous mutations in the *LAMA2* gene [25, 100]. Such heterogeneity is somewhat reflected in MDC1A fibroblasts presented in this study, whereby M1 cells carrying abnormal splicing in the final exon of *LAMA2* lead to detectable LAMA2 protein. In contrast, M2 and M3 cells have minimum to no expression of *LAMA2*. Although not examined in this study, the position of this mutation at the 65th exon in M1 might lead to an mRNA transcript less susceptible to nonsense-mediated mRNA decay than compared to M2 and M3 cells, leading to the expression of LAMA2 protein in M1 cells. The exact functional impairments of the protein are unknown. This bolsters the claim to develop a functional assay to understand the impact of these mutations in cells. Based on the presence of LAMA2 expression, the individual should likely exhibit a milder clinical presentation. However, the clinical phenotype of M1 is required to validate this claim further to relate the genotype-phenotype correlation in M1.

Furthermore, I investigated in research databases such as Leiden Open Variation Database (LOVD) for patient data with similar mutations to understand the effect of M1 mutation. Interestingly, in LOVD, another study reported a patient with a similar M1 mutation resulting in abnormal splicing in *LAMA2* [59]. Similarly, M2 mutation has been reported in several muscular dystrophy studies [9, 204]. Collectively, the data acknowledges the heterogeneity in LAMA2 expression in MDC1A fibroblasts.

To upregulate LAMA1 in these MDC1A fibroblasts, I designed a CRISPR activation system with Cas9 protein derived from *Staphylococcus aureus,* VP64 transactivation domain with different sgRNAs binding to the proximal promoter of *LAMA1*. The delivery of CRISPR components via electroporation was successful in the MDC1A cells. Albeit the same electroporation conditions would not work for all the cells, and the conditions need to be optimized

with a specific Cas9-sgRNA to Cells ratio for each cell line. Furthermore, the CRISPR activation system can also be modified in the future by switching the VP64 transactivation domain to a more powerful transcriptional activator such as VPR[135]. Future applications to the clinic would require dual AAVs to package the necessary CRISPRa components. Therefore, technological improvement would involve miniaturizing the CRISPRa components that can reduce the number of AAVs, or utilization of alternative delivery modality with no size constraints.

The study acknowledges that treatment of disease at the genomic level must contend with significant inter-individual natural genetic variation. The presence of single nucleotide polymorphism (SNP) in a population underrepresented in the human reference genomes could lead to disruption of the targeted sequence or cause unintended genome modifications/off-targets [205, 206]. Recently, Cancellieri et al. developed a computational method to predict the impact of SNP and off-target sequences across diverse human populations; aptly termed CRISPRme [207]. However, it is currently limited to the prediction of *S. pyogenes*-derived Cas9 targets, whereas the recognition sequence of *S. aureus*-derived Cas9 was not yet included at the time of preparation of this manuscript. In the future, variant-aware target assessments are expected to become integral to therapeutic genome editing evaluation, including CRISPRa-modulation of gene expression presented here.

Collectively, the results of our study highlight the efficacy of CRISPRa as a means to upregulate a critical disease-modifying gene, e.g., *LAMA1*, in MDC1A cells regardless of the specific nature of the *LAMA2* mutation. To the best of our knowledge, this is the first time this approach has been used to target human *LAMA1* in fibroblasts derived from individuals diagnosed with MDC1A.

3.0 Transcriptomic analysis reveals dysregulation of wound-healing mechanism in MDC1A fibroblasts

3.1 Introduction

MDC1A is caused by the mutations in *LAMA2*, which encode for α2 chain subunit of the Laminin-211 protein complex [36, 37]. The laminin-211 is expressed in the basement membrane surrounding the muscle fibers. It attaches to the muscle cell via cell surface receptors - Integrin α7β1 and dystroglycan. The absence of the laminin α2 chain leads to disruption of the laminin complex and dysregulation of Integrin α7β1 and dystroglycan-mediated signaling pathway and other cellular mechanisms [208]. The disrupted pathways and cell-signaling mechanisms vary based on the cell type. Such tissue-specific gene expression profiles can be captured by RNA-sequencing technology [56, 209, 210]. To our knowledge, gene expression profiling studies have been done in MDC1A mouse model and myoblasts from MDC1A individuals but never in MDC1A fibroblasts [211, 212]. Therefore, **I aim to identify the novel biological pathways between the MDC1A and the control fibroblasts. In addition, I aim to evaluate the effect of the CRISPR activation system on MDC1A-treated cells.** This work would enable us to understand the impact of *LAMA2* loss on a global scale and to develop functional assays for in-vitro analysis in fibroblast models. Further, it will provide information on the effects of *LAMA1* upregulation in the dysregulated pathways.

3.2 Methods

3.2.1 Cell culture growth conditions

Healthy human fibroblasts (PCS-201-01-80825173 and PCS-201-01-70004547, referred to as C1 and C2, respectively) were purchased from American Type Culture Collection (ATCC, Manassas, VA, USA). MDC1A fibroblasts were obtained, as mentioned in the previous section 2.2.1. Fibroblasts were cultured in Dulbecco's Modified Eagle Medium (DMEM) (cat. 10013CM, Corning, VA, USA), supplemented with 15% heat-inactivated fetal bovine serum (FBS) (cat. 10082-147, Gibco, MA, USA), 1% L-glutamine (cat. 15140-122, Gibco, MA, USA), 1% penicillin/streptomycin (cat. 15140-122, Gibco, MA, USA). The culture flasks were incubated at 37°C in a 5% CO_2 atmosphere.

3.2.2 Electroporation of fibroblasts and RNA isolation

Each patient cell M1, M2, and M3 was transfected with *Sa*dCas9-2XVP64 plasmid for the vector group, and *Sa*dCas9-2XVP64-sgRNA10, *Sa*dCas9-2XVP64-sgRNA11, and *Sa*dCas9-2XVP64-sgRNA12 for the treatment group. The fibroblasts were electroporated based on the protocol mentioned above in section 2.2.4. RNA was extracted 96 hours post-electroporation. Total RNA was isolated from the cultured cells using the Nucleospin RNA Plus kit (740984, Machery Nagel, CA, USA) per the manufacturer's instructions. The RNA concentration and purity were checked by a Qubit fluorometer (Invitrogen, CA, USA). RNA Integrity number (RIN) samples above nine were selected for downstream processing.

3.2.3 RT-qPCR

The cDNA synthesis was performed using 500µg of RNA from each sample using iScript reverse transcription supermix (1708840, Bio-Rad) per the manufacturer's protocol. qPCR was done using Power Track SYBR Green Master Mix (A46109, applied biosystems) on Quant Studio 5 Real-Time PCR system. *GAPDH* was used as an internal control, and the $2^{-\Delta\Delta Ct}$ method [213] was used to calculate the fold change in expression between the treatment groups. All the primers used for qPCR were synthesized by Integrated DNA technologies and are listed in Table 5.

Table 5. Primers used for qPCR

Gene	Forward primer	Reverse Primer
GAPDH	GTCTCCTCTGACTTCAACAGCG	ACCACCCTGTTGCTGTAGCCAA
LAMA2	TGCTGTCCTGAATCTTGCTTC	AGCATTTGTAATCGGGTGTCTC
LAMA1	GTCAGCGACTCAGAGTGTTTG	CTTGGGTGAAAGATCGTCAGC
TGFB2	CAGCACACTCGATATGGACCA	CCTCGGGCTCAGGATAGTCT
FGFR2	AGCACCATACTGGACCAACAC	GGCAGCGAAACTTGACAGTG
ACTA2	GTGTTGCCCCTGAAGAGCAT	GCTGGGACATTGAAAGTCTCA
MMP10	GACAGAAGATGCATCAGGCAC	GGCGAGCTCTGTGAATGAGT

3.2.4 RNA sequencing and bioinformatics analysis

RNA sequencing was performed by the Health Sciences Sequencing core at UPMC Children's Hospital of Pittsburgh using Illumina NextSeq2000 system producing 202-bp paired ends. The resulting raw FASTQ reads from RNA sequencing were imported to the CLC Genomics Workbench version 22.0.2 software (Qiagen, USA). The quality check was performed using the

"*QC for sequencing reads*" function to generate a quality control report. The "*RNA-Seq analysis*" function was used to map the reads. All the reads were aligned to the GRCh38 human genome. Principle component analysis was performed by the function "*PCA for RNA-Seq*" to generate a PCA plot. The differential gene expressions between the groups were performed using the "*Differential expression for RNA-Seq*" function. Finally, Heatmaps were created using the function *"Create Heat map for RNA-Seq"* [214].

3.2.5 Ingenuity Pathway analysis

The list of differentially expressed genes, including the gene identifiers, expression values (log_2fold changes), and FDR p-values from the CLC Genomics workbench, were uploaded in the IPA software (Ingenuity Systems, QIAGEN). The "*Core analysis*" function in the software was used to identify the canonical pathway, upstream analysis, disease functions, and gene networks. The canonical pathways enriched by the differentially expressed genes were plotted according to p-values. The Z-score was used to predict the activation/inhibition state of the pathway/function/regulator [215, 216].

3.2.6 Statistical analyses

Statistical analyses were performed using GraphPad Prism 9 (GraphPad, San Diego, CA, USA). For the comparison of two groups, t-test was utilized and for the comparison of multiple groups, one-way ANOVA followed by Dunnett's multiple comparison test was used. For all the analysis, statistical significance defined as $P \leq 0.05$.

3.3 Results

3.3.1 Heterogeneity in *LAMA2* expression in MDC1A cells

The transcriptome data were analyzed to see the differences in the expression of genes between the MDC1A patient cells and controls. I investigated the expression of *LAMA2* to understand the expression of the causative gene for MDC1A and to confirm whether the transcriptome data correlates with the protein expression observed in Chapter 2. The control cells C1 and C2 were used as a baseline for observing the expression of *LAMA2* in MDC1A cells (M1, M2, M3). First, I compared individual MDC1A fibroblast to the control group. The cell line M1 showed no significant downregulated expression of *LAMA2* (log2fold change of -0.05; q-value =1.0). This is in conjunction with the protein expression data, in which I observed the M1 to show *LAMA2* expression. The M2 and M3 cells had a significantly downregulated *LAMA2* expression with log_2fold change of -5.06 (q-value = 6.32 $x10^{-35}$) and -5.14 (q-value = 5.44 $x10^{-34}$) (Figure 11A-C). Secondly, all the MDC1A cells (M1 + M2 + M3) were combined and compared them with the control group. The *LAMA2* expression was not significantly downregulated (log_2fold change -2.01; F.D.R p-value = 0.25) (Figure 11D). As this combination would not help to understand the key molecular differences between the patient and control group, M1 was excluded from further analysis. The expression of *LAMA2* in the patient group consisting of M2 and M3 against the control group was observed and *LAMA2* was significantly downregulated with a log_2fold-change of -5.1 (F.D.R p-value= $4.69x10^{-49}$). I proceeded with this analysis between the patient group (M2 + M3) against the control group (C1 +C2) for investigating downstream analysis (Figure 11E-F).

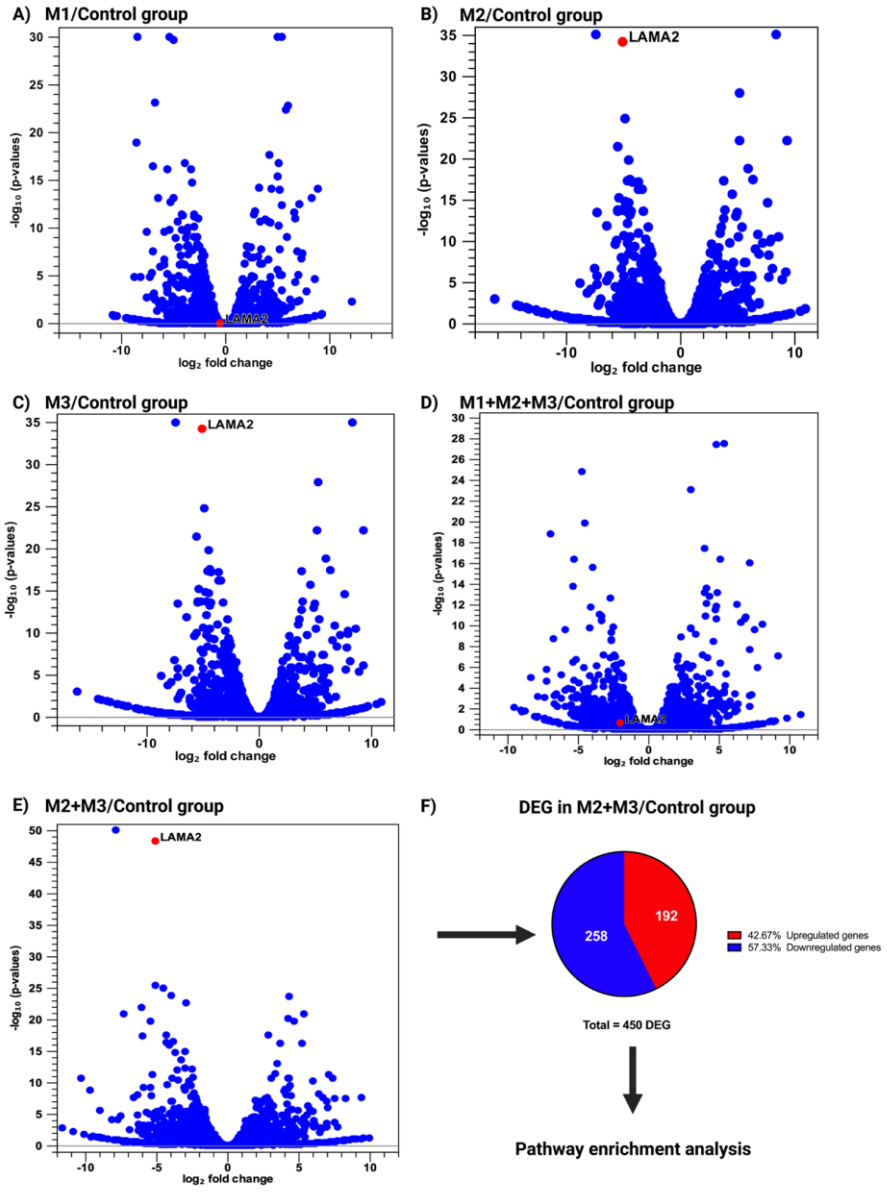

Figure 11. Molecular profiles of MDC1A and control cells

(A-E) Volcano plots provide visual documentation of genes that are differentially expressed genes in MDC1A and control cells. The x-axis represents the $\log_2$ fold change and the y-axis represents the false discovery rate (FDR) *p*-value for each differentially expressed gene (blue dots); *LAMA2* is indicated by a red dot. (F) Pie chart depicting the amount of differentially expressed genes. The upregualted genes are indicated by red and downregualted genes are indicated by blue.

3.3.2 Biological pathways different between MDC1A and control group

To capture the transcriptomic differences between MDC1A and the control fibroblasts, I utilized M2 + M3 cells against the control group. Differentially expressed genes were filtered based on the criteria two criteria: absolute log_2fold change > 2 and False discovery rate (FDR) p-value (q-value) ≤ 0.05. Interestingly, the majority of them have downregulated genes. Out of 450 differentially expressed genes (DEG), 258 (57.33 %) are down-regulated genes and 192 (42%) are upregulated genes. Few of the differentially expressed genes are highlighted in Figure 12 and Table 6 and the complete list of DEG is available in Appendix A.

Table 6. Top 10 DEGs between MDC1A and healthy control

Gene	Chromosome	Max group mean	Log_2 fold change	Fold change	FDR p-value	ENSEMBL
HOXC10	12	25.25	-7.87	-233.19	2.38E-61	ENSG00000180818
LAMA2	6	17.64	-5.1	-34.24	4.69E-49	ENSG00000196569
IGF2	11	49.58	-5.09	-34.07	3.67E-26	ENSG00000167244
GRIA1	5	12.65	-4.5	-22.58	1.11E-25	ENSG00000155511
ADH1B	4	16.54	-3.99	-15.84	1.52E-24	ENSG00000196616
ERAP2	5	5.31	4.35	20.43	2.08E-24	ENSG00000164308
COL15A1	9	39.81	-2.92	-7.58	2.61E-23	ENSG00000204291
PITX1	5	7.41	-6.04	-65.68	1.19E-22	ENSG00000069011
SDK1	7	1.33	-7.33	-160.55	1.18E-21	ENSG00000146555
NRN1	6	68.58	5.35	40.84	1.39E-21	ENSG00000124785

The top five dysregulated pathways are cAMP response element-binding protein (CREB) signaling in neurons, hepatic fibrosis/hepatic stellate cell activation, axonal guidance signaling, cardiac hypertrophy signaling, and pulmonary fibrosis idiopathic signaling as shown in Figure 13.

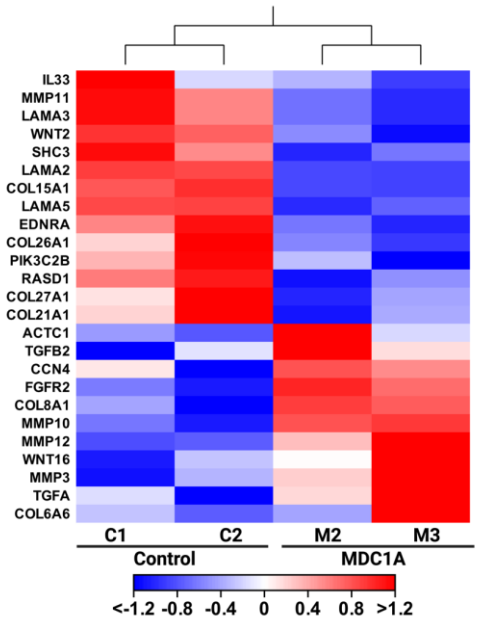

Figure 12. Heatmap of the DEGs involved in wound healing and fibrosis pathways

Downregulated genes are indicated in blue, and upregulated genes are indicated in red. The tree denotes the hierarchical clustering between the different groups. C1-C2, control cells; M2-M3, MDC1A cells.

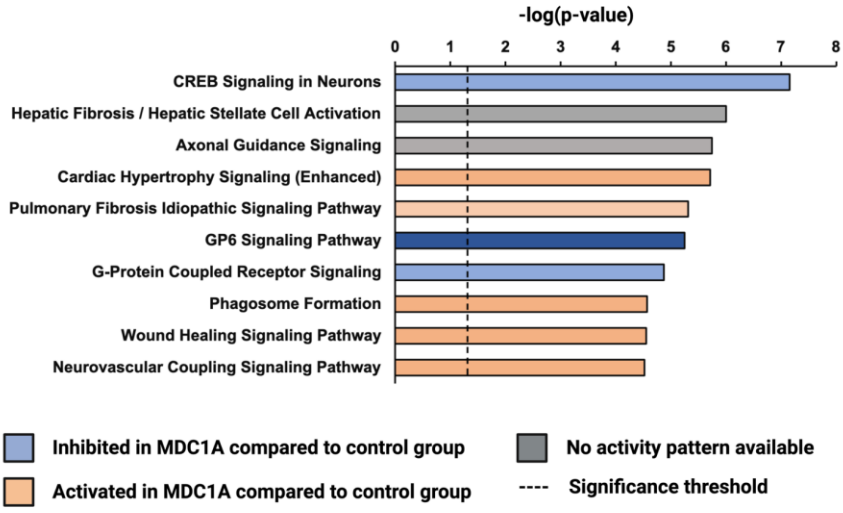

Figure 13. Canonical pathways identified by IPA

The x-axis represents the individual pathways, and the y-axis represents the IPA z-score. A negative z-score indicates the pathway is inhibited, while a positive z-score means that the pathway is activated in MDC1A cells. Gray-colored

bars indicate that no activity pattern is available. The specific pathways highlighted were based on our analysis of 450 differentially expressed genes (DEGs) identified in a comparison of MDC1A and control fibroblasts.

3.3.3 *LAMA2* is associated with Glycoprotein 6 and wound healing pathways

I investigated the pathways directly associated with *LAMA2* and observed that *LAMA2* was associated with two canonical pathways - wound healing and the GP6 signaling pathway. The wound healing signaling pathway had a positive z-score of 0.5 and -log(p-value) = 4.55, indicating an overall predicted activation state of the pathway, while the GP6 signaling pathway had a negative z-score of -1.732 and -log(p-value) = 5.25 showing an overall predicted inhibition state. (Figure 13). For this study, the focus was restricted to the wound healing pathway to understand the direct impact of the loss of *LAMA2*. The list of genes involved in this pathway is tabulated in Table 7. Few of these genes were analyzed to validate the transcriptomic data as shown in Figure 14. *LAMA2* was significantly downregulated in the M2 and M3 samples compared to the control group. Likewise, *FGFR2*, *TGFB2*, and *MMP10* show an increase in mRNA expression compared to the control group similar to the transcriptomic data.

Table 7. Genes involved in wound healing pathway between MDC1A and healthy control

Symbol	Entrez Gene Name	Gene Symbol	Log Ratio	False Discovery Rate (q-value)	Location
COL15A1	collagen type XV alpha 1 chain	ENSG00000204291	-2.92	2.61E-23	Extracellular Space
COL21A1	collagen type XXI alpha 1 chain	ENSG00000124749	-3.31	0.0000206	Extracellular Space
COL26A1	collagen type XXVI alpha 1 chain	ENSG00000160963	-5.7	0.02	Extracellular Space
COL27A1	collagen type XXVII alpha 1 chain	ENSG00000196739	-2.01	0.000374	Extracellular Space
COL6A6	collagen type VI alpha 6 chain	ENSG00000206384	3.63	0.00324	Extracellular Space
COL8A1	collagen type VIII alpha 1 chain	ENSG00000144810	2.88	0.000000804	Extracellular Space
FGFR2	fibroblast growth factor receptor 2	ENSG00000066468	6.02	5.74E-11	Plasma Membrane
IL33	interleukin 33	ENSG00000137033	-6.21	0.00131	Extracellular Space

LAMA2	laminin subunit alpha 2	ENSG00000196569	-5.1	4.69E-49	Extracellular Space
LAMA3	laminin subunit alpha 3	ENSG00000053747	-3.66	1.92E-15	Extracellular Space
LAMA5	laminin subunit alpha 5	ENSG00000130702	-2.42	1.56E-11	Extracellular Space
MMP10	matrix metallopeptidase 10	ENSG00000166670	4.67	0.00115	Extracellular Space
RASD1	ras related dexamethasone induced 1	ENSG00000108551	-3.48	0.000848	Cytoplasm
SHC3	SHC adaptor protein 3	ENSG00000148082	-3.9	2.04E-11	Cytoplasm
TGFA	transforming growth factor alpha	ENSG00000163235	4.65	0.00711	Extracellular Space
TGFB2	transforming growth factor beta 2	ENSG00000092969	2.6	0.00415	Extracellular Space

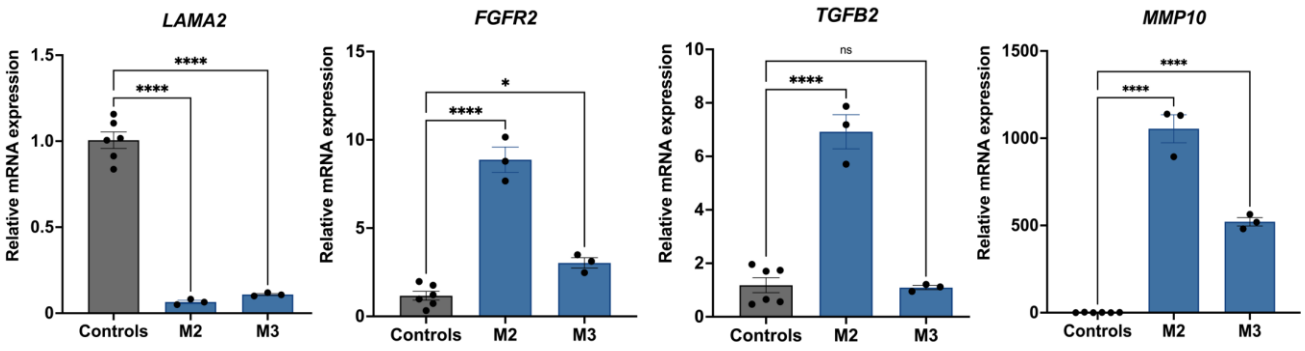

Figure 14. Validation of genes involved in the wound-healing pathway

qPCR analysis in control and MDC1A fibroblasts. Data are presented as fold-change relative to *GAPDH*. The fold change is assessed using the $2^{-\Delta\Delta ct}$ method. The dots represent individual cq measurements, and the data are plotted as mean ± s.e. M2-M3, MDC1A cells. *$P \leq 0.05$, **** $P \leq 0.0001$, ns = not significant; One-way ANOVA.

3.3.4 Gene expression profile shows upregulation of *LAMA1* by CRISPRa system

I analyzed the global transcriptome to understand the changes in gene expression after transfection with the CRISPR activation system. The MDC1A cell group (M2 + M3) treated with 2XVP64-*Sa*dCas9-sgRNAs10,11,12 was compared against the MDC1A untreated group. The results showed an endogenous increase in the expression of *LAMA1* with a log2fold change of 2.06 (P = 2.66 x10^6). Interestingly, gene expression analysis of MDC1A cells (M2 + M3) transfected

with 2XVP64-*Sa*dCas9 against the MDC1A untreated group, *LAMA1* was not significantly upregulated (Figure 15A-B). Collectively, this data suggests that the sgRNAs designed were very specific in binding to the proximal promoter region of *LAMA1* and increasing the expression of *LAMA1*.

To investigate the effect of LAMA1 on the pathways, I did differential gene expression analysis and filtered based on the two criteria: absolute $\log_2$fold change > 1 and false discovery rate (FDR) p-value (q-value) $\leq$ 0.05. As a result, 510 DEG consisting of 225 (56%) downregulated and 286 (44%) upregulated genes. These genes were mapped by the Ingenuity Pathways Knowledge Base and were used for pathway enrichment analysis (Figure 15C). The top 10 differentially expressed genes are shown in Table 8 and highlighted in Figure 16. The entire list of genes is in Appendix B.

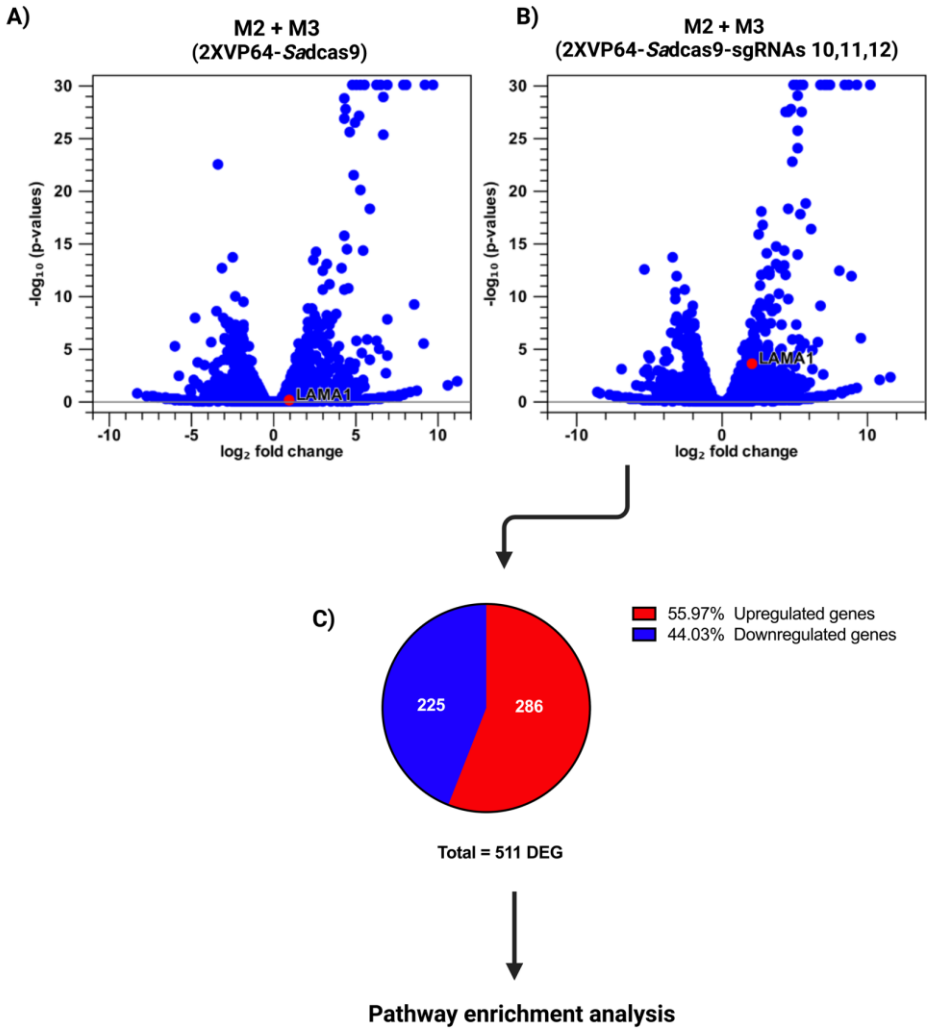

Figure 15. Molecular profiles of MDC1A cells after transfection

(A-B) Volcano plots provide visual documentation of differentially expressed genes in MDC1A transfected genes with 2XVP64-*Sa*dCas9 and 2XVP64-*Sa*dCas9-sgRNAs10,11,12 against the untreated group. The x-axis represents the $\log_2$ fold change, and the y-axis represents the false discovery rate (FDR) *p*-value for each differentially expressed gene (blue dots); *LAMA1* is indicated by a red dot. (C) Pie chart depicting the amount of differentially expressed genes in the MDC1A cells transfected with 2XVP64-*Sa*dCas9-sgRNAs10,11,12s. The upregulated genes are indicated by red, and downregulated genes are indicated by blue.

Table 8. The top 10 DEGs between MDC1A treated with 2XVP64-*Sad*Cas9-sgRNAs10,11,12 and MDC1A untreated cells

Gene	Chromosome	Max group mean	Log_2 fold change	Fold change	FDR p-value	ENSEMBL
OAS1	12	25.04	8.76	433.84	1.97E-78	ENSG00000089127
IFI44L	1	28.59	7.15	142.5	3.86E-65	ENSG00000137959
IFIT2	10	183.55	6.86	115.77	2.27E-57	ENSG00000119922
CMPK2	2	20.82	8.47	354.61	1.62E-50	ENSG00000134326
MX1	21	102.08	7.5	180.44	1.92E-47	ENSG00000157601
HERC5	4	14.37	7.12	139.49	1.50E-43	ENSG00000138646
OASL	12	62.12	9.34	648.67	2.13E-43	ENSG00000135114
PMAIP1	18	89.34	5.46	43.95	7.62E-40	ENSG00000141682
IFIT3	10	261.23	5.62	49.19	7.82E-35	ENSG00000119917
BST2	19	37.18	7.29	155.99	1.89E-34	ENSG00000130303

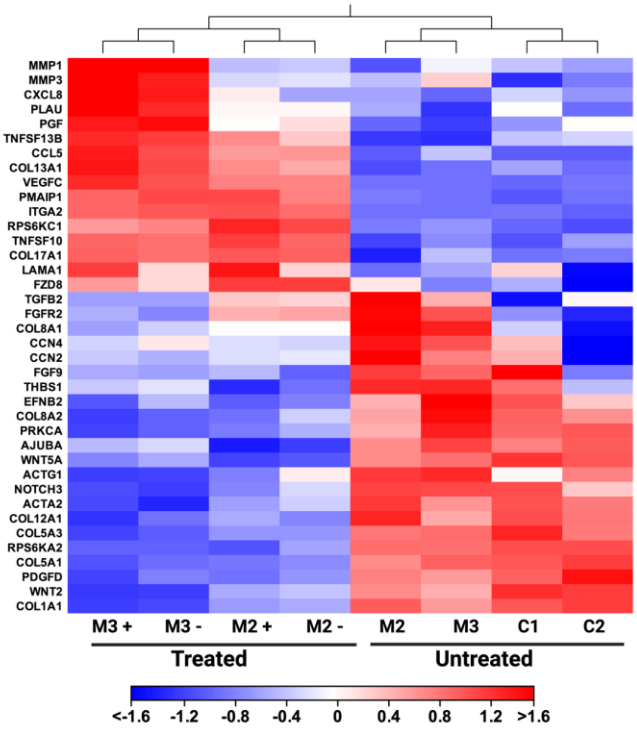

Figure 16. Heatmap of the DEGs involved in wound healing and fibrosis pathways

Downregulated genes are indicated in blue, and upregulated genes are indicated in red. The tree denotes the hierarchical clustering between the different groups. C1-C2, control cells; M2-M3, MDC1A cells.

3.3.5 *LAMA1* is associated with wound healing similar to *LAMA2*

The transcriptomic analysis revealed the inclusion of *LAMA1* in the wound-healing pathway in the MDC1A-treated cells. This suggests that *LAMA1* and *LAMA2* might share similar roles in the wound-healing mechanism. Furthermore, the reversal of the pathway prediction state further supports this argument. For instance, the wound-healing pathway existed in an activation and changed its course to an inhibition state (z score = -0.65). Collectively, this data suggests the possibility that *LAMA1* could have compensated for the lack of *LAMA2* in the MDC1A-treated cells and, thus, the difference in the reversal of the state. In addition to *LAMA1*, the other genes involved in the wound-healing pathway are shown in Table 9. The transcriptomic data was validated for a few genes as shown in Figure 17. *LAMA1* was significantly upregulated in the M2 and M3 samples compared to the control group. Similar to the transcriptomic results, *FGFR2*, *TGFB2*, and *ACTA2* show decreased mRNA expression compared to the untreated group.

Table 9. Genes involved in wound healing pathway between MDC1A treated with 2XVP64-*Sa*dCas9-sgRNAs10,11,12 and MDC1A untreated

Gene	Entrez Gene Name	Gene Symbol	Log Ratio	False Discovery Rate (q-value)	Location
ACTA2	actin alpha 2, smooth muscle	ENSG00000107796	-2.69	2.81E-08	Cytoplasm
CCL5	C-C motif chemokine ligand 5	ENSG00000271503	8.09	4.53E-13	Extracellular Space
COL12A1	collagen type XII alpha 1 chain	ENSG00000111799	-1.8	0.00582	Extracellular Space
COL13A1	collagen type XIII alpha 1 chain	ENSG00000197467	2.35	8.35E-08	Plasma Membrane
COL17A1	collagen type XVII alpha 1 chain	ENSG00000065618	4.9	0.000252	Extracellular Space
COL1A1	collagen type I alpha 1 chain	ENSG00000108821	-1.67	0.00975	Extracellular Space
COL5A1	collagen type V alpha 1 chain	ENSG00000130635	-1.69	0.00406	Extracellular Space
COL5A3	collagen type V alpha 3 chain	ENSG00000080573	-2.56	2.72E-11	Extracellular Space
COL8A1	collagen type VIII alpha 1 chain	ENSG00000144810	-2.23	0.0000335	Extracellular Space

COL8A2	collagen type VIII alpha 2 chain	ENSG00000171812	-1.63	0.000699	Extracellular Space
CXCL8	C-X-C motif chemokine ligand 8	ENSG00000169429	5.47	0.0000111	Extracellular Space
FGFR2	fibroblast growth factor receptor 2	ENSG00000066468	-3	0.00792	Plasma Membrane
LAMA1	laminin subunit alpha 1	ENSG00000101680	2.06	0.000266	Extracellular Space
MMP1	matrix metallopeptidase 1	ENSG00000196611	4.68	0.000205	Extracellular Space
PDGFD	platelet derived growth factor D	ENSG00000170962	-2.97	0.000000295	Extracellular Space
PGF	placental growth factor	ENSG00000119630	3.18	0.00000953	Extracellular Space
PRKCA	protein kinase C alpha	ENSG00000154229	-1.95	0.000419	Cytoplasm
TGFB2	transforming growth factor beta 2	ENSG00000092969	-2.06	0.05	Extracellular Space
TNFSF10	TNF superfamily member 10	ENSG00000121858	6.82	7.75E-10	Extracellular Space
TNFSF13B	TNF superfamily member 13b	ENSG00000102524	4.5	0.000227	Extracellular Space
VEGFC	vascular endothelial growth factor C	ENSG00000150630	1.97	0.0000249	Extracellular Space

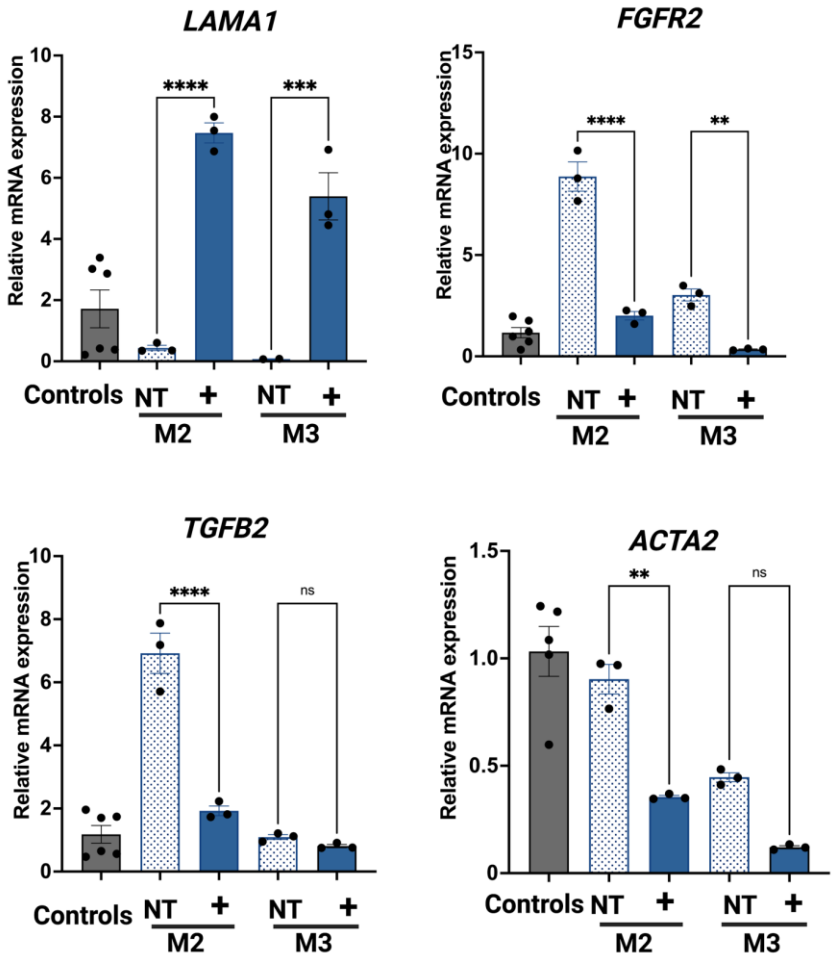

Figure 17. qPCR analysis of genes involved in the wound-healing pathway

qPCR analysis in control and MDC1A fibroblasts. Data are presented as fold-change relative to *GAPDH*. The fold change is assessed using the $2^{-\Delta\Delta ct}$ method. The dots represent individual cq measurements, and the data are plotted as mean ± s.e. NT, Non-transfected; +, Treated with 2XVP64-*Sa*dCas9-sgRNAs10,11,12; M2-M3, MDC1A cells. $^{**}P \leq 0.01$, $^{***}P \leq 0.001$, **** $P \leq 0.0001$, ns = not significant; One-way ANOVA.

3.3.6 Expression of genes associated with immune responses are changed after *LAMA1* upregulation

MDC1A cells treated with 2XVP64-*Sa*dCas9-sgRNAs 10,11,12 showed inhibition of wound-healing signaling pathway and pulmonary fibrosis idiopathic pathway. In addition, the MDC1A treated cells also showed activation of immune-related pathways such as hypercytokinemia, interferon signaling, pathogen induced cytokine storm signaling, and recognition receptors in recognition of bacteria and viruses (Figure 18).

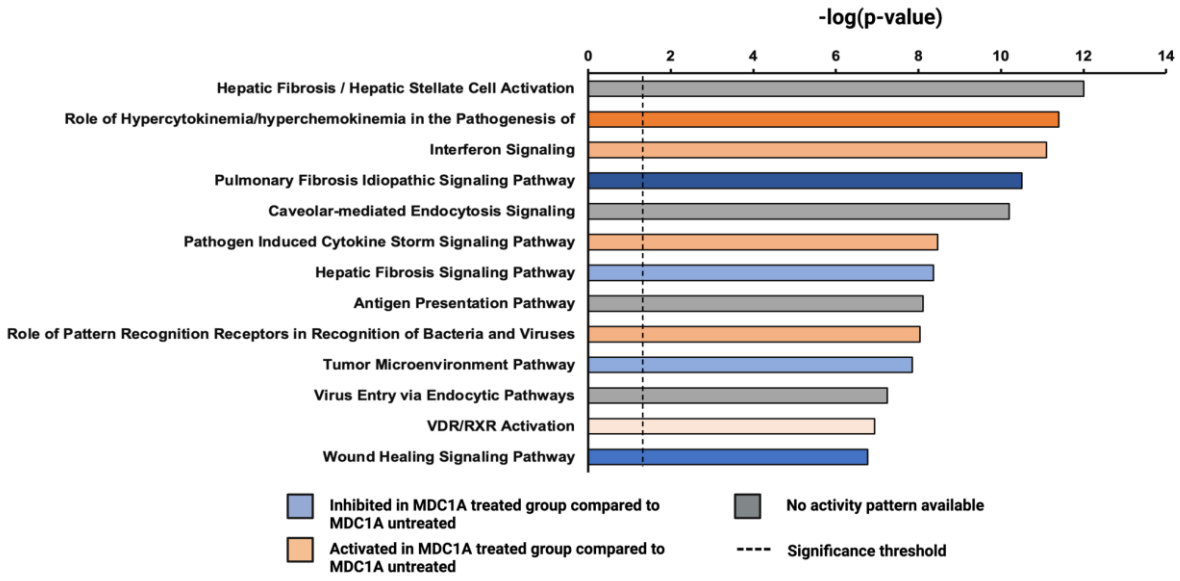

Figure 18. Canonical pathways in the MDC1A treated cells

The x-axis represents the individual pathways, and the y-axis represents the IPA z-score. A negative z-score indicates the pathway is inhibited, while a positive z-score means that the pathway is activated in MDC1A cells. Gray-colored bars indicate that no activity pattern is available. The specific pathways highlighted were based on our analysis of 510 differentially expressed genes (DEGs) identified in a comparison of MDC1A cells treated with 2XVP64-*Sa*dCas9-sgRNAs 10,11,12 and untreated MDC1A cells.

Further, gene expression and pathway analysis for the MDC1A cells treated with 2XVP64-*Sa*dCas9 also resulted in similar immune response profile (Figure 19). Interferon regulatory factors (IRF1, IRF3, IRF5, IRF7) and signal transducer and activator of transcription (STAT1, STAT2) that are known to be associated with type I interferon responses are activated in both the groups [217, 218]. Specifically, the pathways build on linking the 'the accumulation of antigen presenting cells' to the 'antiviral response' to IRF-7, which in turn connected with Interferon signaling. Likewise, a similar network association is also seen in the MDC1A cells treated with 2XVP64-*Sa*dCas9. However, all these pathways are indirectly associated (dotted edges) with each other and give a graphical summary suggesting possible immune responses elicited due to the CRISPR components that need to be validated in multicellular organisms.

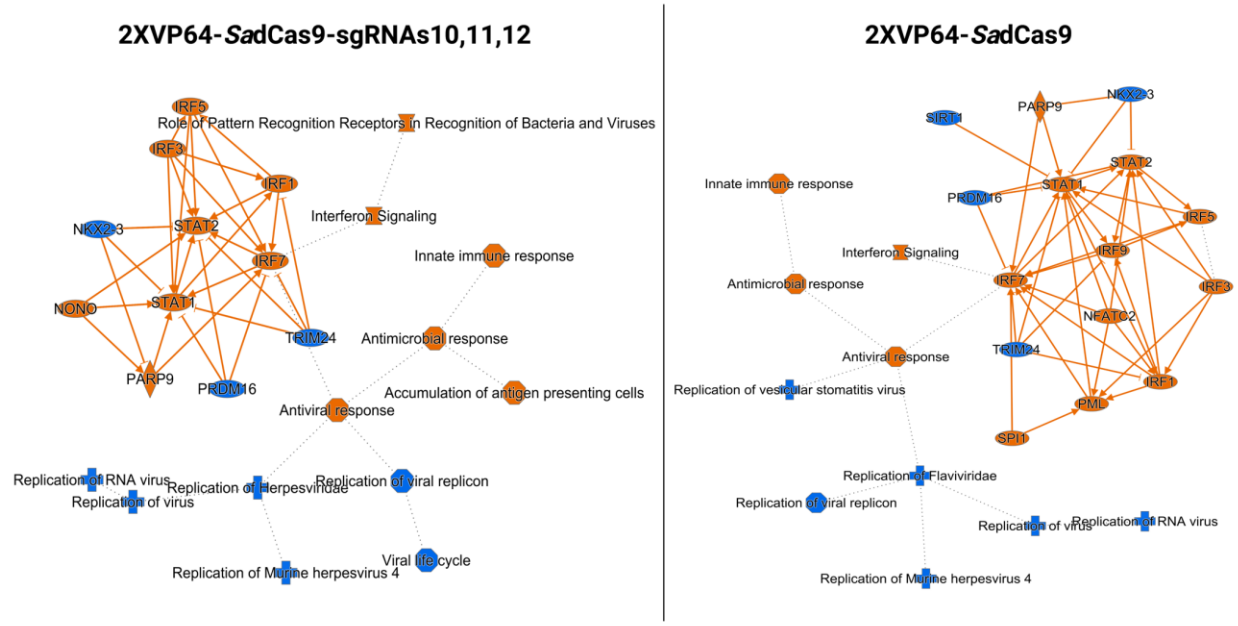

Figure 19. Immune responses in MDC1A treated cells

The graphical summary illustrates the synopsis of the immune responses in the MDC1A cells treated with 2XVP64-*Sa*dCas9-sgRNAs10,11,12 (left) and 2XVP64-*Sa*dCas9 (right). Predicted activation state is represented in orange and predicted inhibition state is represented in blue. The solid edges represent direct relationship and the dotted edges represent indirect relationship.

3.4 Discussion

These data lay the groundwork for identifying the gene expression profile and biological pathways that differ in the MDC1A fibroblasts compared to the healthy controls. Our analysis resulted in pathways reflecting the pathogenesis of MDC1A. Similarly, Yanay et al. 2019 reported differentially expressed genes involved in inflammation and fibrosis pathways in the transcriptomic analysis of the dy^{2J}/dy^{2J} mouse model [211].

Further, the results showed the association of *LAMA2* and *LAMA1* in the wound-healing signaling mechanism. This is significant because functional assays such as migration assay could be used to gauge the association of *LAMA1* and *LAMA2* in MDC1A cells. A similar approach was followed by Fontes-Oliveira et al. 2017, wherein they reported dysregulation of genes involved in oxidative phosphorylation pathways in MDC1A human myoblasts [212]. Subsequently, they utilized functional assays to gauge the MDC1A cells' response to oxidative stress. In addition to revealing the dysregulated pathways and pathways associated with *LAMA2*, the transcriptome data also revelated the upregulation of *LAMA1* in the MDC1A-treated cells only corroborating the efficiency of the CRISPR activation system.

I compared the transcriptomes of cells transfected with 2XVP64-SadCas9 with three sgRNAs to the untransfected cells, rather than (ideally) cells transfected with 2XVP64-SadCas9 with no sgRNA. This comparison was chosen because our objective was to use the CRISPRa method to increase the endogenous expression of only one gene (i.e., LAMA1). The MDC1A fibroblast genomes are overall very similar to one another; thus, our efforts to identify DEGs between these groups yielded no statistically significant results. Inclusion of several additional MDC1A fibroblasts would increase the power of the study and strengthen the transcriptome analyses.

Furthermore, the study recognizes the immune response in the MDC1A treated cells. The immune response might be elicited because Cas9 mRNA could be considered as exogenous mRNA derived from viral infection and induce a type I interferon-mediated immune response in cells and can activate immune responses [219]. Vaidyanathan et al. 2018 demonstrated chemical modifications in the Cas9 mRNA rendered it less immunogenic [220] [221, 222]. The data suggest that the immune response could be due to the components in the plasmid. However, an in vivo model with a complete immune system is essential to address the interaction between the host and the CRISPR activation system. This is beyond the scope of the current study but might be incorporated in the future directions.

4.0 LAMA1 compensates for LAMA2 and rescues aberrant cell migration in MDC1A fibroblasts

4.1 Introduction

Our findings from the transcriptomic analysis revealed the association of *LAMA1* and *LAMA2* in the wound-healing mechanism. I hypothesized that a lack of LAMA2 would lead to aberrant migration, and subsequent LAMA1 upregulation would reduce the aberrant migration in MDC1A fibroblasts. In this chapter, **I aim to analyze the migration potential of MDC1A fibroblasts and, subsequently, the effect of LAMA1 in migration in the MDC1A-treated cells.** This work is essential to answer several questions (i) Do MDC1A fibroblasts exhibit aberrant migration compared to the control group? (ii) Can LAMA1 compensate for the lack of LAMA2 on a functional level by reducing the aberrant migration, (iii) Does the level of LAMA1 upregulation achieved via CRISPRa might be sufficient for compensation? Our findings help to answer these questions to an extent and enabled us to develop a working model that explains the possible aberrant migration and rescue in MDC1A fibroblasts.

In addition to the wound-healing mechanism, I also focused on the mitochondrial bioenergetics in our study. Impairment in mitochondrial bioenergetics is commonly observed in myoblasts and to our knowledge there is no study that examines the same in a MDC1A fibroblast model. To fill this gap, I investigated the mitochondrial respiration in MDC1A fibroblasts and compared to the control group.

4.2 Methods

4.2.1 Cell culture growth conditions

Healthy human fibroblasts (PCS-201-01-80825173 and PCS-201-01-70004547, referred to as C1 and C2, respectively) were purchased from American Type Culture Collection (ATCC, Manassas, VA, USA). In addition to these two control fibroblasts from ATCC, another control fibroblast (#GM08398) purchased from Coriell Institute for Medical Research was used for seahorse analysis. MDC1A fibroblasts were obtained, as mentioned in the previous section 2.2.1. Fibroblasts were cultured in Dulbecco's Modified Eagle Medium (DMEM) (cat. 10013CM, Corning, VA, USA), supplemented with 15% heat-inactivated fetal bovine serum (FBS) (cat. 10082-147, Gibco, MA, USA), 1% L-glutamine (cat. 15140-122, Gibco, MA, USA), 1% penicillin/streptomycin (cat. 15140-122, Gibco, MA, USA). The culture flasks were incubated at 37°C in a 5% CO_2 atmosphere.

4.2.2 Transfection of fibroblasts

Each patient cell M1, M2, and M3 was transfected with *Sa*dCas9-2XVP64 plasmid for the vector group, and *Sa*dCas9-2XVP64-sgRNA10, *Sa*dCas9-2XVP64-sgRNA11, and *Sa*dCas9-2XVP64-sgRNA12 for the treatment group. The third group is the non-transfected/untreated group was also airzapped, so that all the groups have been subjected to the stress of electroporation. The detailed description of electroporation is mentioned above in the section 2.2.4. Twenty-four hours post electroporation, the antibiotic free media was changed to regular growth media as mentioned

in section 2.2.1 and the cultured dishes were incubated at 37°C in a 5% CO_2 atmosphere for three days.

4.2.3 Migration assay

On the day of the assay, fibroblasts from the electroporated dishes were washed and trypsinized and seeded on an IncuCyte Imagelock 96-well plate (cat. 4856, Essen Bioscience, MI, USA) at a density of 10,000 cells per well. The culture plates were incubated overnight at 37°C in a 5% CO_2 atmosphere. One day later (t = 0) a wound of uniform width was created in the monolayer using the IncuCyte 96-well wound maker (cat. no, 4563, Essen Bioscience, MI, USA) according to the manufacturer's protocol. The plate was monitored in real-time by IncuCyte until the end of the experiment at t = 24 hrs. The analyses were done using the IncuCyte scratch wound analysis software module (cat. 9600-0012, Essen Bioscience, MI, USA)[223]

4.2.4 Proliferation assay

Three control (C2) and MDC1A (M1) cell replicates were seeded at 100,000 cells per well in a six-well plate. The cells were made to rest for an hour in the hood to prevent edge effects and then transferred to the IncuCyte to monitor for proliferation and cell growth. Measurements were taken at 3 hours intervals for a total of 60 hours. The data were normalized based on the images taken at the 0-hour scan using the IncuCyte software module. The normalized data were used to plot the proliferation growth curve.

4.2.5 Measurement of mitochondrial respiration

Mitochondrial respiration was assessed using electron transport chain inhibitors such as oligomycin, FCCP, and rotenone using Seahorse XFe96 Extracellular Flux Analyzer (Agilent technologies, Santa Clara, CA). Firstly, the basal respiration rate is measured. Secondly, an injection of oligomycin is provided. It inhibits the ATP synthase in the electron transport chain (ETC), resulting in low ATP production. Subsequently, FCCP inhibitor is added, which results in uncoupled respiration, making the cells reach their maximum respiration capacity. Finally, rotenone is added, inhibiting the complex I of the OXPHOS system and thereby shutting down the ETC. The difference between basal respiration and maximal respiration will yield the spare respiratory capacity (Figures 20-21).

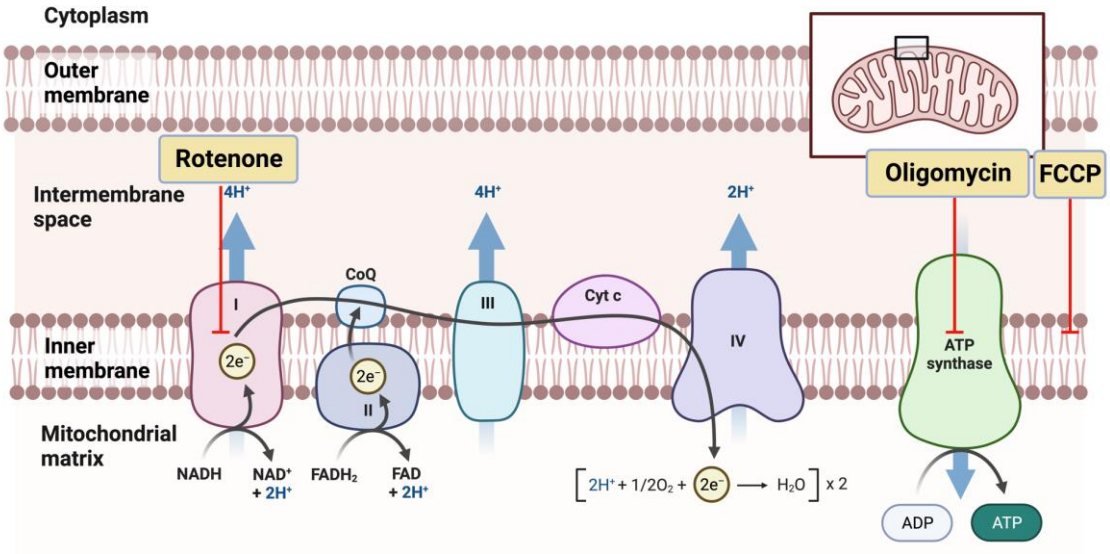

Figure 20. Principle of bioenergetics

Oxygen consumption rate (OCR) is measured in real-time with injections of oligomycin, FCCP, and rotenone to inhibit ATP synthase, uncoupled respiration, and complex I of OXPHOS system, respectively. (The figure was created with BioRender.com).

Fibroblasts were seeded at a density of 10,000/well in regular growth media on a 96-well seahorse plate coated with poly-D-Lysine. The cells were allowed to rest in the hood for an hour to avoid edging effects and then placed in the incubator at 37°C; 5% CO_2 atmosphere overnight. On the day of the assay, the growth media was replaced by XF Assay media (Agilent technologies, Santa Clara, CA), supplemented with 1mM sodium pyruvate, 2mM L-glutamine and 10mM glucose and were incubated for 1 hr in without CO_2. ATP synthase inhibitor oligomycin (1.5 μM), proton ionophore fluorocarbonyl cyanide phenylhydrazone (1 μM) and complex I inhibitor rotenone (0.5 μM) were injected to the Seahorse analyzer. Mitochondrial function parameters such as basal respiration, maximal respiration, ATP production, spare respiration, non-mitochondrial respiration were analysed. Six-eight technical replicates were used per patient fibroblast and average values for each All the fibroblast conditions were analyzed as 6-8 replicates per primary fibroblast and data were analyzed to give average values for each condition. OCR data was normalized against the protein concentration and reported as pmol/min/mg.

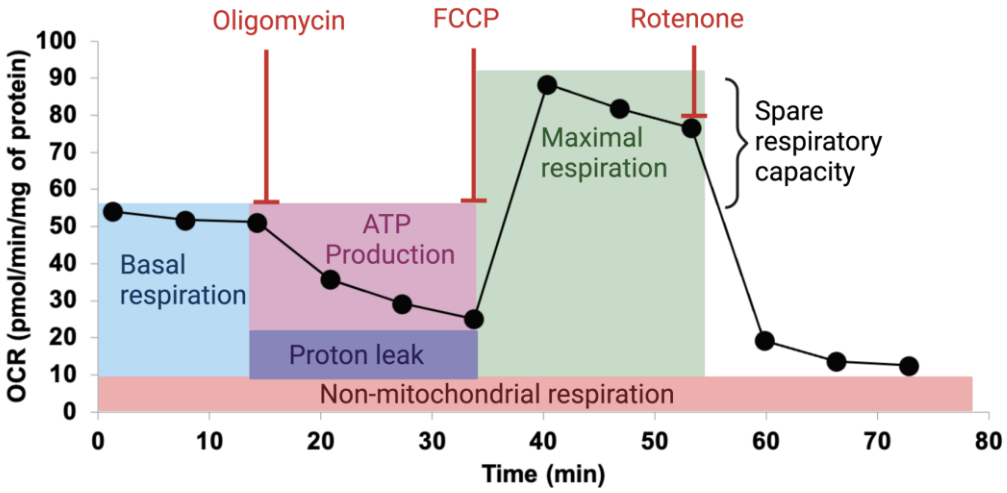

Figure 21. Seahorse assay

The cells were seeded at a concentration of 30,000 cells per well. Oligomycin (1.5 µM), FCCP (1 µM), and rotenone (0.5 µM) were injected to the cells and processed by Seahorse XFe96 analyzer.

4.2.6 Statistical analyses

Statistical analyses were performed using GraphPad Prism 9 (GraphPad, San Diego, CA, USA). For the comparison of two groups, student's t-test was utilized and for the comparison of multiple groups, one-way ANOVA followed by Dunnett's multiple comparison test was used. For all the analysis, statistical significance defined as $P \leq 0.05$.

4.3 Results

4.3.1 MDC1A cells show aberrant migration compared to the control group

I performed migration assays by creating wounds in MDC1A and control cell monolayers and monitoring their closure in real-time using IncuCyte. Relative wound density was used as a marker of cell migration into the wounded region and was measured every 2 hours in a 24-hour period (Figure 22).

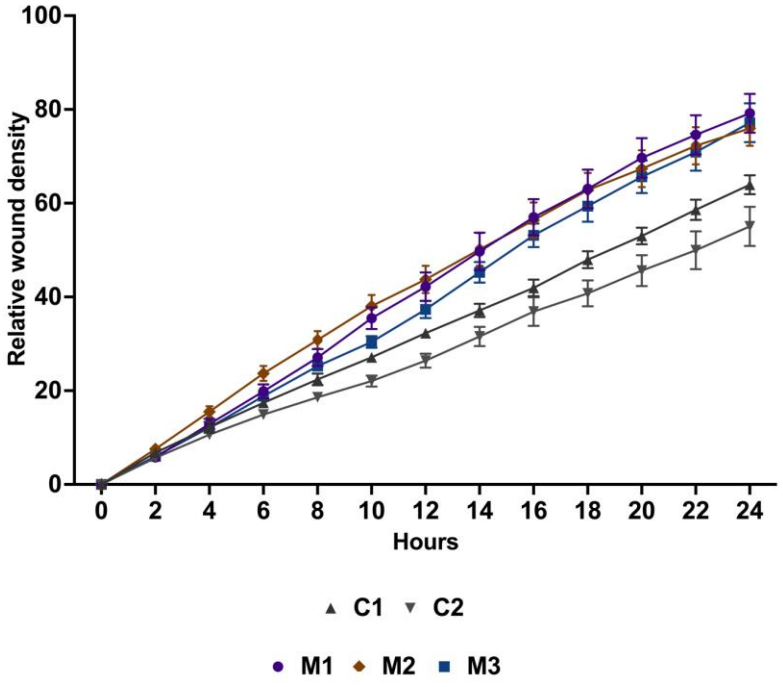

Figure 22. Migration of MDC1A cells versus controls

Wound density is plotted as a continuous function of time, beginning from 0 hr and ending at 24 hrs. C1-2, control cells. M1-3, MDC1A cells. Data are represented as mean ± s.e from n = 5-6 replicates per cell line.

Statistical analyses were performed on data collected at the 14- and 24-hour time points. Our findings revealed an overall trend in which the wounds created in the MDC1A cell monolayers closed more rapidly than those in the control groups (Figure 23A). At 14 hrs, the M1 and M2 MDC1A cells exhibited a relative wound density that was significantly higher than that achieved by control cells (C1) with *P* values of 0.02 for each; by contrast, no significant differences were observed in experiments performed with M3 cells. At 14 hours, all three sets of MDC1A cells (M1, M2, and M3) exhibited relative wound densities that were higher than that sustained by control C2 cells with *P* values of 0.002, 0.002, and 0.02, respectively (Figure 23B). At 24 hours, M1 and M3 cell monolayers maintained relative wound densities that were higher than those exhibited by C1 with *P* values of 0.01 and 0.05, respectively; by contrast, the differences in wound density exhibited by M2 did not achieve statistical significance. At 24 hours, all M1, M2, and M3 cells exhibited relative wound densities that were higher than that of C2 with *P* values of 0.002, 0.007, and 0.005, respectively (Figure 23C). In addition, the results of proliferation assay yielded no significant difference in cell growth and proliferation between control and MDC1A cells (Appendix B). Collectively, these results suggest that MDC1A cells promote more rapid wound closure than healthy controls.

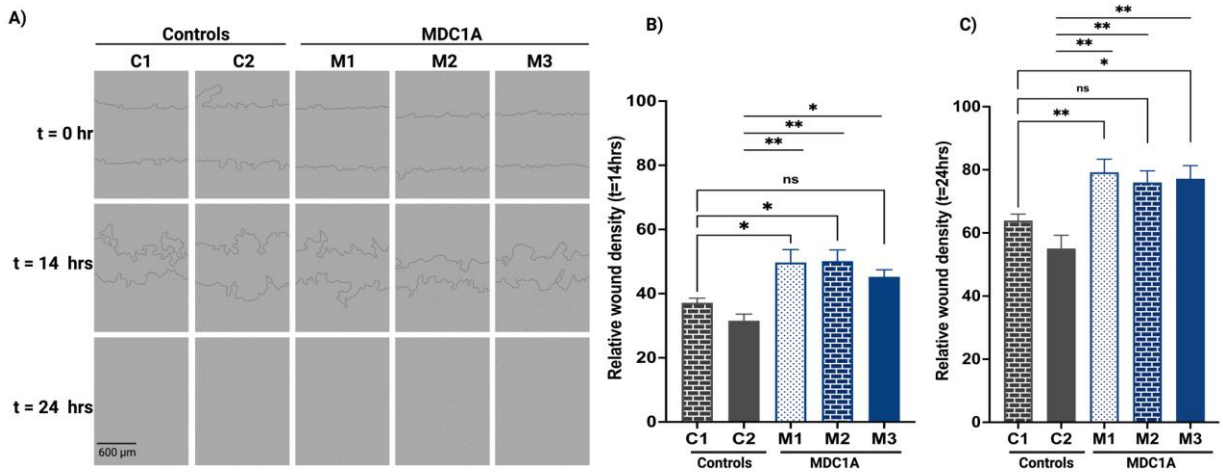

Figure 23. MDC1A cells migrate and close wounds more rapidly than control cells.

(A) The upper panel shows scratch wounds made in control and MDC1A monolayers at t = 0. The middle and bottom panels show the areas covered by these cells at t = 14 hours and t = 24 hours, respectively. (B-C) Quantification of relative wound density at t = 14 hours and t = 24 hours, respectively. Statistical comparisons were made between MDC1A and control cells to capture the inter-individual variations. C1-2, control cells; M1-3, MDC1A cells. Data are presented as mean ± s.e.; n = 5-6 replicates per condition; *$P \leq 0.05$, **$P \leq 0.01$, ns = not significant ; one-way ANOVA.

4.3.2 LAMA1 upregulation rescues aberrant migration in MDC1A cells

Subsequently, I tested whether the designed CRISPR activation system can induce increased expression of human *LAMA1* in MDC1A fibroblasts and assessed its impact on cellular migration. MDC1A cells (M1, M2, M3) were electroporated with 2XVP64-*Sa*dCas9 only or in conjunctions with the sgRNAs 10+11+12; the latter resulted in robust LAMA1 expression at 96 hours post-transfection. When coupled to migration assay, LAMA1 upregulation significantly reduced wound closure in all the MDC1A fibroblasts. Statistical quantification was done at 14 hrs. LAMA1 upregulated M1 cells have a significant reduction in wound closure (P = 0.001) and

comparable wound density to healthy control. The migration assay also revealed a significant reduction of wound density in the M2 cells following LAMA1 upregulation (P = 0.01) to a comparable level at the healthy control. Comparison of the effect of 2XVP64-*Sa*dCas9 only or in conjunctions with the sgRNAs 10+11+12 in the M3 cells also revealed a significant reduction in wound closure (P < 0.0001) towards the level exhibited by the healthy controls, albeit did not reach to similar migration level in healthy control. When coupled to migration assay, LAMA1 upregulation significantly reduced wound closure in all the MDC1A fibroblasts and relative wound density was calculated every 2 hours (Figures 24-25). Collectively, our findings revealed that CRISPRa-mediated *LAMA1* upregulation reduced the overactive migration in MDC1A fibroblasts.

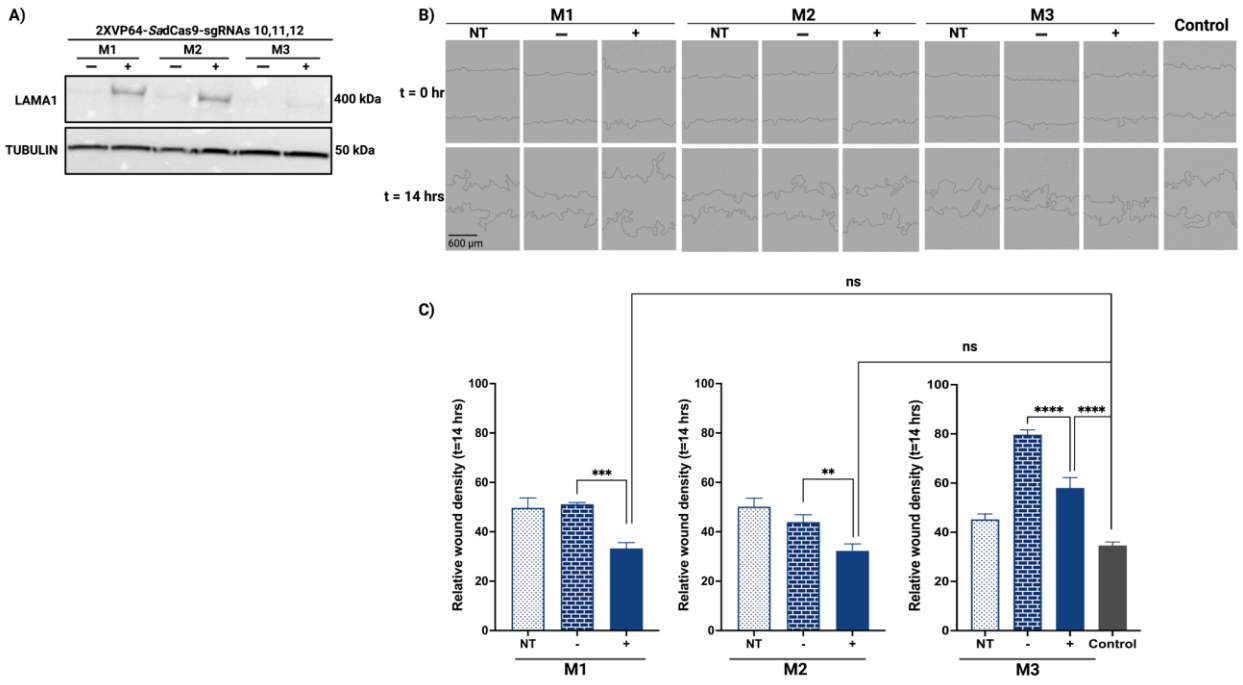

Figure 24. LAMA1 upregulation reduces migration in MDC1A fibroblasts

A). Western blot analysis of LAMA1 expression in control and MDC1A fibroblasts at 96 hours post-transfection. β-TUBULIN is used as the loading control, and quantification was done as a fold change in expression relative to the β-

TUBULIN. B). The upper panel shows the migration of the cells at the beginning of the wound (0hr) and at 14hrs in MDC1A and control group. C). The bottom panel shows the quantification of relative wound density measured at 14hrs. The control cells were combined, and statistical comparisons were made with reference to the control group and to the group with no guides. C1-2, control cells. M1-3, MDC1A cells. NT, non-transfected. '-' 2XVP64-*Sa*dCas9 with no guides. '+' 2XVP64-*Sa*dCas9 with three guides. Data are represented as mean ± s.e from n = 5-6 replicates per cell line. $^{**}P \leq 0.01$, $^{***}P \leq 0.001$, **** $P \leq 0.0001$, ns = not significant; one-way ANOVA.

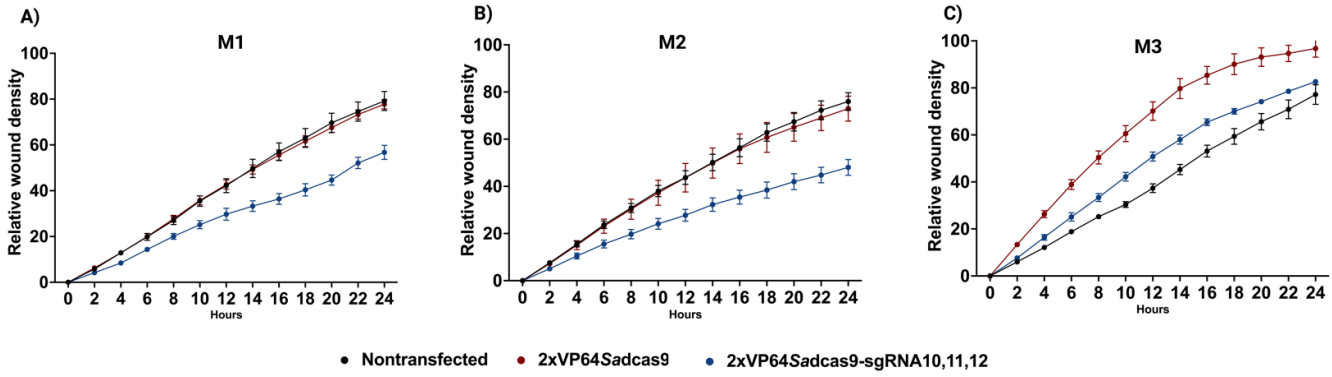

Figure 25. Migration of MDC1A cells treated with CRISPRa

A-C) Wound density is plotted as a continuous function of time, beginning from 0 hr and ending at 24 hrs. M1-3, MDC1A cells. NT, non-transfected. '-' 2XVP64-*Sa*dCas9 with no guides. '+' 2XVP64-*Sa*dCas9 with three guides. Data are represented as mean ± s.e from n = 5-6 replicates per cell line.

4.3.3 Working model demonstrating the wound-healing mechanism

Signal transduction begins with the binding of a ligand to the membrane-bound receptor and triggering a cascade of mechanisms, then transfers to the transcription factors in the nucleus and ends with regulation of the expression of the downstream genes [224]. This signaling mechanisms are essential for various cellular responses such as proliferation, differentiation, metabolism, repair and death [225]. Several bioinformatic tools are available to construct pathways

based on the gene expression data and public availability of the protein-protein interaction data [226]. I employed IPA to construct pathways for the wound-healing mechanism observed in the MDC1A treated cells.

The IPA illustrated the two stages of wound healing mechanism after a skin injury. The first stage comprises of inflammatory phase wherein the signaling mechanism is centered around stoping the progress of the wound and in eliminating the pathogens. In the second stage comprising of proliferative phase, the responses revolve around wound contraction and closure of the skin, The pathway tracker illustrated few of the genes that is involved in the wound healing mechanism as shown in Figure 26. They include genes encoding fibroblast growth factor receptor 2 (*FGFR2*), transforming growth factor beta 2 (*TGF-β2*), and actin alpha 2, smooth muscle (*ACTA2*).

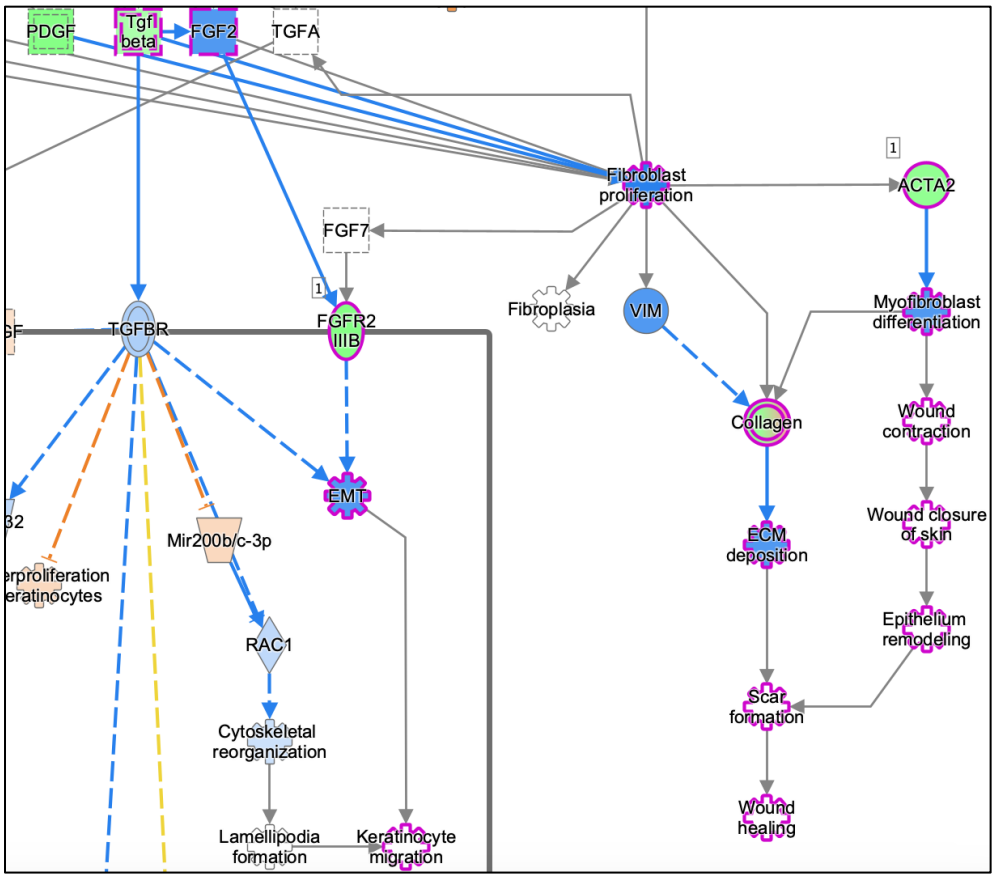

Figure 26. Ingenuity pathway analysis of differentially expressed genes in the MDC1A fibroblasts transfected with 2XVP64-*Sad*Cas9-sgRNAs10,11,12

Nodes represent the molecules in the pathway and the shapes of the nodes represent the functional class of the product: growth factor/cytokine (square), transmembrane receptor (veritcal ellipse), complex/group/other (circle). Genes that are up-regulated are depicted in red nodes and that are down-regualted are depicted in green nodes. The edges represent the biological relationship between the nodes. Solid or broken edges represent the direct or indirect relationship, respecitvely. The orange line indicates predicted upegulation, blue line indicates predicted inhibition and yellow line indicates contrary finding. The genes that are focussed in this study are highlighted in pink.

RT-qPCR analysis revealed increased expression of fibroblast growth factor receptor 2 (*FGFR2*), transforming growth factor beta 2 (*TGFβ2*), and actin alpha 2, smooth muscle (*ACTA2*) in the MDC1A fibroblasts compared to the healthy control groups. Importantly, the expression of

FGFR2, *TGFβ-2*, and *ACTA2* were reduced in *LAMA1*-upregulated cells (i.e., electroporated with 2XVP64-*Sa*dCas9 and sgRNAs 10+11+12) (previously Figure 17). Based on these observations in the transcriptomic and pathway analysis I postulated a model to explain the wound-healing mechanism observed in MDC1A fibroblasts and how *LAMA1* upregulation rescued this phenotype (Figure 27). MDC1A fibroblasts express high levels of *FGFR2* and *TGFβ2*, which in turn interact with *ACTA2* and likely affects myofibroblast differentiation and its associated wound contraction and -closure mechanisms. Upon *LAMA1* upregulation, the signaling mechanisms are downregulated leading to decreased expression of *FGFR2*, *TGFβ-2*, and *ACTA2* in the MDC1A treated cells. This might result in decreased myofibroblast differentiation and its associated wound contraction and wound closure mechanism and thereby the MDC1A treated cells exhibit reduced migration.

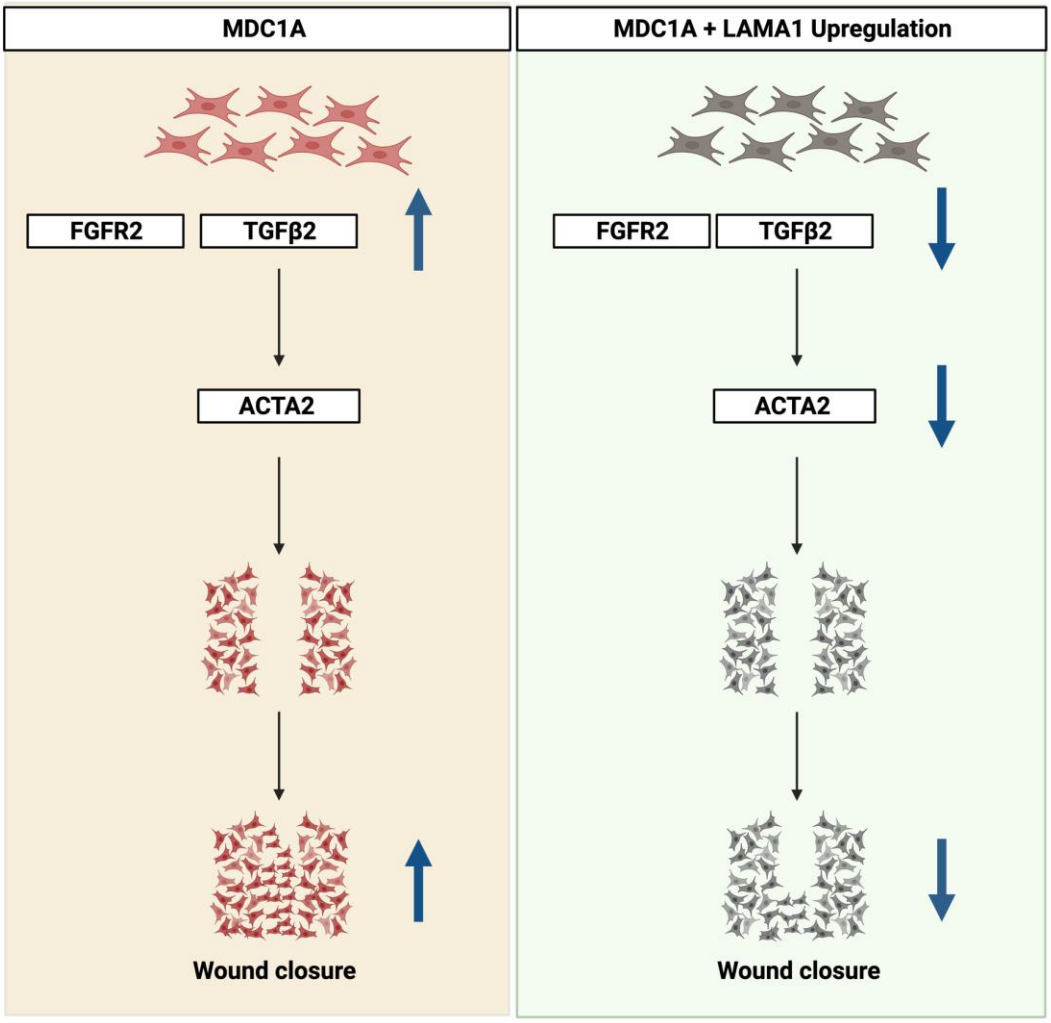

Figure 27. A working model of wound-healing mechanism

The left panel illustrates the migration in MDC1A fibroblasts. These cells express high levels of *FGFR2* and *TGFβ2*; these mediators interact with *ACTA2* to facilitate increased migration and wound contraction. The right panel shows the signaling mechanisms that are downregulated in response to the upregulation of *LAMA1*, thereby resulting in reduced migration. (The figure was created with BioRender.com).

4.3.4 Another functional assay: Bioenergetic profile of MDC1A fibroblasts

I investigated another functional assay prior to the transcriptomic analysis of the MDC1A fibroblasts. In 2014, de Oliveira et al. did a proteomic analysis of the diaphragm and gastrocnemius muscles from the MDC1A mouse model dy^{3k}/dy^{3k}. Using the PANTHER classification system, they categorized the differentially expressed proteins are involved in various biological processes. The study reported that the majority of the differentially expressed proteins to be involved in different metabolic processes comprising glycolysis, fatty acid β-oxidation, tricarboxylic acid cycle, respiratory electron transport, and oxidative phosphorylation [227]. In 2017, Fontes-Oliveira et al. analyzed the orthologue genes in muscle cells of MDC1A patients. They concluded that genes related to metabolic processes phosphofructokinase (*PFK*), glycogen phosphorylase (*PYGM*), isocitrate dehydrogenase (*IDH3*), and adenine nucleotide translocator (*ANT1*) were significantly dysregulated. Further, the study revealed the MDC1A myoblasts have decreased mitochondrial respiration and increased glycolysis compared to control myoblasts. The study suggested that the MDC1A myoblasts, due to a dysregulated bioenergetic profile, have a low mitochondrial respiration rate that is compensated by a high glycolysis rate [212].

To my knowledge, no studies have been done on the MDC1A fibroblast model system. Therefore, to determine whether MDC1A fibroblasts exhibit impaired bioenergetics, I analyzed the mitochondrial respiration rate of MDC1A and control fibroblasts using a Seahorse analyzer (Figure 28). The study revealed a trend wherein MDC1A fibroblasts exhibit a low oxygen consumption rate for non-mitochondrial oxygen consumption, basal respiration, maximal respiration, ATP production, and spare respiratory capacity. Although I observed a trend in the bioenergetic profile between MDC1A and control fibroblasts, excluding the basal respiration rate, the results were not statistically significant for other parameters (Figure 29).

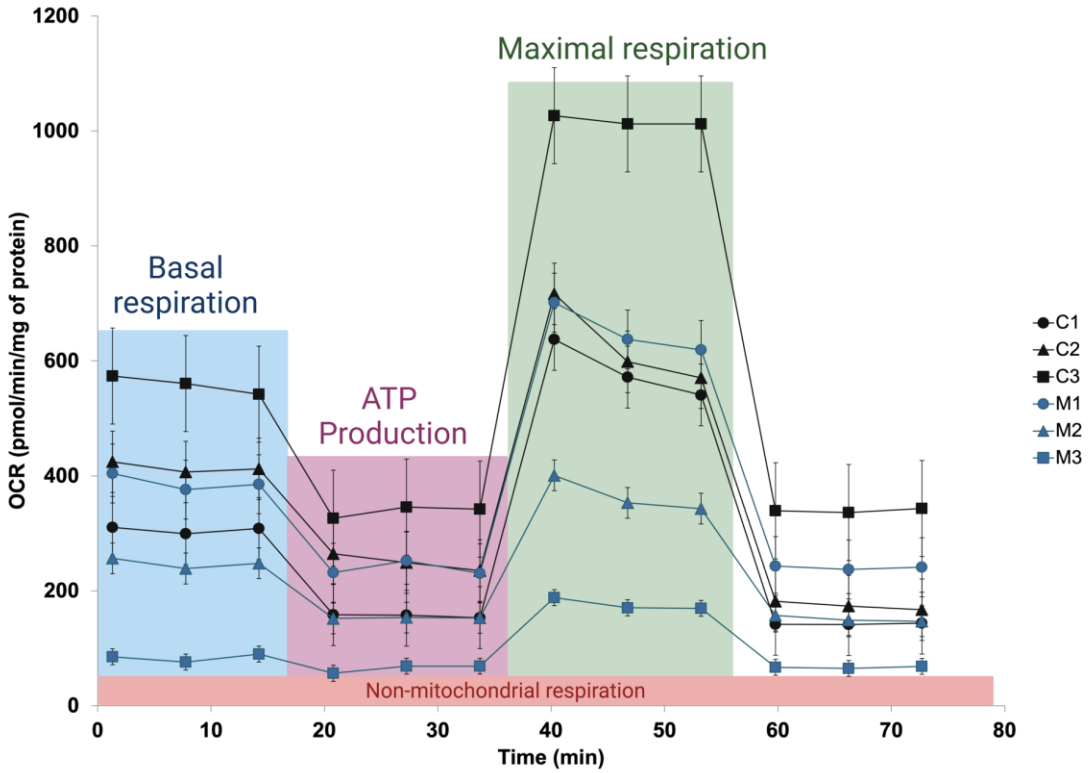

Figure 28. Bioenergetic profile of MDC1A and control fibroblasts

The figure illustrates the real-time oxygen consumption rate (OCR) in the MDC1A and control fibroblasts upon the addition of inhibitors, oligomycin, FCCP, and rotenone in the Seahorse analyzer. Each dot represents mean $\pm$ s.e. n = 6 to 8 technical replicates.

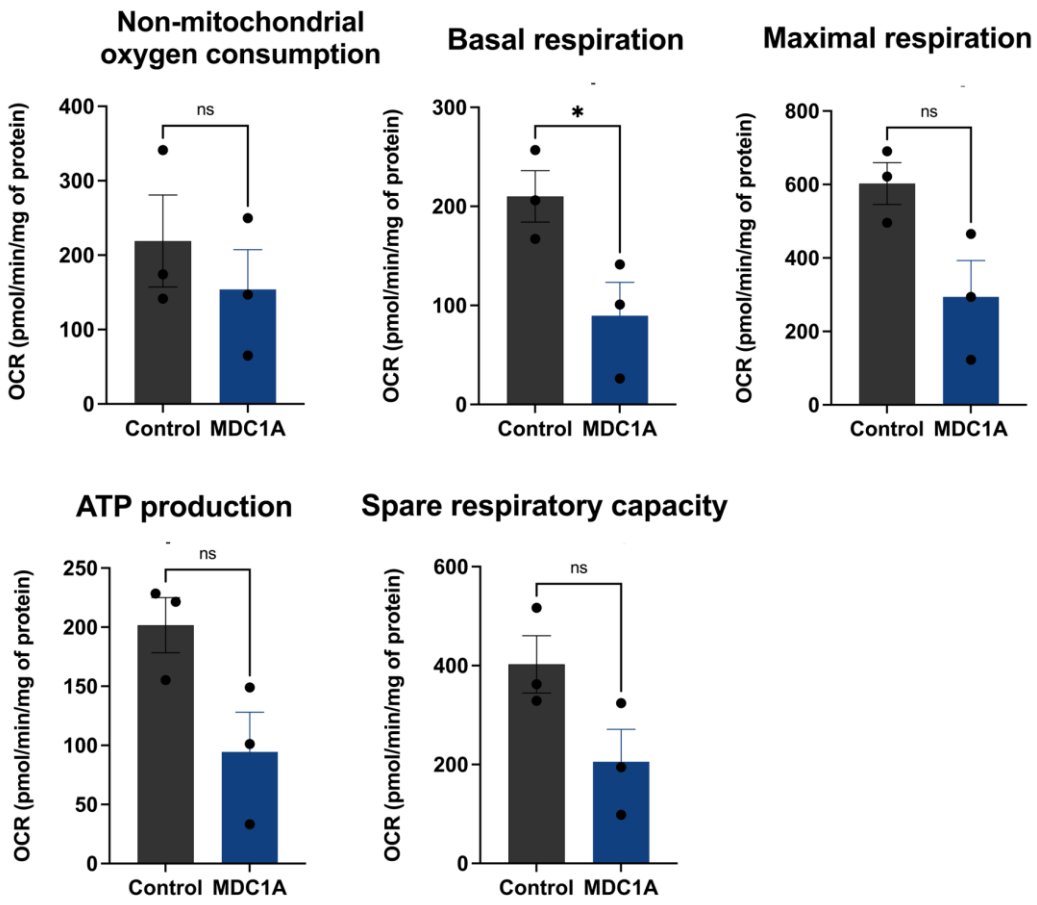

Figure 29. Mitochondrial respiration in MDC1A fibroblasts

The MDC1A fibroblasts exhibit an overall trend with low levels of basal respiration, ATP production, maximal respiration, and spare respiratory capacity compared to the control group. Each dot represents the pooled value of each control and MDC1A fibroblast. Data are represented as mean ± s.e. Statistical significance was assessed by unpaired t-test. * $P < 0.05$.

4.4 Discussion

This study shows that MDC1A fibroblasts despite having varied expression of LAMA2, are functionally impaired and show aberrant migration. The study also demonstrates that the LAMA1 upregulation achieved via CRISPRa was sufficient to reduce the migration in MDC1A cells.

As an essential component of the extracellular matrix (ECM), LAMA2 serves as an anchor that provides stability and restricts aberrant migration. Anchoring activity disappears in the absence of LAMA2; this triggers a cell-signaling response leading to increased migration. Our transcriptomic analysis revealed that MDC1A fibroblasts express high levels of *FGFR2, TGFβ2,* and *ACTA2* – all of them have been implicated in wound healing processes [228-231].

Albeit underexplored in the context of MDC1A, several studies of tumor-related responses have highlighted cell migration mediated by LAMA2. For example, Liang *et al*. reported *LAMA2* downregulation in lung adenocarcinoma cells and found that *LAMA2* knockdown in these cells also promoted migration [232]. Similarly, Wang *et al*. reported that overexpression or demethylation of *LAMA2* suppressed the invasiveness of pituitary adenoma cells [233]. Others have reported that *LAMA2* can serve as a tumor suppressor gene [234] and that inactivation of *LAMA2* may lead to tumor progression [235-239]. Finally, Chermula *et al*. reported a role *LAMA2* in porcine oocyte migration[240]. Collectively, these findings provide strong documentation of the contributions of *LAMA2* to the cellular migration process and are consistent with our work in the context of muscular dystrophy. When *LAMA1* was upregulated using CRISPRa in MDC1A fibroblasts, the overactive migration was curbed and the expression of *FGFR2, TGFβ2,* and *ACTA2* was reduced. Our working model thus centers on the ability of LAMA1 to also anchor the

ECM and reduce aberrant migration, similar to LAMA2; thereby expanding the potential compensatory mechanism between these two proteins.

5.0 General discussion

5.1 Summary of the dissertation research

5.1.1 CRISPR activation system induces LAMA1 upregulation

The work in this dissertation provides evidence that the CRISPR activation system could serve as a mutation-independent approach to upregulate *LAMA1* in the MDC1A fibroblasts regardless of the mutation. MDC1A is caused by mutations in the *LAMA2* gene [36, 37] encoding for laminin-α2 chain, which combines with β1 and γ1 chains to form laminin-211 protein complex in the basement membrane [40, 41]. It provides stability and forms a connecting link between the basement membrane and the cell surface receptors [42]. Lack of laminin-211 results in hypotonia, delayed motor development, and skeletal deformations [7, 8]. The mutations occurring at *LAMA2* are heterogeneous, with more than 300 documented so far [59]. In my study, I used fibroblasts derived from MDC1A patients with different mutations. Instead of correcting the individual mutation in each of the MDC1A cells, I focused on upregulating *LAMA1*, a disease modifier of MDC1A, encoding for the laminin-α1 chain. It shares many similar traits as laminin-α2. Structurally, like the laminin-α2 chain, the laminin-α1 chain combines with β1 and γ1 to form a heterotrimeric complex laminin-211[241]. It was replaced by LAMA2 at nine gestational weeks[58, 65]. Further, it interacts with similar cell surface receptors integrin α7β1 and dystroglycan as LAMA2 [67] [46]. Thereby, similar to LAMA2, it establishes a connection between the basement membrane and cytoskeleton and helps in the downstream signaling process

in the cell. Owing to the aforementioned reasons *LAMA1* is a promising candidate to compensate for the lack of *LAMA2*.

Therefore, to increase the endogenous expression of *LAMA1*, I employed a CRISPR activation system comprising *Sa*dCas9, VP64 transactivation domain, and sgRNAs. I designed multiple sgRNAs and screened for the best combination to induce maximum expression of *LAMA1*. Out of various combinations, CRISPRa with sgRNAs 10,11,12 showed maximum upregulation of *LAMA1* in MDC1A-derived fibroblasts. The works provides evidence for the efficiency and adaptability of CRISPRa for the treating MDC1A cells regardless of the mutation in the *LAMA2* gene.

5.1.2 Transcriptomic analysis reveals dysregulation of wound-healing mechanism in MDC1A fibroblasts

The laminin α2 chain connects the basement membrane to the cytoskeleton [45, 46]. The absence of laminin α2 chain leads to disruption of the laminin complex, and the downstream Integrin α7β1 and dystroglycan-mediated signaling are disrupted [208]. The disrupted pathways and cell-signaling mechanisms vary based on the cell type, and with the help of RNA-sequencing, such tissue-specific gene expression profiles can be documented [56, 209, 210]. To our knowledge, gene expression profile has never been done in MDC1A fibroblasts from humans. The work in this dissertation lays the foundation for documenting the transcriptomic profiles in MDC1A fibroblasts. I analyzed the transcriptomic data and identified the different biological pathways between the MDC1A and the control fibroblasts such as hepatic fibrosis, pulmonary fibrosis, axonal guidance, wound-healing mechanism, and phagosome formation. Out of these pathways, *LAMA2* was directly associated with the wound healing pathway with a predicted activation state,

implying that a lack of *LAMA2* leads to an activated wound healing pathway. Furthermore, some genes involved in the wound healing mechanisms, such as *FGFR2*, *TGFβ2*, and *ACTA2*, were also increased in the MDC1A cells. After treatment with CRISPRa, the MDC1A cells revealed significant upregulation of *LAMA1* with an association with the wound healing pathway but with an inhibitory effect. Further, the expression of the wound healing genes- *FGFR2*, *TGFβ2*, and *ACTA2*- were reduced in the MDC1A treated cells.

Overall, the findings once again corroborate the upregulation of *LAMA1* by CRISPRa but very importantly, it reveals that the lack of *LAMA2* activated the wound healing pathway. At the same time, upregulation of *LAMA1* reversed the pathway to an inhibitory state suggesting that *LAMA1* can compensate for *LAMA2*.

5.1.3 LAMA1 rescues cellular migrations in MDC1A fibroblasts

Our findings from the transcriptomic study directed us to observe the cellular migrations in MDC1A cells. Our study showed that all three MDC1A fibroblasts exhibit aberrant migration compared to the control group, as expected from the transcriptomic data. Notably, M1 also showed overactive migration even though it showed LAMA2 expression in the protein expression and transcriptome data. It could be because M1 cells have a mutation impacting the polar residues at the region beyond the G5- globular domain in the *LAMA2* gene. The position of this mutation might lead to the expression of sufficiently stable transcript and protein in M1 cells. It could be possible that LAMA2 might still be attached to the basement membrane, but its functionally hampered and unable to perform the downstream cell-signaling process, resulting in aberrant migration in M1 cells. In the future, and if it is feasible to access the skin samples of M1,

immunostaining it to understand the localization of the LAMA2 in M1 cells would help us to make inferences and add more validation to the proposed phenomena.

MDC1A cells, upon *LAMA1* upregulation mediated by CRISPRa, showed reduced migration. Based on our findings, LAMA2 might serve as an anchor that provides stability and restricts aberrant migration. Lack of LAMA2 removes the anchoring activity and disrupts downstream cell-signaling resulting in increased migration. When CRISPRa increases *LAMA1*, the LAMA1 serves as an anchor, thereby rescuing the aberrant migration exhibited by the MDC1A cells. Albeit not related to muscular dystrophy, several oncological studies have reported the inactivation of *LAMA2* leading to tumor progression [235-239]. Finally, I developed a model suggesting a possible wound healing mechanism where lack of LAMA2 leads to high expression of *FGFR2, TGFβ2,* and *ACTA2,* which in turn causes myofibroblast differentiation and its associated wound contraction and wound closure mechanisms, increasing the migration. Similarly, upregulation of *LAMA1* leads to reduced expression of *FGFR2, TGFβ2,* and *ACTA2* and decreased myofibroblast differentiation and its associated wound closure mechanisms, reducing migration.

5.2 Limitations and future considerations

5.2.1 Design and efficiency of the CRISPR system

Several considerations were taken into account while designing sgRNAs, such as their proximity to the promoter of the *LAMA1* gene and the length of the sgRNAs to be within 19-21 bp to maximize the gene expression [202, 242]. However, studies have demonstrated that not all the sgRNAs bind to the complementary region efficiently[243, 244]. Therefore, I designed multiple

sgRNAs, and the optimal sgRNAs were screened from the preliminary pool. However, the GC content of the sgRNAs was not considered at the time of the study. Designing sgRNAs with low GC content ($\leq$ 35%) is more favorable because the sgRNAs with high GC content has the potential to form strong DNA-RNA hybrid even with 4-5 mismatches in the target sequence [205, 245]. Further, to upregulate *LAMA1* using CRISPRa, I employed a combination of three sgRNAs based on the previous studies suggesting a synergistic effect of sgRNAs causes an increase in endogenous expression of a target gene [110, 131, 203] [246]. However, using three sgRNAs in three different plasmids would lead to a high concentration of Cas9. In the future, our research group aims to design a CRISPR system consisting of miniaturized tripartite activators can upregulate the target gene efficiently with one sgRNA. This would be advantageous for a few reasons. First, it would significantly reduce the concentration of the Cas9, by reducing the number of plasmids required for transfection. Second, previous studies have suggested that an increased ratio of sgRNA to Cas9 will tend to produce maximum efficiency[247-249]. Albeit there is no limitation for the plasmid capacity in the electroporation method, this would be beneficial when viral vectors such as AAVs for in vivo gene delivery.

5.2.2 Off-target effects and single nucleotide polymorphisms

The presence of single nucleotide polymorphism (SNPs) in the PAM or the complementary region of the sgRNA could disrupt the targeted sequence. Likewise, the presence of SNPs sometimes might cause unexpected off-target sites facilitating sgRNA binding. Disruption of the targeted sequence will lead to the non-binding of the sgRNA, and thereby CRISPRa would not work in the designated cell type. However, binding at unexpected off-target sites might lead to unintended genome modifications, such as tumor suppressing genes [205]. There are several

bioinformatic tools to streamline the CRISPR off-target effects. However, these tools are built based on common SNPs based on the human reference genome, which does not account for genetic variants in a specific population [206]. For instance, Cancellieri et al. demonstrated that sgRNA used in preclinical studies for β-thalassemia, has no off-target sites based on the human reference genome. However, when it was matched against 1000G variants, it showed a potential off-target site in the African population with a high on-target score suggesting a high probability of binding to the off-target site. However, it is currently limited to the prediction of *S. pyogenes*-derived Cas9 targets, whereas the recognition sequence of *S. aureus*-derived Cas9 was not yet included at the time of preparation of this manuscript. In the future, variant-aware target assessments are expected to become integral to therapeutic genome editing evaluation, including CRISPRa-modulation of gene expression presented here [207].

5.2.3 Transcriptomic analysis

In the transcriptomic analysis, I compared the 2XVP64-*Sa*dCas9-sgRNAs10,11,12 treated cells to untreated cells rather than the 2XVP64-*Sa*dCas9 treated cells. The comparison was chosen because our objective was to use the CRISPRa method to increase the endogenous expression of only one gene (i.e., *LAMA1*). Both the groups are similar except for the sgRNAs in the MDC1A treated cells. Further, the MDC1A fibroblast genomes are overall very similar to one another; thus, our efforts to identify DEGs between these groups yielded no statistically significant results. The inclusion of several MDC1A fibroblasts would have increased the statistical power of the transcriptomic analysis. Even though the study was started with three MDC1A fibroblasts, one of the patient cells exhibited LAMA2 expression and was excluded from the transcriptomic analysis

and included in the treatment of the CRISPR activation system and migration assay. In future, several MDC1A fibroblasts would be included in our study.

5.2.4 Immunogenicity

The transcriptomic analysis showed the activation of immune-related pathways in the MDC1A treated cells. However, our cellular model system hampers further investigation due to the lack of an immune system. Nevertheless, this laid the foundation for our future directions to investigate the immune response due to the CRISPR components in animal models with immune system[250]. The immune response could arise from *Staphylococcus aureus*, Cas9, or delivery vectors such as AAVs. For instance, a humoral and a cell-mediated immune response are observed against *Staphylococcus aureus*, which causes common infections in humans [251, 252]. Similarly, pre-existing immunity to Cas9 in the form of Cas9 reactive T cells has been reported [253, 254] [219, 255]. This implies that for an individual with Cas9 reactive T cells, the cells expressing Cas9 protein would be recognized by the cytotoxic T-lymphocytes (CTL) via MHC class-II molecules in the antigen-presenting cells. This would activate CTLs that target and destroy the cell, which might lead to tissue toxicity [255]. This would not be a problem in ex vivo therapy mainly because Cas9 could express transiently using RNPs. Therefore, the antigen would not be expressed on the cells during transplantation back to the body. However, it poses problems during in vivo delivery using viral vectors, leading to long-term expression of Cas9 [253, 256].

Similar to Cas9, the major challenge to the use of AAVs is the pre-existing immunity in individuals against several serotypes of AAV[257, 258] that causes a similar immune response as mentioned above. In addition to the seroprevalence, determining an optimal dose required for efficient upregulation of the target gene without creating an immune response is essential.

Moreover, due to the formation of neutralizing antibodies (NAb) to AAV during the first dose of administration, further, re-dosing is a challenge. These challenges could be overcome by engineering the AAV capsid that prevents binding of NAbs [259], plasmapheresis for low-NAb titre individuals [260, 261]. Overall, checking for pre-existing immunity to Cas9 or AAVs in people is essential before enrolling them in gene therapy trials. Additionally, providing immunosuppression drugs such as corticosteroids during the initial stages after gene therapy would also help the individuals and with the recent advancements in delivery vectors including nanoparticles, very soon platforms would emerge that circumvents the current challenges[256].

5.2.5 Conclusion

In summary, our study demonstrates the feasibility of CRISPRa-mediated upregulation of human *LAMA1* in MDC1A cells, and at the same time highlights the compensatory mechanism between these two genes. This strategy might be adapted to address other neuromuscular diseases and inherited conditions in which strong compensatory mechanisms have been identified [262-264]. Finally, the application of migration assay as a functional outcome measure in fibroblasts from affected individuals also illustrates a robust and scalable pipeline in drug discovery and screening in MDC1A and potentially other ECM-related muscular dystrophies.

Appendix A sgRNAS 10,11,12 shows high expression in HeLa cells

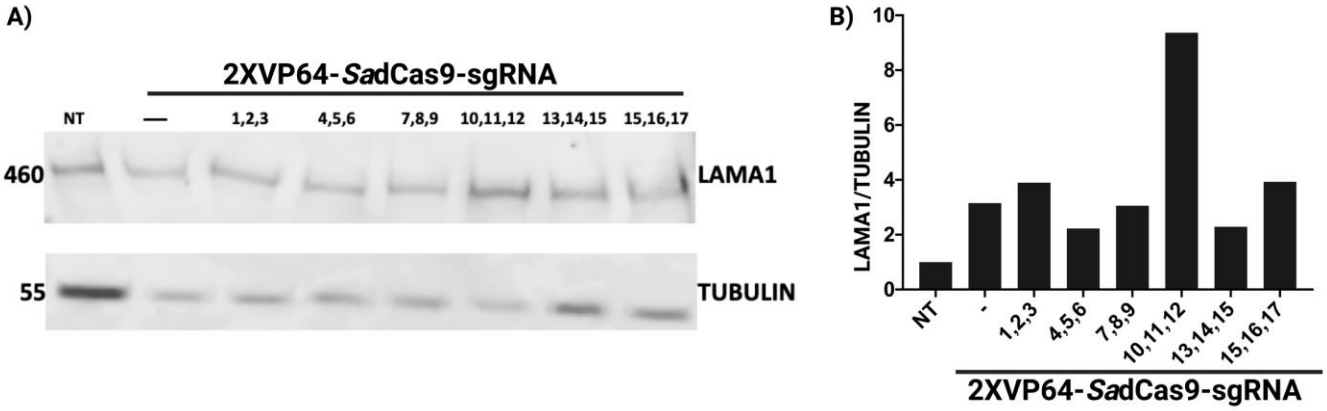

Appendix Figure 1.

Western blot analysis of the combination of optimal sgRNAs for LAMA1 expression. NT, non-transfected. '-' 2XVP64-*Sa*dCas9 with no guides. β-TUBULIN is used as the loading control, and quantification was done as a fold change in expression relative to the β-TUBULIN.

Appendix B Proliferation assay between MDC1A and control group

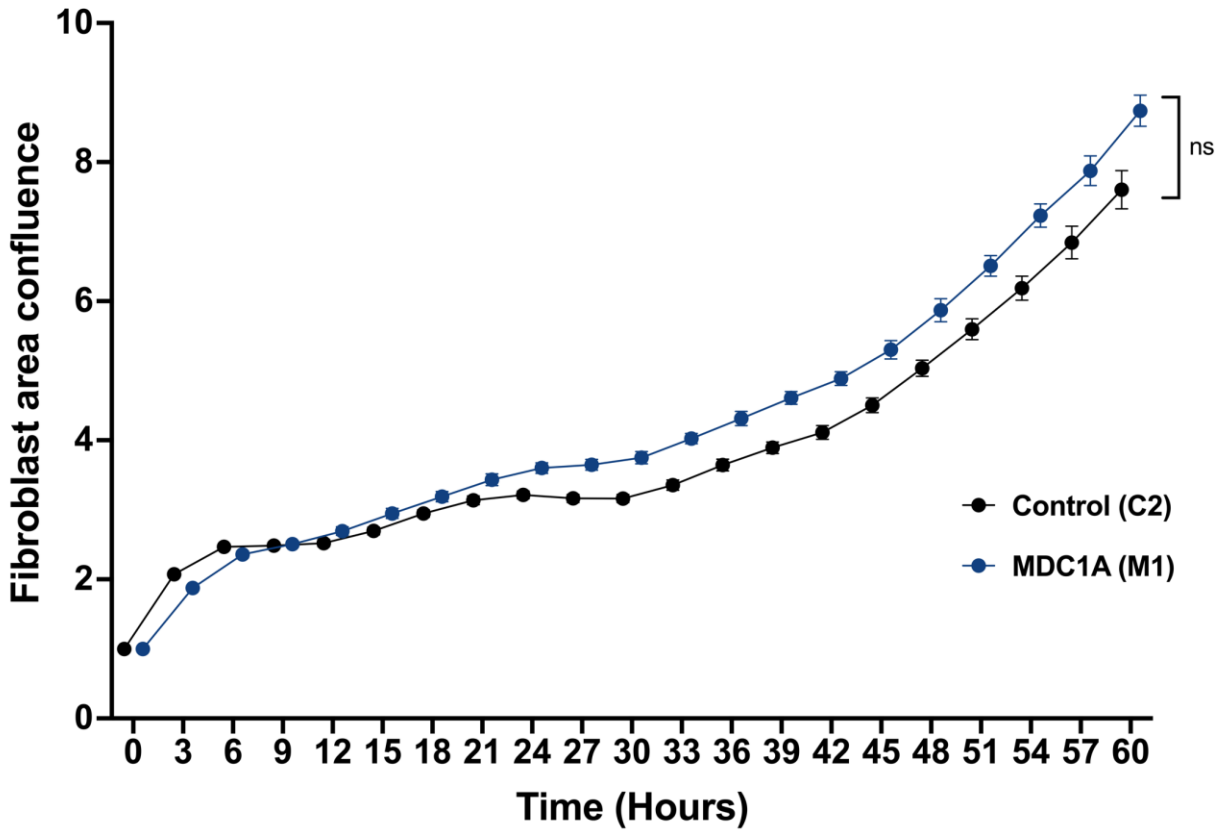

Appendix Figure 2.

Proliferation assay illustrating the cell-growth between MDC1A (M1) and control group (C2). The X-axis represents the time in hours and the Y-axis represents the fibroblast area confluence. Data are represented as mean ± s.e from a total of n = 3 replicates per cell group. Statistical significance was assessed by unpaired t-test, ns; non-significant; student's t-test.

Appendix C DEG between MDC1A and healthy controls

Appendix Table 1.

Name	Chromosome	Max group mean	Log_2 fold change	Fold change	FDR p-value	ENSEMBL
HOXC10	12	25.25	-7.87	-233.19	2.38E-61	ENSG00000180818
LAMA2	6	17.64	-5.1	-34.24	4.69E-49	ENSG00000196569
IGF2	11	49.58	-5.09	-34.07	3.67E-26	ENSG00000167244
GRIA1	5	12.65	-4.5	-22.58	1.11E-25	ENSG00000155511
ADH1B	4	16.54	-3.99	-15.84	1.52E-24	ENSG00000196616
ERAP2	5	5.31	4.35	20.43	2.08E-24	ENSG00000164308
COL15A1	9	39.81	-2.92	-7.58	2.61E-23	ENSG00000204291
PITX1	5	7.41	-6.04	-65.68	1.19E-22	ENSG00000069011
SDK1	7	1.33	-7.33	-160.55	1.18E-21	ENSG00000146555
NRN1	6	68.58	5.35	40.84	1.39E-21	ENSG00000124785
TSPAN18	11	8.17	4.29	19.59	6.90E-21	ENSG00000157570
ELFN2	22	1.86	-5.41	-42.45	1.65E-20	ENSG00000166897
DKK2	4	8.33	4.71	26.14	2.01E-20	ENSG00000155011
TMTC1	12	20.63	-4.27	-19.29	3.02E-18	ENSG00000133687
FOXD1	5	41.57	2.87	7.3	3.45E-18	ENSG00000251493
OGN	9	4.39	-5.96	-62.16	4.37E-18	ENSG00000106809
TBX2	17	12.51	-3.82	-14.12	3.21Ev - 17	ENSG00000121068
SLC2A12	6	3.95	-4.32	-20.02	3.73E-17	ENSG00000146411
PODXL	7	29.37	5.24	37.68	5.64E-17	ENSG00000128567
TENM2	5	24.98	3.68	12.85	6.59E-17	ENSG00000145934
EPHB6	7	26.34	-4.12	-17.33	1.27E-16	ENSG00000106123
CPZ	4	36.12	-2.98	-7.9	1.39E-15	ENSG00000109625
LAMA3	18	3.51	-3.66	-12.61	1.92E-15	ENSG00000053747
ARRDC4	15	28.06	-3.27	-9.65	2.93E-14	ENSG00000140450
IL7R	5	22.48	3.5	11.29	9.36E-14	ENSG00000168685
IL17RD	3	4.22	-3	-8	6.24E-13	ENSG00000144730
SIM1	6	9.59	-2.52	-5.74	7.39E-13	ENSG00000112246
MITF	3	5.26	-3.54	-11.63	1.06E-12	ENSG00000187098
CPE	4	7.62	3.34	10.12	3.55E-12	ENSG00000109472
ADAMTS15	11	5.78	-5.27	-38.67	4.91E-12	ENSG00000166106
LHX9	1	12.19	7.11	137.78	6.52E-12	ENSG00000143355
LAMA5	20	5.75	-2.42	-5.36	1.56E-11	ENSG00000130702
HOXC8	12	23.47	4.31	19.79	1.85E-11	ENSG00000037965
ACTC1	15	106.61	7.37	165.47	1.85E-11	ENSG00000159251
ZFY	Y	2.88	-10.3	-1,260.37	1.85E-11	ENSG00000067646
SHC3	9	2.01	-3.9	-14.89	2.04E-11	ENSG00000148082
HSPB7	1	92.94	3.1	8.6	2.06E-11	ENSG00000173641

EN1	2	12.06	4.26	19.15	2.36E-11	ENSG00000163064
AR	X	4.04	-3.48	-11.13	4.60E-11	ENSG00000169083
TOR4A	9	8.4	-2.69	-6.44	5.52E-11	ENSG00000198113
FGFR2	10	0.69	6.02	64.86	5.74E-11	ENSG00000066468
RIPOR3	20	3.52	-4.26	-19.18	2.17E-10	ENSG00000042062
ROR2	9	6.14	-2.74	-6.67	2.20E-10	ENSG00000169071
MEIS1	2	11.78	-2.56	-5.89	2.76E-10	ENSG00000143995
EDIL3	5	27.29	4.41	21.32	2.92E-10	ENSG00000164176
ISL2	15	10.47	-5.42	-42.82	5.58E-10	ENSG00000159556
PCSK6	15	0.67	-5.89	-59.26	6.30E-10	ENSG00000140479
OSR2	8	134.48	-3.03	-8.16	6.62E-10	ENSG00000164920
CCDC85A	2	2.8	4.26	19.1	9.75E-10	ENSG00000055813
ZIC1	3	2.54	4.05	16.59	1.08E-09	ENSG00000152977
HOXC11	12	3.11	-9.68	-819.86	1.76E-09	ENSG00000123388
EDNRA	4	5.45	-2.99	-7.93	1.82E-09	ENSG00000151617
LNX1	4	2.18	3.96	15.59	2.73E-09	ENSG00000072201
SMPDL3A	6	18.6	-2.38	-5.2	4.19E-09	ENSG00000172594
ITGB2	21	1.61	6.43	86.09	7.31E-09	ENSG00000160255
HAS2	8	27.69	4.1	17.16	8.49E-09	ENSG00000170961
RASL12	15	1.82	-6.32	-79.68	9.93E-09	ENSG00000103710
SCIN	7	1.3	4.48	22.35	1.07E-08	ENSG00000006747
WNT2	7	26.81	-2.37	-5.15	1.07E-08	ENSG00000105989
AARD	8	3.64	-5.37	-41.27	1.31E-08	ENSG00000205002
GOLGA8A	15	15.02	-2.59	-6.03	1.59E-08	ENSG00000175265
ADD2	2	0.66	9.4	677.54	2.11E-08	ENSG00000075340
CACNA1H	16	0.73	-6.59	-96.07	2.12E-08	ENSG00000196557
HAPLN1	5	29.19	6.69	103.55	2.25E-08	ENSG00000145681
MARCKSL1	1	29.57	-2.2	-4.61	2.57E-08	ENSG00000175130
MYPN	10	3.16	2.79	6.91	2.57E-08	ENSG00000138347
RHOJ	14	12.15	-2.36	-5.12	2.67E-08	ENSG00000126785
HOXB6	17	3.54	7.57	189.68	2.99E-08	ENSG00000108511
FGL2	7	3.21	8.29	313.75	3.00E-08	ENSG00000127951
ZNF385D	3	1.92	2.67	6.37	3.05E-08	ENSG00000151789
RASL10B	17	3.63	-3.89	-14.83	8.34E-08	ENSG00000270885
ABCA1	9	7.28	-2.17	-4.51	8.47E-08	ENSG00000165029
SCN9A	2	0.82	-3.97	-15.7	9.37E-08	ENSG00000169432
AMPH	7	5.58	2.51	5.69	1.03E-07	ENSG00000078053
ITGA8	10	4.78	2.91	7.51	1.03E-07	ENSG00000077943
C11orf87	11	7.61	2.75	6.72	1.03E-07	ENSG00000185742
HOXB7	17	4.23	7	127.76	1.05E-07	ENSG00000260027
OSR1	2	16.1	2.29	4.89	1.09E-07	ENSG00000143867
GLIPR1	12	38.58	2.36	5.12	1.33E-07	ENSG00000139278
CH25H	10	12.37	2.99	7.94	1.83E-07	ENSG00000138135
C11orf96	11	3.98	4.19	18.31	2.32E-07	ENSG00000187479
NRG1	8	3.27	2.09	4.26	2.41E-07	ENSG00000157168
MICAL2	11	14.22	2.33	5.03	2.96E-07	ENSG00000133816
NBPF3	1	13.95	-2.36	-5.14	3.24E-07	ENSG00000142794

PHACTR3	20	2.19	5.64	49.88	4.45E-07	ENSG00000087495
SFRP2	4	61.28	3.2	9.17	4.61E-07	ENSG00000145423
NPIPA1	16	23.2	-2.02	-4.07	5.39E-07	ENSG00000183426
CRLF1	19	38.17	-2.45	-5.48	5.46E-07	ENSG00000006016
COL8A1	3	233.93	2.88	7.36	8.04E-07	ENSG00000144810
RPS4Y1	Y	164.19	-16.21	-75,747.44	8.58E-07	ENSG00000129824
HOXB5	17	2.96	7.08	135.06	9.34E-07	ENSG00000120075
MAMDC2	9	3.83	-3.41	-10.67	1.04E-06	ENSG00000165072
PRPS1	X	37.83	2.05	4.13	1.08E-06	ENSG00000147224
SGCD	5	23.09	2.14	4.4	1.12E-06	ENSG00000170624
TRHDE	12	3.84	-2.11	-4.33	1.23E-06	ENSG00000072657
CFD	19	9.51	-2.51	-5.71	1.23E-06	ENSG00000197766
PNMA2	8	3.84	-3.75	-13.46	1.57E-06	ENSG00000240694
SYNGR3	16	1.64	-4.59	-24.13	1.64E-06	ENSG00000127561
RIPK4	21	2.22	4.55	23.46	1.91E-06	ENSG00000183421
CDH8	16	0.56	5.82	56.52	2.16E-06	ENSG00000150394
TSPAN13	7	10.93	2.64	6.22	2.30E-06	ENSG00000106537
ARMH4	14	3.62	2.4	5.26	2.36E-06	ENSG00000139971
STRA6	15	0.92	-8.94	-490.68	2.44E-06	ENSG00000137868
L1CAM	X	6.53	-3.3	-9.82	2.44E-06	ENSG00000198910
HOXD3	2	1.55	4.97	31.33	2.55E-06	ENSG00000128652
PTGDS	9	14.27	-2.36	-5.13	2.56E-06	ENSG00000107317
PALM	19	14.21	-2.3	-4.91	3.04E-06	ENSG00000099864
SPON2	4	49.76	-2.32	-5	3.18E-06	ENSG00000159674
GALNT5	2	38.56	3.02	8.12	3.27E-06	ENSG00000136542
HOXB3	17	3.45	4.26	19.11	3.56E-06	ENSG00000120093
ID4	6	8.38	3.06	8.34	3.77E-06	ENSG00000172201
RIMS1	6	4.88	5.99	63.68	4.35E-06	ENSG00000079841
TCF21	6	3.12	-4.95	-30.95	4.37E-06	ENSG00000118526
FOXF2	6	57.29	-2.91	-7.5	4.43E-06	ENSG00000137273
EMILIN3	20	1	-5.73	-53.08	5.55E-06	ENSG00000183798
APBA2	15	1.99	-5.04	-32.89	5.81E-06	ENSG00000034053
GUCY1B1	4	6.45	-2.67	-6.36	5.98E-06	ENSG00000061918
DSP	6	24.27	2.87	7.31	6.45E-06	ENSG00000096696
TFAP2A	6	5.7	-2.78	-6.86	6.68E-06	ENSG00000137203
ZNF423	16	0.92	-4.03	-16.35	6.84E-06	ENSG00000102935
MMP11	22	9.21	-2.22	-4.66	7.93E-06	ENSG00000099953
GOLGA8B	15	12.1	-2.51	-5.69	8.95E-06	ENSG00000215252
HOMER2	15	0.63	3.3	9.83	9.19E-06	ENSG00000103942
GUCY1A1	4	1.08	-3.73	-13.31	1.03E-05	ENSG00000164116
MYO15B	17	0.74	-5.47	-44.35	1.12E-05	ENSG00000266714
FOXF1	16	2.79	-4.07	-16.76	1.13E-05	ENSG00000103241
PCSK1	5	0.99	5.58	47.77	1.28E-05	ENSG00000175426
HOXB13	17	0.85	-6.34	-81.21	1.33E-05	ENSG00000159184
AFF2	X	0.7	3.87	14.64	1.44E-05	ENSG00000155966
MME	3	91.97	-2.47	-5.55	1.57E-05	ENSG00000196549

KRT19	17	34.94	-2.1	-4.3	1.61E-05	ENSG00000171345
ADRA2A	10	20.12	3.17	8.98	1.87E-05	ENSG00000150594
OSBPL10	3	2.48	-2.02	-4.05	1.93E-05	ENSG00000144645
LYPD6B	2	8.47	4.19	18.29	2.06E-05	ENSG00000150556
COL21A1	6	3.82	-3.31	-9.9	2.06E-05	ENSG00000124749
GPRC5B	16	2.35	-3.1	-8.57	2.08E-05	ENSG00000167191
LTBP4	19	27.89	-2.16	-4.46	2.11E-05	ENSG00000090006
HPSE2	10	0.98	-7.54	-185.7	2.22E-05	ENSG00000172987
MSX1	4	10.55	2.44	5.43	2.39E-05	ENSG00000163132
OXTR	3	79.65	2.42	5.36	2.65E-05	ENSG00000180914
USP9Y	Y	5.11	-14.29	-19,994.46	2.65E-05	ENSG00000114374
HOXA13	7	3.68	-3.34	-10.12	2.73E-05	ENSG00000106031
TCIM	8	2.2	-4.55	-23.37	2.78E-05	ENSG00000176907
FBN2	5	324.05	-3.31	-9.92	2.93E-05	ENSG00000138829
C10orf105	10	2.22	-3.82	-14.12	3.30E-05	ENSG00000214688
B3GNT5	3	1.02	-4.98	-31.67	3.64E-05	ENSG00000176597
PLEKHA6	1	0.7	-3.87	-14.67	3.69E-05	ENSG00000143850
GPC4	X	7.8	2.49	5.62	3.76E-05	ENSG00000076716
INSYN2B	5	4.08	2.25	4.75	3.99E-05	ENSG00000204767
KCNJ6	21	0.38	5.38	41.57	4.10E-05	ENSG00000157542
DDX3Y	Y	9.13	-14	-16,372.73	4.36E-05	ENSG00000067048
PRRT2	16	5.32	-2.19	-4.55	4.39E-05	ENSG00000167371
SEMA4D	9	0.34	-5.11	-34.61	4.73E-05	ENSG00000187764
GABBR2	9	10.38	3.35	10.18	4.73E-05	ENSG00000136928
PTGER3	1	0.69	4.81	27.99	5.80E-05	ENSG00000050628
CLEC2B	12	9.44	2.47	5.53	5.81E-05	ENSG00000110852
TBX4	17	1.27	-4.98	-31.51	5.84E-05	ENSG00000121075
ADAM33	20	96.23	-2.2	-4.6	5.84E-05	ENSG00000149451
DENND2A	7	4.17	-2.05	-4.15	6.15E-05	ENSG00000146966
PNMA8A	19	2.18	-3.25	-9.51	6.30E-05	ENSG00000182013
B4GALNT4	11	4.18	-2.96	-7.8	6.88E-05	ENSG00000182272
THBD	20	3.32	4.11	17.27	7.55E-05	ENSG00000178726
KCNN2	5	0.62	-7.7	-207.25	7.65E-05	ENSG00000080709
LZTS1	8	3.02	2.84	7.14	7.91E-05	ENSG00000061337
TBC1D3D	17	2.72	-8.1	-274.84	7.91E-05	ENSG00000274419
SLC35F2	11	3.15	2.69	6.45	8.43E-05	ENSG00000110660
MAB21L1	13	27.11	-2.77	-6.83	8.64E-05	ENSG00000180660
GJD3	17	3.77	-2.38	-5.22	9.43E-05	ENSG00000183153
FABP3	1	24.72	-2.58	-5.99	9.53E-05	ENSG00000121769
ADRA2C	4	1.53	4.2	18.35	9.53E-05	ENSG00000184160
KDM5D	Y	4.35	-13.5	-11,550.37	1.01E-04	ENSG00000012817
IFI30	19	14.9	2.39	5.23	1.05E-04	ENSG00000216490
PLCB4	20	7.78	2.18	4.54	1.12E-04	ENSG00000101333

CLEC2A		12	1.9	6.06	66.68	1.24E-04	ENSG00000188393
DMKN		19	8.71	-2.33	-5.05	1.24E-04	ENSG00000161249
BDKRB2		14	11.86	-2.65	-6.27	1.25E-04	ENSG00000168398
SLC38A11		2	0.64	-4.47	-22.16	1.34E-04	ENSG00000169507
MMP12		11	1.62	5.2	36.87	1.46E-04	ENSG00000262406
NLGN4Y	Y		3.06	-13.23	-9,638.01	1.47E-04	ENSG00000165246
MMP3		11	209.6	2.56	5.89	1.53E-04	ENSG00000149968
AKAP6		14	1.07	2.6	6.07	1.53E-04	ENSG00000151320
C1R		12	384.68	-2.24	-4.73	1.54E-04	ENSG00000159403
PRLR		5	0.9	4.46	22.07	1.57E-04	ENSG00000113494
TENM3		4	10.11	2.08	4.23	1.62E-04	ENSG00000218336
PTPRN2		7	0.81	-3.88	-14.75	1.70E-04	ENSG00000155093
NKX2-6		8	1.25	7.51	182.23	2.06E-04	ENSG00000180053
PI16		6	13.93	5.39	41.92	2.10E-04	ENSG00000164530
F2RL2		5	13.37	-2.23	-4.68	2.12E-04	ENSG00000164220
TTC9		14	0.89	3.96	15.55	2.12E-04	ENSG00000133985
PPARG		3	2.72	-2.66	-6.32	2.32E-04	ENSG00000132170
ARRB1		11	3.14	-2.12	-4.36	2.32E-04	ENSG00000137486
HOXB4		17	2.26	4.58	23.88	2.34E-04	ENSG00000182742
PTGIS		20	45.42	-2.16	-4.47	2.38E-04	ENSG00000124212
DYSF		2	0.52	3.85	14.41	2.41E-04	ENSG00000135636
PLEKHG1		6	0.84	-3.37	-10.33	2.57E-04	ENSG00000120278
ELANE		19	2.74	-4.34	-20.21	2.64E-04	ENSG00000197561
EPGN		4	0.96	6.96	124.54	2.74E-04	ENSG00000182585
LAT		16	3.69	-3.05	-8.28	2.94E-04	ENSG00000213658
TNIP3		4	0.6	5.53	46.32	3.06E-04	ENSG00000050730
PCSK9		1	3.75	-2.25	-4.76	3.10E-04	ENSG00000169174
HOXD8		2	4.38	2.65	6.28	3.36E-04	ENSG00000175879
HOXD4		2	3.73	3.61	12.17	3.64E-04	ENSG00000170166
COL27A1		9	8.63	-2.01	-4.04	3.74E-04	ENSG00000196739
C1S		12	169.59	-2.14	-4.41	3.74E-04	ENSG00000182326
PAX6		11	0.11	6.14	70.46	3.99E-04	ENSG00000007372
SLC26A7		8	0.41	-6.28	-77.86	4.12E-04	ENSG00000147606
CILP		15	0.38	-4.6	-24.25	4.18E-04	ENSG00000138615
ALPL		1	2.05	-4.32	-20.02	4.25E-04	ENSG00000162551
F8A2	X		4.09	-4.02	-16.25	4.37E-04	ENSG00000288709
APCDD1		18	45.16	-2.55	-5.84	4.47E-04	ENSG00000154856
BMP4		14	3.72	-3.58	-11.97	4.97E-04	ENSG00000125378
RASGRF2		5	0.25	-4.77	-27.21	5.24E-04	ENSG00000113319
TAFA5		22	33.01	3.26	9.58	5.32E-04	ENSG00000219438
ST6GALNAC5		1	2.86	2.89	7.4	5.42E-04	ENSG00000117069
NLGN4X	X		0.21	-5.52	-45.98	5.68E-04	ENSG00000146938
PNMA8B		19	2.47	-2.3	-4.91	6.03E-04	ENSG00000204851
DTX4		11	2.23	-2.45	-5.45	6.21E-04	ENSG00000110042
C1QTNF7		4	0.35	-5.36	-41.06	6.37E-04	ENSG00000163145
C1orf226		1	0.54	-4.3	-19.64	6.43E-04	ENSG00000239887
CDH3		16	0.44	-5.9	-59.54	6.43E-04	ENSG00000062038

SHISA9	16	0.48	6.03	65.15	6.45E-04	ENSG00000237515
MSTN	2	0.92	5.4	42.27	6.58E-04	ENSG00000138379
C4B	6	0.68	-3.59	-12.02	7.12E-04	ENSG00000224389
GLDN	15	0.48	-3.94	-15.32	7.12E-04	ENSG00000186417
GLCCI1	7	3.07	-2.16	-4.46	7.20E-04	ENSG00000106415
APOE	19	3.89	-3.24	-9.48	7.51E-04	ENSG00000130203
RASD1	17	3.13	-3.48	-11.12	8.48E-04	ENSG00000108551
RNF144A	2	2.09	-2.93	-7.6	8.78E-04	ENSG00000151692
PPP4R4	14	0.73	-3.99	-15.92	8.83E-04	ENSG00000119698
CMKLR1	12	0.26	6.07	67.03	9.97E-04	ENSG00000174600
UTY	Y	1.39	-12.1	-4,376.03	9.97E-04	ENSG00000183878
ELN	7	265.89	2.2	4.61	1.01E-03	ENSG00000049540
ICAM5	19	0.61	-4.57	-23.68	1.08E-03	ENSG00000105376
CSGALNACT1	8	1.66	4.67	25.44	1.08E-03	ENSG00000147408
GBP5	1	0.16	6.97	125.42	1.12E-03	ENSG00000154451
EVI2A	17	1.23	3.66	12.61	1.12E-03	ENSG00000126860
CDH10	5	0.87	7.76	216.46	1.15E-03	ENSG00000040731
MMP10	11	0.89	4.67	25.47	1.15E-03	ENSG00000166670
PLPP2	19	3.47	-3.25	-9.54	1.15E-03	ENSG00000141934
OTULINL	5	0.64	-3.63	-12.39	1.23E-03	ENSG00000145569
SLCO2A1	3	0.59	4.58	23.86	1.26E-03	ENSG00000174640
NTRK3	15	0.06	5.43	43.12	1.28E-03	ENSG00000140538
DYNC1I1	7	0.45	4.37	20.66	1.30E-03	ENSG00000158560
IL33	9	0.82	-6.21	-73.81	1.31E-03	ENSG00000137033
ARHGAP6	X	1.98	-2.25	-4.76	1.32E-03	ENSG00000047648
IGFBPL1	9	0.99	4.4	21.11	1.37E-03	ENSG00000137142
RNF144B	6	3.95	2.4	5.28	1.42E-03	ENSG00000137393
ITGA10	1	1.25	3.05	8.27	1.58E-03	ENSG00000143127
ALDH1A3	15	8.08	2.57	5.95	1.60E-03	ENSG00000184254
WNT16	7	3.08	3.51	11.37	1.67E-03	ENSG00000002745
CYP24A1	20	0.9	-5.23	-37.51	1.67E-03	ENSG00000019186
THNSL2	2	7.02	-3.9	-14.94	1.74E-03	ENSG00000144115
PDE3B	11	0.25	-6.02	-64.75	1.74E-03	ENSG00000152270
BCAM	19	6.49	-2.03	-4.07	1.75E-03	ENSG00000187244
EIF1AY	Y	6.46	-11.65	-3,215.35	1.76E-03	ENSG00000198692
SYNPO2L	10	0.51	4.54	23.3	1.77E-03	ENSG00000166317
MCAM	11	9.43	2.12	4.35	1.77E-03	ENSG00000076706
MYH1	17	0.4	6.54	93.28	1.82E-03	ENSG00000109061
SYTL5	X	0.29	-4.76	-27.13	1.86E-03	ENSG00000147041
RUNX3	1	3.52	2.59	6.04	1.87E-03	ENSG00000020633
FMO1	1	0.7	-4.55	-23.37	1.89E-03	ENSG00000010932
gene: ENSG00000288637	4	0.18	-5.6	-48.54	1.94E-03	ENSG00000288637
CHRDL1	X	4.72	-3.48	-11.15	1.94E-03	ENSG00000101938
GBX2	2	0.55	6.65	100.2	2.02E-03	ENSG00000168505
OSBPL6	2	0.98	2.03	4.09	2.04E-03	ENSG00000079156
NFE2L3	7	1.26	-3.41	-10.62	2.04E-03	ENSG00000050344
RSPO2	8	0.39	-6.01	-64.58	2.07E-03	ENSG00000147655

ADA2	22	1.21	-2.35	-5.11	2.07E-03	ENSG00000093072
SMIM43	4	3.48	3.08	8.46	2.09E-03	ENSG00000164112
TNK1	17	0.91	-3.72	-13.13	2.14E-03	ENSG00000174292
TRPV2	17	24.25	2.29	4.89	2.17E-03	ENSG00000187688
LXN	3	14.66	-2.07	-4.21	2.30E-03	ENSG00000079257
KRT8	12	1.69	-2.63	-6.17	2.32E-03	ENSG00000170421
OBSCN	1	0.37	-2.06	-4.16	2.38E-03	ENSG00000154358
RGPD2	2	0.5	3.54	11.64	2.40E-03	ENSG00000185304
PDPN	1	4.83	-2.26	-4.78	2.43E-03	ENSG00000162493
ST6GAL1	3	0.29	-4.96	-31.07	2.43E-03	ENSG00000073849
CACNG7	19	0.51	-4.86	-29.09	2.44E-03	ENSG00000105605
FHAD1	1	0.21	4.77	27.29	2.45E-03	ENSG00000142621
DOK6	18	1.21	2.54	5.81	2.46E-03	ENSG00000206052
PKD1L2	16	0.9	-3.22	-9.31	2.46E-03	ENSG00000166473
CPNE8	12	1.27	3.2	9.18	2.49E-03	ENSG00000139117
ICAM1	19	7.94	-2.33	-5.02	2.52E-03	ENSG00000090339
GDF7	2	0.12	-5.66	-50.62	2.58E-03	ENSG00000143869
ANO4	12	1.89	-2.41	-5.3	2.62E-03	ENSG00000151572
ATP1A2	1	0.45	-4.22	-18.7	2.63E-03	ENSG00000018625
RARRES1	3	1.98	-3.59	-12.07	2.74E-03	ENSG00000118849
HTR2B	2	1.27	-3.66	-12.67	2.77E-03	ENSG00000135914
B3GALT2	1	6.97	2.15	4.44	2.83E-03	ENSG00000162630
PRSS3	9	6.33	-2.71	-6.54	2.89E-03	ENSG00000010438
SLC38A5	X	6.48	2.09	4.25	2.92E-03	ENSG00000017483
KIAA1755	20	0.91	-2.96	-7.78	2.97E-03	ENSG00000149633
ST8SIA2	15	1.26	2.73	6.63	3.12E-03	ENSG00000140557
COL6A6	3	0.95	3.63	12.35	3.24E-03	ENSG00000206384
KIF26A	14	1.33	-4.12	-17.41	3.28E-03	ENSG00000066735
ENPP4	6	0.7	4.76	27.15	3.28E-03	ENSG00000001561
SEC31B	10	1.94	-2.34	-5.07	3.33E-03	ENSG00000075826
PRXL2A	10	0.89	-3.12	-8.69	3.34E-03	ENSG00000122378
HIF3A	19	0.28	-4.53	-23.07	3.39E-03	ENSG00000124440
SLITRK6	13	0.35	-6.89	-118.51	3.52E-03	ENSG00000184564
SIRPB1	20	0.39	4.79	27.66	3.52E-03	ENSG00000101307
F8A3	X	3.53	-3.64	-12.5	3.52E-03	ENSG00000277150
LRATD2	8	0.27	4.49	22.45	3.66E-03	ENSG00000168672
COLGALT2	1	1.63	2.24	4.74	3.81E-03	ENSG00000198756
GSTM1	1	1.47	4.32	20.04	3.81E-03	ENSG00000134184
PDE1C	7	6.86	2.49	5.62	3.92E-03	ENSG00000154678
SCG2	2	0.81	4.67	25.52	4.02E-03	ENSG00000171951
TGFB2	1	2.47	2.6	6.05	4.15E-03	ENSG00000092969
NDNF	4	15.11	2.77	6.82	4.22E-03	ENSG00000173376
ZDHHC15	X	0.15	5.39	41.93	4.24E-03	ENSG00000102383
CYP2S1	19	0.43	-5.65	-50.39	4.31E-03	ENSG00000167600
MAOA	X	0.85	-2.95	-7.74	4.33E-03	ENSG00000189221
MYH2	17	1.48	4.78	27.38	4.35E-03	ENSG00000125414
PLPPR4	1	3	-2.27	-4.83	4.38E-03	ENSG00000117600

CNTNAP3B	9	0.09	-6.25	-76.08	4.38E-03	ENSG00000154529
IGF1	12	0.22	-3.8	-13.95	4.95E-03	ENSG00000017427
GREM2	1	32.93	2.48	5.59	5.04E-03	ENSG00000180875
PDCD6-AHRR	5	0.86	-10.88	-1,878.60	5.32E-03	ENSG00000288622
MKRN3	15	0.19	-4.46	-22.08	5.33E-03	ENSG00000179455
OMD	9	1.76	-2.66	-6.33	5.36E-03	ENSG00000127083
ITGA9	3	0.16	4.94	30.79	5.49E-03	ENSG00000144668
EGFLAM	5	0.46	-4.01	-16.12	5.54E-03	ENSG00000164318
STYK1	12	0.44	4.06	16.67	5.54E-03	ENSG00000060140
ANKRD1	10	5.27	3.77	13.62	5.86E-03	ENSG00000148677
FRMPD3	X	0.24	3.93	15.24	5.87E-03	ENSG00000147234
KCNAB1	3	0.29	4.58	23.94	5.87E-03	ENSG00000169282
LCNL1	9	0.8	-4.16	-17.82	5.92E-03	ENSG00000214402
GABRA5	15	0.43	4.26	19.15	6.13E-03	ENSG00000186297
ALDH1A1	9	280.12	-4.58	-23.85	6.34E-03	ENSG00000165092
EPHB1	3	0.9	3	8	6.37E-03	ENSG00000154928
STMN2	8	7.01	-2.02	-4.06	6.81E-03	ENSG00000104435
TGFA	2	0.44	4.65	25.18	7.11E-03	ENSG00000163235
DLX1	2	1.08	3.28	9.72	7.39E-03	ENSG00000144355
MFAP3L	4	1.84	2.3	4.91	7.55E-03	ENSG00000198948
KCNH5	14	0.21	-4.01	-16.13	8.95E-03	ENSG00000140015
TDRD9	14	0.23	-4.16	-17.87	9.02E-03	ENSG00000156414
CADM3	1	0.27	6.53	92.19	9.08E-03	ENSG00000162706
BMPR1B	4	0.53	3.26	9.55	9.08E-03	ENSG00000138696
CRACD	4	0.52	-3.21	-9.24	9.10E-03	ENSG00000109265
PCDH1	5	0.43	3.32	9.96	9.56E-03	ENSG00000156453
CORIN	4	1.93	-3.85	-14.38	9.76E-03	ENSG00000145244
ANO3	11	1.33	-2.6	-6.07	0.01	ENSG00000134343
GRIN3B	19	1.25	-2.78	-6.86	0.01	ENSG00000116032
PLEKHA7	11	0.38	3.22	9.33	0.01	ENSG00000166689
SHOX	X	2.7	2.83	7.1	0.01	ENSG00000185960
ADRA1D	20	2.57	2.22	4.64	0.01	ENSG00000171873
STXBP2	19	1.89	-2.75	-6.72	0.01	ENSG00000076944
EREG	4	0.15	-4.94	-30.63	0.01	ENSG00000124882
ABI3	17	0.54	5.31	39.57	0.01	ENSG00000108798
AQP1	7	2.81	2.29	4.88	0.01	ENSG00000240583
GREB1L	18	0.41	3.26	9.56	0.01	ENSG00000141449
KCNAB3	17	0.86	-2.92	-7.57	0.01	ENSG00000170049
RNF182	6	1.69	2.46	5.5	0.01	ENSG00000180537
SLC10A6	4	0.43	-5	-32.09	0.01	ENSG00000145283
MC4R	18	1.06	3.8	13.89	0.01	ENSG00000166603
PADI2	1	0.62	4.05	16.56	0.01	ENSG00000117115
STUM	1	0.12	-4.16	-17.89	0.01	ENSG00000203685
RGL3	19	0.5	-3.6	-12.17	0.01	ENSG00000205517
SEMA4G	10	1.34	-2.5	-5.65	0.01	ENSG00000095539
SBSPON	8	0.79	-10.09	-1,088.27	0.02	ENSG00000164764
PIK3C2B	1	1.02	-2.41	-5.3	0.02	ENSG00000133056

HHEX	10	1.12	-3.32	-9.98	0.02	ENSG00000152804
CD79B	17	0.64	-5.97	-62.59	0.02	ENSG00000007312
ADHFE1	8	2.21	-2.59	-6	0.02	ENSG00000147576
CNKSR2	X	0.45	2.35	5.11	0.02	ENSG00000149970
NPTX1	17	2.19	-2.26	-4.81	0.02	ENSG00000171246
NDUFA4L2	12	7.04	-2.11	-4.33	0.02	ENSG00000185633
NOXA1	9	1.08	-3.43	-10.75	0.02	ENSG00000188747
ZIC4	3	0.85	3.05	8.27	0.02	ENSG00000174963
gene:ENSG00000244255	6	0.16	-4.81	-28.14	0.02	ENSG00000244255
PDE8B	5	0.14	-4.22	-18.67	0.02	ENSG00000113231
BCL2L11	2	0.97	-2.37	-5.16	0.02	ENSG00000153094
gene:ENSG00000287908	12	1.13	-2.83	-7.09	0.02	ENSG00000287908
MGAT3	22	0.1	-5.57	-47.4	0.02	ENSG00000128268
CD36	7	0.22	-3.55	-11.68	0.02	ENSG00000135218
FAT3	11	0.49	2.76	6.77	0.02	ENSG00000165323
RFLNA	12	0.87	2.94	7.66	0.02	ENSG00000178882
NPIPB15	16	2.07	-2.69	-6.47	0.02	ENSG00000196436
GRHL1	2	0.9	-2.86	-7.25	0.02	ENSG00000134317
TM6SF1	15	0.24	-5.55	-46.76	0.02	ENSG00000136404
PTPRQ	12	0.84	-2.35	-5.09	0.02	ENSG00000139304
FCRLA	1	0.94	3.21	9.22	0.02	ENSG00000132185
MEDAG	13	13.33	2.05	4.15	0.02	ENSG00000102802
CNGA3	2	0.29	4.54	23.32	0.02	ENSG00000144191
FGFBP2	4	0.62	-5.79	-55.39	0.02	ENSG00000137441
COL26A1	7	0.22	-5.7	-51.94	0.02	ENSG00000160963
SLITRK1	13	0.87	4.76	27.12	0.02	ENSG00000178235
FCHO1	19	0.44	-3.52	-11.46	0.02	ENSG00000130475
SYNDIG1	20	2.21	2.81	6.99	0.02	ENSG00000101463
ITGA11	15	81.81	2.14	4.42	0.02	ENSG00000137809
GAL	11	3.32	3.01	8.03	0.02	ENSG00000069482
NAP1L3	X	2.18	2.29	4.88	0.02	ENSG00000186310
TMEM178A	2	1.25	-3.35	-10.22	0.02	ENSG00000152154
gene:ENSG00000287542	4	1.56	2.03	4.1	0.02	ENSG00000287542
GPC3	X	0.31	-3.79	-13.86	0.02	ENSG00000147257
STON2	14	0.33	2.85	7.23	0.02	ENSG00000140022
ST8SIA1	12	0.21	3.08	8.44	0.02	ENSG00000111728
SAP25	7	1.97	-3.17	-8.97	0.02	ENSG00000205307
PABPC1L	20	3.08	-2.06	-4.17	0.02	ENSG00000101104
KCNJ15	21	0.32	3.56	11.83	0.03	ENSG00000157551
C16orf74	16	2.17	-2.53	-5.76	0.03	ENSG00000154102
CD7	17	0.61	-3.51	-11.37	0.03	ENSG00000173762
KRT18	12	5.19	-2.38	-5.22	0.03	ENSG00000111057
CLUL1	18	0.18	-4.81	-28.02	0.03	ENSG00000079101
CCN4	8	5.08	2.04	4.11	0.03	ENSG00000104415
NTSR1	20	0.24	-3.98	-15.77	0.03	ENSG00000101188
HGF	7	1.12	-2.29	-4.9	0.03	ENSG00000019991
PTGER1	19	3	-2.71	-6.56	0.03	ENSG00000160951

STON1-GTF2A1L	2	0.6	-3.73	-13.22	0.03	ENSG00000068781
BLOC1S5-TXNDC5	6	0.39	-4.5	-22.57	0.03	ENSG00000259040
TMEM108	3	0.07	-4.23	-18.82	0.03	ENSG00000144868
PTPRB	12	0.85	3.48	11.17	0.03	ENSG00000127329
HTR1B	6	0.24	-3.91	-15.05	0.03	ENSG00000135312
ERG	21	0.22	4.43	21.58	0.03	ENSG00000157554
TNFRSF25	1	1.69	-2.79	-6.92	0.03	ENSG00000215788
EPS8L1	19	0.54	-3.12	-8.7	0.03	ENSG00000131037
ADAMTSL3	15	0.35	4.87	29.29	0.03	ENSG00000156218
ISL1	5	0.81	-9.48	-716.19	0.03	ENSG00000016082
INHBE	12	2.08	-2.49	-5.63	0.03	ENSG00000139269
KLHL13	X	0.33	-2.93	-7.61	0.04	ENSG00000003096
FXYD1	19	4.14	-2.28	-4.87	0.04	ENSG00000266964
CYP2D6	22	0.28	-4.42	-21.43	0.04	ENSG00000100197
SHANK2	11	0.87	-2.11	-4.31	0.04	ENSG00000162105
CFI	4	1.72	-3.43	-10.76	0.04	ENSG00000205403
KRTAP1-1	17	0.66	4.18	18.13	0.04	ENSG00000188581
ADGRB3	6	0.13	-4.62	-24.62	0.04	ENSG00000135298
EGFL6	X	2.14	-2.37	-5.19	0.04	ENSG00000198759
SEC14L5	16	0.18	-3.26	-9.58	0.04	ENSG00000103184
PDZD2	5	0.06	-3.81	-13.99	0.04	ENSG00000133401
MOV10L1	22	0.58	-2.58	-5.96	0.04	ENSG00000073146
TRIM17	1	0.13	-4.43	-21.49	0.04	ENSG00000162931
KCTD4	13	0.68	3.6	12.13	0.04	ENSG00000180332
PLK5	19	0.58	-9.58	-764.98	0.04	ENSG00000185988
TFPI2	7	7.93	2.29	4.89	0.04	ENSG00000105825
APBB1IP	10	2.44	2.36	5.15	0.04	ENSG00000077420
MAFB	20	2.64	2.08	4.23	0.04	ENSG00000204103
TMEM176B	7	0.5	-3.44	-10.82	0.05	ENSG00000106565
RGS11	16	3.63	-2.02	-4.05	0.05	ENSG00000076344
PSG1	19	7.82	2.05	4.15	0.05	ENSG00000231924
GAD1	2	0.15	3.45	10.91	0.05	ENSG00000128683
RGS2	1	3.86	-2.49	-5.6	0.05	ENSG00000116741
SOSTDC1	7	0.21	-5.4	-42.11	0.05	ENSG00000171243
FAM162B	6	1.56	-9.21	-590.23	0.05	ENSG00000183807
gene:ENSG00000285839	1	0.39	-3.7	-12.95	0.05	ENSG00000285839
UBE2QL1	5	0.09	4.66	25.32	0.05	ENSG00000215218
AP1M2	19	0.27	4.59	24.01	0.05	ENSG00000129354
PAX9	14	0.37	4.02	16.21	0.05	ENSG00000198807
CGNL1	15	0.79	2.24	4.74	0.05	ENSG00000128849
TLCD4	1	0.23	3.01	8.07	0.05	ENSG00000152078
PCSK2	20	0.1	5.48	44.5	0.05	ENSG00000125851
ATP6V1G3	1	0.87	3.52	11.47	0.05	ENSG00000151418
ABCA9	17	0.8	-2.22	-4.65	0.05	ENSG00000154258

Appendix D DEG in the MDC1A treated cells Vs MDC1A untreated

Appendix Table 2.

Name	Chromosome	Max group mean	Log_2 fold change	Fold change	FDR p-value	ENSEMBL
OAS1	12	25.04	8.76	433.84	1.97E-78	ENSG00000089127
IFI44L	1	28.59	7.15	142.5	3.86E-65	ENSG00000137959
IFIT2	10	183.55	6.86	115.77	2.27E-57	ENSG00000119922
CMPK2	2	20.82	8.47	354.61	1.62E-50	ENSG00000134326
MX1	21	102.08	7.5	180.44	1.92E-47	ENSG00000157601
HERC5	4	14.37	7.12	139.49	1.50E-43	ENSG00000138646
OASL	12	62.12	9.34	648.67	2.13E-43	ENSG00000135114
PMAIP1	18	89.34	5.46	43.95	7.62E-40	ENSG00000141682
IFIT3	10	261.23	5.62	49.19	7.82E-35	ENSG00000119917
BST2	19	37.18	7.29	155.99	1.89E-34	ENSG00000130303
IFIT1	10	106.01	5.59	48.28	6.32E-34	ENSG00000185745
RSAD2	2	100.52	10.26	1,230.17	8.34E-34	ENSG00000134321
IFI44	1	136.18	4.97	31.26	2.26E-33	ENSG00000137965
ITGA2	5	72.04	5.18	36.15	5.27E-33	ENSG00000164171
OAS3	12	29.39	5.25	38.15	9.00E-30	ENSG00000111331
IFIH1	2	21.34	4.78	27.44	1.86E-28	ENSG00000115267
DDX58	9	42.67	4.63	24.81	2.90E-28	ENSG00000107201
IFI6	1	1,426.24	5.51	45.52	3.28E-28	ENSG00000126709
DDX60	4	17.42	4.4	21.05	3.46E-28	ENSG00000137628
HERC6	4	52.54	5.21	36.97	2.24E-26	ENSG00000138642
IFI27	14	29.38	5.23	37.55	9.62E-25	ENSG00000165949
ISG15	1	564.65	4.91	29.97	1.84E-23	ENSG00000187608
OAS2	12	36.54	5.77	54.66	1.42E-19	ENSG00000111335
CTSS	1	9.18	4.61	24.5	5.65E-19	ENSG00000163131
SAMD9	7	34.55	2.78	6.88	9.66E-19	ENSG00000205413
GBP4	1	4.68	5.39	41.88	1.51E-18	ENSG00000162654
PLSCR1	3	43.67	2.85	7.22	1.90E-17	ENSG00000188313
NCF2	1	12.05	6.12	69.79	4.35E-17	ENSG00000116701
PARP14	3	27.4	2.56	5.9	1.36E-16	ENSG00000173193
IFITM1	11	359.15	3.79	13.8	1.81E-15	ENSG00000185885
SPP1	4	12.09	4.35	20.45	5.13E-15	ENSG00000118785
XAF1	17	29.52	3.16	8.94	8.17E-15	ENSG00000132530
MX2	21	42.49	5.22	37.26	1.32E-14	ENSG00000183486
TSPAN18	11	8.17	-3.39	-10.48	2.10E-14	ENSG00000157570
HLA-F	6	11.75	3.78	13.72	8.10E-14	ENSG00000204642
PLAAT4	11	23.97	4.28	19.41	1.20E-13	ENSG00000133321
USP18	22	23.16	4.08	16.87	2.21E-13	ENSG00000184979
WNT2	7	4.8	-5.27	-38.5	2.73E-13	ENSG00000105989

EPSTI1	13	15.17	3.21	9.28	3.61E-13	ENSG00000133106
CCL5	17	10.61	8.09	273.1	4.53E-13	ENSG00000271503
CDCP1	3	6.3	3.27	9.65	5.96E-13	ENSG00000163814
CCL26	7	23.35	4.39	20.91	9.14E-13	ENSG00000006606
IRF7	11	17.91	3.27	9.64	1.04E-12	ENSG00000185507
TRIM14	9	15.75	2.76	6.77	1.13E-12	ENSG00000106785
ACTN2	1	2.26	8.97	502.79	1.20E-12	ENSG00000077522
LMOD1	1	17.72	-3.11	-8.61	1.23E-12	ENSG00000163431
DHX58	17	17.39	2.7	6.49	1.08E-11	ENSG00000108771
COL5A3	19	10.3	-2.56	-5.91	2.72E-11	ENSG00000080573
DHRS3	1	14.34	-3.2	-9.19	4.45E-11	ENSG00000162496
THEMIS2	1	8.42	3.96	15.54	5.45E-11	ENSG00000130775
RTP4	3	10.74	4.63	24.71	2.02E-10	ENSG00000136514
TNFAIP3	6	9.07	3.33	10.07	2.02E-10	ENSG00000118503
CEMIP	15	364.55	-3.19	-9.1	2.23E-10	ENSG00000103888
PARP12	7	13.62	2.61	6.12	5.39E-10	ENSG00000059378
TNFSF10	3	3.1	6.82	112.88	7.75E-10	ENSG00000121858
AKR1C1	10	27.89	2.88	7.35	8.63E-10	ENSG00000187134
NT5DC2	3	37.54	-1.97	-3.92	9.10E-10	ENSG00000168268
TMEM158	3	55.27	3.27	9.67	1.12E-09	ENSG00000249992
ADRA1D	20	17.4	2.49	5.6	1.52E-09	ENSG00000171873
ISG20	15	11.09	3.73	13.27	1.71E-09	ENSG00000172183
TYMP	22	56.84	3.48	11.2	2.74E-09	ENSG00000025708
CRISPLD2	16	13.18	-2.02	-4.04	3.74E-09	ENSG00000103196
XKR8	1	24.68	2.38	5.2	4.05E-09	ENSG00000158156
NOTCH3	19	7.8	-2.31	-4.96	6.48E-09	ENSG00000074181
SAMD9L	7	25.95	2.65	6.29	9.82E-09	ENSG00000177409
AKAP6	14	1.07	-3.08	-8.46	1.02E-08	ENSG00000151320
PRICKLE1	12	2.1	-3.19	-9.13	2.01E-08	ENSG00000139174
LMCD1	3	21.15	-2.41	-5.32	2.81E-08	ENSG00000071282
ACTA2	10	168.57	-2.69	-6.45	2.81E-08	ENSG00000107796
SOD2	6	35.51	2.93	7.62	3.54E-08	ENSG00000112096
CFH	1	22.33	3.4	10.57	4.02E-08	ENSG00000000971
RHOB	2	34.94	-1.88	-3.68	4.13E-08	ENSG00000143878
IFI35	17	66.71	2.01	4.02	4.34E-08	ENSG00000068079
BATF2	11	5.9	4.17	18.01	5.49E-08	ENSG00000168062
FOXF1	16	6.28	5.12	34.76	5.68E-08	ENSG00000103241
ASNS	7	24.43	-1.83	-3.56	6.50E-08	ENSG00000070669
HELZ2	20	16.87	2.59	6.03	6.50E-08	ENSG00000130589
COL13A1	10	20.11	2.35	5.1	8.35E-08	ENSG00000197467
RFX8	2	13.53	2.59	6.04	8.58E-08	ENSG00000196460
F3	1	25.79	-2.27	-4.83	8.62E-08	ENSG00000117525
EFNB2	13	20.2	-2.29	-4.9	9.21E-08	ENSG00000125266
SYNPO2	4	9.82	-2.61	-6.1	9.89E-08	ENSG00000172403
ELN	7	265.89	-2.55	-5.85	1.07E-07	ENSG00000049540
ADM2	22	7.56	-2.78	-6.87	1.13E-07	ENSG00000128165
HLA-B	6	488.53	3.02	8.11	2.55E-07	ENSG00000234745

RCAN2	6	22.97	-2.12	-4.35	2.62E-07	ENSG00000172348
PDGFD	11	4.4	-2.97	-7.81	2.95E-07	ENSG00000170962
CNN1	19	13.14	-3.46	-10.97	2.98E-07	ENSG00000130176
PARP9	3	21.01	2.21	4.64	2.99E-07	ENSG00000138496
PNP	14	23.95	2.17	4.51	4.05E-07	ENSG00000198805
RFLNB	17	42.68	-2.24	-4.74	5.53E-07	ENSG00000183688
B4GALT5	20	73.94	2.26	4.77	7.84E-07	ENSG00000158470
CNTN6	3	2.15	9.58	765.74	9.51E-07	ENSG00000134115
DAPK1	9	2.71	-2.92	-7.56	1.04E-06	ENSG00000196730
ARID5B	10	25.25	-1.82	-3.54	1.05E-06	ENSG00000150347
KCND3	1	6.86	-2.99	-7.92	1.18E-06	ENSG00000171385
SVEP1	9	10.73	-2.16	-4.48	1.35E-06	ENSG00000165124
SLC16A6	17	4.27	5.35	40.83	1.39E-06	ENSG00000108932
IL4I1	19	2.86	4.88	29.52	1.42E-06	ENSG00000104951
SLC7A11	4	10.8	-2.71	-6.53	1.45E-06	ENSG00000151012
NREP	5	30.73	-1.92	-3.77	2.11E-06	ENSG00000134986
WNT5A	3	64.5	-2.49	-5.63	2.31E-06	ENSG00000114251
SLCO4A1	20	1.15	6.66	100.85	2.37E-06	ENSG00000101187
ZC3HAV1	7	34.5	1.99	3.98	2.43E-06	ENSG00000105939
GRIP2	3	0.56	5.72	52.55	2.98E-06	ENSG00000144596
MKX	10	19.17	-1.72	-3.29	2.98E-06	ENSG00000150051
TAGLN	11	232.98	-2.97	-7.83	2.98E-06	ENSG00000149591
SHROOM3	4	8.71	-3.06	-8.33	3.14E-06	ENSG00000138771
METTL7A	12	11.96	2.51	5.69	3.27E-06	ENSG00000185432
PARP10	8	13.46	2.02	4.07	3.88E-06	ENSG00000178685
COMP	19	20.01	-2.77	-6.84	4.38E-06	ENSG00000105664
NLRC5	16	8.88	1.6	3.02	4.57E-06	ENSG00000140853
KCNQ5	6	12.98	3.22	9.29	5.09E-06	ENSG00000185760
LGALS3BP	17	56.53	2.37	5.18	5.28E-06	ENSG00000108679
SAMHD1	20	20.37	2.24	4.72	5.57E-06	ENSG00000101347
ETV1	7	5.23	2.03	4.09	5.87E-06	ENSG00000006468
CNIH3	1	15.69	2.23	4.7	6.91E-06	ENSG00000143786
ADRA2A	10	20.12	-2.35	-5.11	6.91E-06	ENSG00000150594
C11orf87	11	7.61	-2.52	-5.73	6.91E-06	ENSG00000185742
PSMB9	6	32.02	2.34	5.07	7.28E-06	ENSG00000240065
SP110	2	6.75	1.72	3.3	7.28E-06	ENSG00000135899
DDX60L	4	9.07	1.84	3.57	7.38E-06	ENSG00000181381
LBH	2	125.25	-2.27	-4.84	7.86E-06	ENSG00000213626
FHL1	X	40.61	-1.87	-3.66	9.45E-06	ENSG00000022267
PGF	14	16.51	3.18	9.04	9.53E-06	ENSG00000119630
RHEBL1	12	5.18	4.11	17.31	9.63E-06	ENSG00000167550
PCK2	14	21.75	-1.69	-3.22	9.98E-06	ENSG00000100889
SLC15A3	11	16.4	2.53	5.79	1.10E-05	ENSG00000110446
CXCL8	4	3.45	5.47	44.37	1.11E-05	ENSG00000169429
TAP2	6	13.5	1.69	3.22	1.15E-05	ENSG00000204267
HRK	12	1.03	4.08	16.86	1.29E-05	ENSG00000135116
CRYM	16	1.23	6.25	76.31	1.48E-05	ENSG00000103316

SP100	2	25.77	1.48	2.79	1.59E-05	ENSG00000067066
BTN3A3	6	14.65	1.88	3.69	1.68E-05	ENSG00000111801
GJD3	17	5.53	2.81	7	1.68E-05	ENSG00000183153
EFR3B	2	1.76	3.25	9.52	1.75E-05	ENSG00000084710
DKK2	4	8.33	-3.81	-14.07	1.80E-05	ENSG00000155011
CFB	6	10.59	2.7	6.5	1.82E-05	ENSG00000243649
TAP1	6	59.04	2.17	4.49	1.86E-05	ENSG00000168394
TYSND1	10	8.82	2.14	4.42	1.95E-05	ENSG00000156521
VEGFC	4	132.38	1.97	3.91	2.49E-05	ENSG00000150630
SIPA1L2	1	4.62	-1.88	-3.69	2.96E-05	ENSG00000116991
GPC4	X	7.8	-2.38	-5.19	2.97E-05	ENSG00000076716
COL8A1	3	233.93	-2.23	-4.7	3.35E-05	ENSG00000144810
SQOR	15	40.27	2.12	4.34	3.36E-05	ENSG00000137767
ACO1	9	13.81	-1.62	-3.08	3.86E-05	ENSG00000122729
FGF9	13	0.6	-5	-31.99	4.70E-05	ENSG00000102678
PENK	8	8.31	2.21	4.64	4.72E-05	ENSG00000181195
TNFRSF8	1	0.74	5.17	36	4.77E-05	ENSG00000120949
AFF3	2	3.48	-2.32	-4.98	6.24E-05	ENSG00000144218
SLC7A5	16	52.76	-1.81	-3.51	6.49E-05	ENSG00000103257
TRIM22	11	45.5	1.7	3.24	6.49E-05	ENSG00000132274
UBE2L6	11	70.34	1.88	3.68	6.63E-05	ENSG00000156587
PDE1C	7	6.86	-2.25	-4.75	6.75E-05	ENSG00000154678
IRAG1	11	2.09	-3.63	-12.4	8.00E-05	ENSG00000072952
DIO2	14	3.16	-4.92	-30.37	8.00E-05	ENSG00000211448
ITPR3	6	28.46	1.84	3.57	8.07E-05	ENSG00000096433
SLC6A15	12	1.01	3.01	8.06	8.07E-05	ENSG00000072041
ANGPTL4	19	7.25	2.6	6.07	8.08E-05	ENSG00000167772
CDH11	16	48.7	-2.01	-4.03	8.46E-05	ENSG00000140937
CNN2	19	204.57	-2.02	-4.05	8.61E-05	ENSG00000064666
GBP5	1	2.69	3.78	13.75	9.30E-05	ENSG00000154451
THBS1	15	1,760.26	-2.29	-4.89	9.30E-05	ENSG00000137801
PDE5A	4	4.01	-2.11	-4.31	1.05E-04	ENSG00000138735
DTX3L	3	32.68	1.75	3.36	1.14E-04	ENSG00000163840
SMOX	20	17.14	1.78	3.44	1.14E-04	ENSG00000088826
ADAMTS5	21	17.41	-1.75	-3.36	1.18E-04	ENSG00000154736
PLAU	10	34.83	2.18	4.53	1.42E-04	ENSG00000122861
PHACTR3	20	2.19	-3.87	-14.57	1.42E-04	ENSG00000087495
SUMF1	3	9.71	-1.54	-2.9	1.45E-04	ENSG00000144455
CBS	21	17.9	-1.68	-3.2	1.51E-04	ENSG00000160200
AKR1C2	10	26.23	2.92	7.56	1.61E-04	ENSG00000151632
KCNB1	20	0.56	-3.79	-13.79	1.72E-04	ENSG00000158445
LOXL3	2	34.26	1.98	3.94	1.87E-04	ENSG00000115318
VGLL3	3	34.77	-2.01	-4.02	1.96E-04	ENSG00000206538
MMP1	11	1,690.07	4.68	25.58	2.05E-04	ENSG00000196611
HLA-C	6	968.07	2.31	4.98	2.12E-04	ENSG00000204525
PSAT1	9	78.91	-2.07	-4.21	2.22E-04	ENSG00000135069
TNFSF13B	13	1.65	4.5	22.62	2.27E-04	ENSG00000102524

COL17A1	10	0.63	4.9	29.95	2.52E-04	ENSG00000065618
SNX18	5	17.74	-1.64	-3.12	2.59E-04	ENSG00000178996
LAMA1	18	1.96	2.06	4.18	2.66E-04	ENSG00000101680
IFI30	19	70.82	1.99	3.96	2.68E-04	ENSG00000216490
FAM172A	5	5.49	-2.18	-4.52	3.23E-04	ENSG00000113391
CCN4	8	5.08	-2.06	-4.17	3.23E-04	ENSG00000104415
B2M	15	1,936.65	2.1	4.28	3.23E-04	ENSG00000166710
ODF3B	22	6.7	3.34	10.13	3.23E-04	ENSG00000177989
PODXL	7	277.77	2.97	7.83	3.28E-04	ENSG00000128567
SHFL	19	31	1.4	2.63	3.28E-04	ENSG00000130813
TMEM51	1	2.78	3.36	10.29	3.37E-04	ENSG00000171729
APOL1	22	13.58	3.32	10.02	3.64E-04	ENSG00000100342
BAG2	6	12.01	-1.35	-2.54	3.81E-04	ENSG00000112208
RENBP	X	13.16	2.72	6.58	3.87E-04	ENSG00000102032
VSIR	10	23.11	-1.9	-3.73	4.06E-04	ENSG00000107738
HK2	2	26.22	2.13	4.37	4.07E-04	ENSG00000159399
PRKCA	17	14.78	-1.95	-3.87	4.19E-04	ENSG00000154229
STING1	5	137.22	1.97	3.92	4.23E-04	ENSG00000184584
NEDD9	6	5.06	-2.3	-4.94	4.36E-04	ENSG00000111859
SLC5A3	21	41.08	2.28	4.84	4.43E-04	ENSG00000198743
HMGA2	12	4.06	2.16	4.45	4.51E-04	ENSG00000149948
GASK1B	4	4.02	-1.9	-3.73	4.66E-04	ENSG00000164125
ITGB3	17	7.91	2.24	4.72	4.66E-04	ENSG00000259207
KLF4	9	31.48	1.5	2.83	4.70E-04	ENSG00000136826
ITGA11	15	81.81	-2.03	-4.08	4.70E-04	ENSG00000137809
MYOC	1	3	5.03	32.71	4.80E-04	ENSG00000034971
TNFRSF21	6	26.77	2.12	4.35	4.93E-04	ENSG00000146072
SEPTIN11	4	157.76	-1.91	-3.77	5.01E-04	ENSG00000138758
DUSP6	12	6.66	2.18	4.52	5.03E-04	ENSG00000139318
BDKRB1	14	14.72	2.31	4.96	5.06E-04	ENSG00000100739
CXCL1	4	11.75	3.43	10.8	5.29E-04	ENSG00000163739
CCN2	6	409.12	-2.08	-4.24	5.29E-04	ENSG00000118523
ERAP2	5	20.75	1.7	3.24	5.33E-04	ENSG00000164308
DUSP4	8	3.41	2.16	4.46	5.42E-04	ENSG00000120875
CTSK	1	406.02	2.1	4.3	5.71E-04	ENSG00000143387
ARHGAP27	17	1.77	2.78	6.89	5.71E-04	ENSG00000159314
MAMLD1	X	9.14	-1.82	-3.53	6.30E-04	ENSG00000013619
AJUBA	14	14.36	-1.49	-2.81	6.36E-04	ENSG00000129474
APOL3	22	6.15	1.91	3.75	6.36E-04	ENSG00000128284
HMGCS1	5	30.43	1.88	3.69	6.56E-04	ENSG00000112972
TRIM21	11	24.13	1.59	3.01	6.74E-04	ENSG00000132109
OLFM2	19	6.09	-2.22	-4.67	6.74E-04	ENSG00000105088
PHGDH	1	31.4	-1.55	-2.94	6.95E-04	ENSG00000092621
COL8A2	1	13.58	-1.63	-3.09	6.99E-04	ENSG00000171812
ETV7	6	3.38	3.24	9.46	7.02E-04	ENSG00000010030
MT2A	16	682.75	2.01	4.02	7.19E-04	ENSG00000125148
PLXNA2	1	4.02	1.8	3.49	7.39E-04	ENSG00000076356

PKP4	2	9.68	-1.34	-2.53	7.39E-04	ENSG00000144283
gene:ENSG00000288637	4	0.32	6.29	78.26	7.66E-04	ENSG00000288637
MYH1	17	0.4	-6.88	-117.53	7.72E-04	ENSG00000109061
TENM2	5	24.98	-1.97	-3.91	8.12E-04	ENSG00000145934
ZNF469	16	2.42	-1.71	-3.26	8.55E-04	ENSG00000225614
PTGIS	20	9.37	-2.07	-4.21	8.79E-04	ENSG00000124212
MYH2	17	1.48	-5.12	-34.69	8.87E-04	ENSG00000125414
CALD1	7	306.05	-1.87	-3.65	9.15E-04	ENSG00000122786
BTN3A1	6	11.89	1.82	3.53	9.21E-04	ENSG00000026950
TMEM132A	11	14.12	2.27	4.82	9.21E-04	ENSG00000006118
NAALADL2	3	1.97	-2	-4	9.24E-04	ENSG00000177694
RAB30	11	3.13	-1.51	-2.85	9.72E-04	ENSG00000137502
FZD8	10	5.63	2.49	5.6	9.78E-04	ENSG00000177283
NRROS	3	1.01	4.18	18.08	1.01E-03	ENSG00000174004
ZMAT3	3	8.81	-1.54	-2.92	1.09E-03	ENSG00000172667
ESM1	5	3.23	3.01	8.04	1.09E-03	ENSG00000164283
NT5E	6	285.46	1.77	3.42	1.16E-03	ENSG00000135318
ADH1B	4	0.96	-4.34	-20.29	1.20E-03	ENSG00000196616
LY6E	8	521.4	2.21	4.62	1.20E-03	ENSG00000160932
RPS6KC1	1	18.36	1.46	2.74	1.22E-03	ENSG00000136643
UBA7	3	19.71	1.46	2.75	1.27E-03	ENSG00000182179
TNFRSF10D	8	8.86	-1.86	-3.64	1.32E-03	ENSG00000173530
UBE4B	1	11.84	-1.15	-2.22	1.33E-03	ENSG00000130939
AKAP12	6	21.17	-1.84	-3.58	1.38E-03	ENSG00000131016
FOXC1	6	6.72	-2.04	-4.1	1.41E-03	ENSG00000054598
ACAN	15	52.64	-5.32	-39.99	1.45E-03	ENSG00000157766
E2F7	12	3.21	1.81	3.52	1.48E-03	ENSG00000165891
MYL9	20	363.99	-1.72	-3.29	1.48E-03	ENSG00000101335
RNF149	2	23.76	1.18	2.27	1.60E-03	ENSG00000163162
PRELP	1	10.15	-2.01	-4.03	1.65E-03	ENSG00000188783
TNFSF18	1	1.02	-4.05	-16.61	1.67E-03	ENSG00000120337
PRSS35	6	1.86	3.82	14.17	1.73E-03	ENSG00000146250
SH2D5	1	5.4	2.01	4.02	1.77E-03	ENSG00000189410
PXDN	2	109.44	-1.69	-3.22	1.99E-03	ENSG00000130508
CYP1B1	2	20.89	-1.66	-3.16	1.99E-03	ENSG00000138061
RHOBTB1	10	9.1	-1.64	-3.12	2.02E-03	ENSG00000072422
RPS6KA2	6	26.99	-1.3	-2.46	2.15E-03	ENSG00000071242
IRF1	5	11.91	1.65	3.15	2.23E-03	ENSG00000125347
KLF5	13	4.72	-1.98	-3.94	2.33E-03	ENSG00000102554
C3	19	1.58	3.53	11.57	2.36E-03	ENSG00000125730
NOTUM	17	1.5	4.37	20.64	2.38E-03	ENSG00000185269
IDI1	10	25.42	1.24	2.36	2.48E-03	ENSG00000067064
PSME2	14	55.51	1.23	2.34	2.48E-03	ENSG00000100911
LAP3	4	52.22	1.48	2.79	2.51E-03	ENSG00000002549
FOSL1	11	136.85	1.54	2.92	2.63E-03	ENSG00000175592
DUSP8	11	0.53	-3.78	-13.72	2.67E-03	ENSG00000184545
PRRG4	11	0.32	7.02	129.9	2.67E-03	ENSG00000135378

IGFBP3	7	1,895.10	-2.15	-4.43	2.70E-03	ENSG00000146674
CLDN4	7	0.63	3.77	13.62	2.72E-03	ENSG00000189143
IRAK2	3	3.54	2.31	4.96	2.74E-03	ENSG00000134070
HES4	1	4.98	3.41	10.66	2.75E-03	ENSG00000188290
ALPK2	18	34.79	-1.54	-2.91	2.75E-03	ENSG00000198796
NPC1	18	24.57	1.53	2.89	2.78E-03	ENSG00000141458
ADGRG1	16	3.37	2.69	6.44	2.87E-03	ENSG00000205336
ARHGAP28	18	0.49	-3.35	-10.19	3.02E-03	ENSG00000088756
IL15RA	10	4.94	1.96	3.89	3.17E-03	ENSG00000134470
NNMT	11	80.2	-1.6	-3.02	3.21E-03	ENSG00000166741
STRIP2	7	1.7	2.54	5.81	3.33E-03	ENSG00000128578
ANGPTL2	9	150.54	1.71	3.27	3.33E-03	ENSG00000136859
OXTR	3	79.65	-2.48	-5.59	3.40E-03	ENSG00000180914
P4HA3	11	10.64	1.58	3	3.40E-03	ENSG00000149380
CYP24A1	20	0.76	4.79	27.66	3.40E-03	ENSG00000019186
PSMB8	6	47.37	1.3	2.46	3.46E-03	ENSG00000204264
CERK	22	14.31	-1.34	-2.53	3.55E-03	ENSG00000100422
STEAP4	7	0.1	-4.93	-30.59	3.64E-03	ENSG00000127954
EFEMP1	2	111.67	-2.14	-4.39	3.68E-03	ENSG00000115380
EHBP1	2	31.23	-1.11	-2.15	4.01E-03	ENSG00000115504
ADM	11	209.45	-1.79	-3.47	4.01E-03	ENSG00000148926
CPT1B	22	1.9	3.01	8.04	4.05E-03	ENSG00000205560
COL5A1	9	207.69	-1.69	-3.22	4.06E-03	ENSG00000130635
JADE2	5	7.49	1.16	2.24	4.07E-03	ENSG00000043143
BHLHE40	3	18.24	1.27	2.41	4.08E-03	ENSG00000134107
JDP2	14	15.68	-1.26	-2.4	4.08E-03	ENSG00000140044
TCN2	22	11.92	1.83	3.56	4.10E-03	ENSG00000185339
RIPOR3	20	2.33	3.55	11.74	4.18E-03	ENSG00000042062
RGS17	6	1	2.75	6.74	4.19E-03	ENSG00000091844
TMEM38B	9	4.12	1.76	3.38	4.19E-03	ENSG00000095209
PLEKHA4	19	35.02	1.48	2.79	4.19E-03	ENSG00000105559
ALDH1B1	9	14.32	-1.59	-3.01	4.23E-03	ENSG00000137124
TRIM47	17	7.38	1.84	3.57	4.32E-03	ENSG00000132481
NCR3LG1	11	3.62	1.84	3.58	4.36E-03	ENSG00000188211
WHRN	9	3.86	1.98	3.96	4.42E-03	ENSG00000095397
RNF144A	2	2.2	2.88	7.38	4.48E-03	ENSG00000151692
FARP1	13	9.59	-1.41	-2.65	4.78E-03	ENSG00000152767
ZBTB32	19	4.56	11.67	3,250.75	4.78E-03	ENSG00000011590
CHN1	2	11.51	-1.14	-2.2	4.83E-03	ENSG00000128656
CHEK2	22	3.78	2.03	4.08	4.83E-03	ENSG00000183765
IGFBP5	2	193.26	-2.9	-7.45	4.91E-03	ENSG00000115461
SH2D4A	8	54.55	-1.38	-2.6	5.23E-03	ENSG00000104611
TRPC6	11	2.62	-3.63	-12.41	5.24E-03	ENSG00000137672
DIPK1A	1	16.66	-1.26	-2.4	5.31E-03	ENSG00000154511
MYD88	3	26.53	1.08	2.12	5.36E-03	ENSG00000172936
GYG2	X	1.4	-3.16	-8.94	5.40E-03	ENSG00000056998
IRF9	14	44.72	1.11	2.15	5.68E-03	ENSG00000213928

COL12A1	6	231.92	-1.8	-3.48	5.82E-03	ENSG00000111799
CAPN5	11	19.28	1.02	2.03	6.02E-03	ENSG00000149260
TMEM140	7	5.39	2.61	6.1	6.08E-03	ENSG00000146859
LOXL4	10	32.17	-1.58	-2.99	6.08E-03	ENSG00000138131
SULF2	20	11.17	-1.5	-2.83	6.08E-03	ENSG00000196562
THY1	11	185.06	-1.6	-3.03	6.30E-03	ENSG00000154096
ZNF536	19	3.84	1.98	3.93	6.30E-03	ENSG00000198597
SERAC1	6	5.51	-1.86	-3.64	6.58E-03	ENSG00000122335
TREX1	3	11.34	1.85	3.6	6.72E-03	ENSG00000213689
SCPEP1	17	52.18	1.35	2.55	6.72E-03	ENSG00000121064
CRLF2	X	0.47	5.28	38.77	6.82E-03	ENSG00000205755
SLC31A2	9	20.11	1.34	2.53	6.92E-03	ENSG00000136867
SPON2	4	28.74	1.41	2.65	7.01E-03	ENSG00000159674
SDC2	8	37.38	-1.73	-3.31	7.21E-03	ENSG00000169439
GFRA1	10	13.38	-2.19	-4.56	7.26E-03	ENSG00000151892
ID4	6	8.38	-2.19	-4.55	7.37E-03	ENSG00000172201
NATD1	17	7.22	-1.38	-2.6	7.60E-03	ENSG00000274180
G0S2	1	7.49	4.06	16.71	7.72E-03	ENSG00000123689
PRSS12	4	21.88	-1.54	-2.9	7.86E-03	ENSG00000164099
CD82	11	5.98	2.06	4.17	7.86E-03	ENSG00000085117
FGFR2	10	0.69	-3	-8	7.92E-03	ENSG00000066468
ADAM19	5	5.44	-1.52	-2.88	8.00E-03	ENSG00000135074
KDR	4	0.8	3.98	15.77	8.17E-03	ENSG00000128052
ITGA10	1	5.76	1.94	3.83	8.37E-03	ENSG00000143127
HR	8	2.48	-1.9	-3.73	8.56E-03	ENSG00000168453
PRUNE2	9	5.61	-1.32	-2.5	8.69E-03	ENSG00000106772
PTPRS	19	11.85	-1.17	-2.26	9.10E-03	ENSG00000105426
COL1A1	17	3,546.90	-1.67	-3.18	9.75E-03	ENSG00000108821
GPNMB	7	196.28	1.64	3.13	9.79E-03	ENSG00000136235
TRIM69	15	5.12	1.97	3.91	9.93E-03	ENSG00000185880
LUM	12	367.16	-1.61	-3.05	0.01	ENSG00000139329
ST8SIA4	5	0.21	5.51	45.41	0.01	ENSG00000113532
PDCD6-AHRR	5	0.91	10.87	1,866.62	0.01	ENSG00000288622
ULBP1	6	4.14	-2.23	-4.69	0.01	ENSG00000111981
OLR1	12	0.41	-4.14	-17.69	0.01	ENSG00000173391
TDRD7	9	10.94	1.27	2.41	0.01	ENSG00000196116
AGRN	1	39.9	1.51	2.85	0.01	ENSG00000188157
APOL2	22	39.4	1.42	2.67	0.01	ENSG00000128335
HSPB8	12	13.53	1.39	2.63	0.01	ENSG00000152137
NTSR1	20	0.31	4.24	18.89	0.01	ENSG00000101188
SPHK1	17	21.56	1.08	2.11	0.01	ENSG00000176170
GBP2	1	11.82	1.3	2.46	0.01	ENSG00000162645
DMKN	19	6.91	1.85	3.61	0.01	ENSG00000161249
STAC	3	7.77	-1.89	-3.71	0.01	ENSG00000144681
MYLK	3	23.45	-1.53	-2.88	0.01	ENSG00000065534
RNF144B	6	3.95	-2.01	-4.03	0.01	ENSG00000137393
RAET1G	6	8.17	2.09	4.24	0.01	ENSG00000203722

OAF	11	43.71	1.18	2.27	0.01	ENSG00000184232
SPHKAP	2	0.22	4.46	21.97	0.01	ENSG00000153820
BOK	2	18.84	-1.24	-2.37	0.01	ENSG00000176720
LIMCH1	4	3.68	-1.99	-3.96	0.01	ENSG00000064042
ANKRD10	13	14.87	1.56	2.95	0.01	ENSG00000088448
NEXN	1	13.01	-1.53	-2.88	0.01	ENSG00000162614
STAMBPL1	10	7.03	1.39	2.62	0.01	ENSG00000138134
EIF2AK2	2	22.6	1.25	2.37	0.01	ENSG00000055332
ANKRD13A	12	38.41	-1.03	-2.04	0.01	ENSG00000076513
C1orf198	1	39.38	-1.39	-2.62	0.01	ENSG00000119280
NMT2	10	6.54	-1.34	-2.53	0.01	ENSG00000152465
RABGAP1	9	22.96	-1.35	-2.55	0.01	ENSG00000011454
FAM167B	1	14.38	1.94	3.83	0.01	ENSG00000183615
SLC1A4	2	13.4	-1.15	-2.22	0.02	ENSG00000115902
PPP3CB	10	16.71	-1.06	-2.08	0.02	ENSG00000107758
PI3	20	1.65	6.06	66.75	0.02	ENSG00000124102
PLCG2	16	0.46	3.3	9.86	0.02	ENSG00000197943
RNF41	12	12.76	-1.03	-2.05	0.02	ENSG00000181852
SLC1A5	19	124.83	-1.5	-2.83	0.02	ENSG00000105281
PLA2G4A	1	6.22	2.59	6.03	0.02	ENSG00000116711
BIVM-ERCC5	13	2.52	1.97	3.91	0.02	ENSG00000270181
DACT1	14	3.4	-2.5	-5.67	0.02	ENSG00000165617
PRICKLE2	3	5.8	1.24	2.35	0.02	ENSG00000163637
IFIT5	10	15.5	1.16	2.23	0.02	ENSG00000152778
CNNM1	10	1.84	2.2	4.61	0.02	ENSG00000119946
TRANK1	3	5.34	1.26	2.39	0.02	ENSG00000168016
STARD4	5	7.73	1.21	2.31	0.02	ENSG00000164211
PRDM8	4	6.32	1.62	3.08	0.02	ENSG00000152784
DLC1	8	19.42	-1.11	-2.16	0.02	ENSG00000164741
FLNB	3	31.31	-1.7	-3.24	0.02	ENSG00000136068
VAV3	1	0.63	3.65	12.58	0.02	ENSG00000134215
SCRG1	4	0.65	-4.2	-18.38	0.02	ENSG00000164106
TIAM2	6	1.9	-1.56	-2.95	0.02	ENSG00000146426
ITSN1	21	3.49	-1.03	-2.04	0.02	ENSG00000205726
RNF150	4	5.44	-1.94	-3.83	0.02	ENSG00000170153
ARHGAP22	10	13.53	1.24	2.37	0.02	ENSG00000128805
POU2F2	19	3.22	1.99	3.98	0.02	ENSG00000028277
SMIM29	6	46.92	1.52	2.86	0.02	ENSG00000186577
FGF10	5	0.86	-3.7	-13.01	0.02	ENSG00000070193
TAC3	12	0.57	5.02	32.49	0.02	ENSG00000166863
MARCKS	6	120.36	-1.45	-2.73	0.02	ENSG00000277443
LPP	3	8.07	-1.21	-2.32	0.02	ENSG00000145012
BMP2K	4	13.96	-1.33	-2.52	0.02	ENSG00000138756
MAP7D3	X	8.39	-1.14	-2.21	0.02	ENSG00000129680
TPM2	9	392.17	-1.42	-2.67	0.02	ENSG00000198467
MMP3	11	1,901.74	2.92	7.59	0.02	ENSG00000149968
CHAC1	15	11.14	-1.87	-3.65	0.02	ENSG00000128965

TNFRSF14	1	11.27	1.64	3.11	0.02	ENSG00000157873
RFTN1	3	26.07	-1.24	-2.36	0.02	ENSG00000131378
ADCY8	8	0.18	5.91	60.11	0.02	ENSG00000155897
PABPC4	1	53.37	-1.2	-2.29	0.02	ENSG00000090621
LRP8	1	2.65	1.69	3.23	0.02	ENSG00000157193
AMDHD2	16	13.66	1.32	2.51	0.02	ENSG00000162066
IDO1	8	0.29	4.57	23.77	0.02	ENSG00000131203
FLNC	7	124.16	-1.43	-2.69	0.02	ENSG00000128591
THBD	20	17.37	2.12	4.35	0.02	ENSG00000178726
PYCR1	17	36.77	-1.26	-2.39	0.02	ENSG00000183010
VDR	12	9.85	-1.3	-2.46	0.02	ENSG00000111424
PDE1A	2	0.29	-3.24	-9.43	0.02	ENSG00000115252
M1AP	2	0.47	3.78	13.71	0.02	ENSG00000159374
HSPB6	19	66.1	-1.59	-3.01	0.02	ENSG00000004776
PFKFB4	3	3.99	1.84	3.58	0.02	ENSG00000114268
PKP1	1	0.31	4.07	16.8	0.02	ENSG00000081277
RAB27B	18	2.66	1.75	3.37	0.02	ENSG00000041353
DDAH1	1	59.33	-1.33	-2.52	0.02	ENSG00000153904
ADGRD1	12	4.45	-2.03	-4.09	0.02	ENSG00000111452
ROBO2	3	4.64	-2.17	-4.5	0.03	ENSG00000185008
FNDC3A	13	21.6	1.39	2.61	0.03	ENSG00000102531
PALLD	4	34.74	-1.44	-2.71	0.03	ENSG00000129116
RND3	2	326.32	1.42	2.67	0.03	ENSG00000115963
RRAGD	6	1.53	2.42	5.35	0.03	ENSG00000025039
MSMO1	4	53.88	1.44	2.7	0.03	ENSG00000052802
GOLGA8T	15	0.12	-5.02	-32.41	0.03	ENSG00000261247
ANKFN1	17	0.14	-3.59	-12.06	0.03	ENSG00000153930
ATP1B1	1	8.32	-1.26	-2.39	0.03	ENSG00000143153
FSTL1	3	508.1	-1.53	-2.89	0.03	ENSG00000163430
PARD3B	2	3.92	-1.09	-2.13	0.03	ENSG00000116117
TSPAN2	1	0.69	-2.98	-7.9	0.03	ENSG00000134198
SLCO5A1	8	0.21	3.45	10.93	0.03	ENSG00000137571
SEMA6B	19	0.14	-5.83	-57.04	0.03	ENSG00000167680
PTX3	3	107.52	-1.73	-3.32	0.03	ENSG00000163661
LPXN	11	45.7	1.15	2.22	0.03	ENSG00000110031
NHLRC3	13	6.82	1.69	3.22	0.03	ENSG00000188811
ZNFX1	20	43.88	1.41	2.65	0.03	ENSG00000124201
RAB4A	1	9.6	-1.34	-2.53	0.03	ENSG00000168118
ANKRD33B	5	2.76	-1.72	-3.3	0.03	ENSG00000164236
C15orf48	15	3.62	3.23	9.41	0.03	ENSG00000166920
PPM1K	4	2.58	1.53	2.9	0.03	ENSG00000163644
TLR3	4	2.39	1.71	3.28	0.03	ENSG00000164342
SLC2A13	12	3.74	1.43	2.69	0.03	ENSG00000151229
MAFB	20	9.96	1.65	3.13	0.03	ENSG00000204103
CEMIP2	9	8.65	-1.2	-2.3	0.03	ENSG00000135048
TBL1XR1	3	10.81	-1.26	-2.39	0.03	ENSG00000177565
SWAP70	11	33.68	-1.01	-2.01	0.03	ENSG00000133789

NTN4	12	13.55	-1.58	-2.99	0.03	ENSG00000074527
ENPP1	6	4.89	-1.69	-3.23	0.03	ENSG00000197594
NPC2	14	78.38	1.14	2.2	0.03	ENSG00000119655
PLEKHG2	19	5.99	-1.06	-2.08	0.03	ENSG00000090924
PATL2	15	0.59	3.39	10.5	0.03	ENSG00000229474
CEBPD	8	38.61	-1.43	-2.69	0.04	ENSG00000221869
ATXN1	6	5.43	-1.19	-2.27	0.04	ENSG00000124788
NET1	10	12.57	1.09	2.13	0.04	ENSG00000173848
C10orf105	10	0.14	-4.77	-27.27	0.04	ENSG00000214688
HUNK	21	1.87	-1.63	-3.09	0.04	ENSG00000142149
PFKFB3	10	10.57	1.22	2.32	0.04	ENSG00000170525
HLA-A	6	780.32	1.6	3.03	0.04	ENSG00000206503
KIT	4	7.91	-1.34	-2.54	0.04	ENSG00000157404
ADTRP	6	1.22	2.96	7.79	0.04	ENSG00000111863
CH25H	10	12.37	-1.81	-3.5	0.04	ENSG00000138135
AKR1B1	7	183.37	1.93	3.82	0.04	ENSG00000085662
FBLIM1	1	20.22	-1.06	-2.09	0.04	ENSG00000162458
SGCD	5	23.09	-1.2	-2.3	0.04	ENSG00000170624
HS3ST2	16	0.3	5.83	56.88	0.04	ENSG00000122254
CDC42EP1	22	48.88	-1.22	-2.32	0.04	ENSG00000128283
GCNT4	5	2.38	-1.72	-3.3	0.04	ENSG00000176928
NYAP1	7	0.81	3.06	8.36	0.04	ENSG00000166924
GDF6	8	3.98	-2.49	-5.61	0.04	ENSG00000156466
CD302	2	8.14	-1.22	-2.33	0.04	ENSG00000241399
MXRA5	X	130.49	-1.39	-2.63	0.04	ENSG00000101825
BLOC1S5-TXNDC5	6	0.59	4.91	29.97	0.04	ENSG00000259040
MAP4K4	2	119.86	1.33	2.52	0.04	ENSG00000071054
MEST	7	8.8	-1.96	-3.9	0.04	ENSG00000106484
AQP1	7	2.81	-1.99	-3.98	0.04	ENSG00000240583
TAFA5	22	33.01	-1.28	-2.43	0.04	ENSG00000219438
GSTA1	6	0.38	-5.51	-45.55	0.04	ENSG00000243955
GPC1	2	117.12	-1.32	-2.49	0.04	ENSG00000063660
KAT2A	17	11.76	1.15	2.22	0.04	ENSG00000108773
B3GALT2	1	6.97	-2.88	-7.35	0.04	ENSG00000162630
CHKB-CPT1B	22	0.78	3.12	8.71	0.04	ENSG00000254413
CTSL	9	109.47	1.38	2.61	0.04	ENSG00000135047
ROBO4	11	0.57	2.87	7.31	0.04	ENSG00000154133
ODC1	2	21.99	-1.15	-2.22	0.04	ENSG00000115758
TPD52L1	6	5.25	-3.2	-9.18	0.04	ENSG00000111907
FAT4	4	5.7	-1.25	-2.38	0.05	ENSG00000196159
BAIAP2L1	7	3.52	-1.65	-3.13	0.05	ENSG00000006453
CCDC80	3	243.43	-1.48	-2.78	0.05	ENSG00000091986
TOX	8	5.86	-1.94	-3.84	0.05	ENSG00000198846
INHBB	2	1.3	-2.82	-7.07	0.05	ENSG00000163083
TGFB2	1	2.47	-2.06	-4.16	0.05	ENSG00000092969
SPRY2	13	13.63	1.41	2.66	0.05	ENSG00000136158
HACD4	9	4.89	1.15	2.23	0.05	ENSG00000188921

MT1X	16	22.37	1.54	2.91	0.05	ENSG00000187193
ZDHHC14	6	2.66	1.35	2.56	0.05	ENSG00000175048
ACTG1	17	1,335.93	-1.36	-2.57	0.05	ENSG00000184009
CEACAM1	19	0.14	5.37	41.29	0.05	ENSG00000079385

Bibliography

1. Voit T: **Congenital muscular dystrophies: 1997 update**. *Brain Dev* 1998, **20**(2):65-74.

2. Sframeli M, Sarkozy A, Bertoli M, Astrea G, Hudson J, Scoto M, Mein R, Yau M, Phadke R, Feng L *et al*: **Congenital muscular dystrophies in the UK population: Clinical and molecular spectrum of a large cohort diagnosed over a 12-year period**. *Neuromuscul Disord* 2017, **27**(9):793-803.

3. Mostacciuolo ML, Miorin M, Martinello F, Angelini C, Perini P, Trevisan CP: **Genetic epidemiology of congenital muscular dystrophy in a sample from north-east Italy**. *Hum Genet* 1996, **97**(3):277-279.

4. Norwood FLM, Harling C, Chinnery PF, Eagle M, Bushby K, Straub V: **Prevalence of genetic muscle disease in Northern England: in-depth analysis of a muscle clinic population**. *Brain* 2009, **132**(11):3175-3186.

5. Lake NJ, Phua J, Liu W, Moors T, Axon S, Lek M: **Estimating the prevalence of LAMA2 congenital muscular dystrophy using population genetic databases**. *bioRxiv* 2022:2022.2007.2006.499037.

6. Oliveira J, Parente Freixo J, Santos M, Coelho T: **LAMA2 Muscular Dystrophy**. In: *GeneReviews(®).* Edited by Adam MP, Everman DB, Mirzaa GM, Pagon RA, Wallace SE, Bean LJH, Gripp KW, Amemiya A. Seattle (WA): University of Washington, Seattle. Copyright © 1993-2023, University of Washington, Seattle. GeneReviews is a registered trademark of the University of Washington, Seattle. All rights reserved.; 1993.

7. Jones KJ, Morgan G, Johnston H, Tobias V, Ouvrier RA, Wilkinson I, North KN: **The expanding phenotype of laminin alpha2 chain (merosin) abnormalities: case series and review**. *J Med Genet* 2001, **38**(10):649-657.

8. Muntoni F, Voit T: **The congenital muscular dystrophies in 2004: a century of exciting progress**. *Neuromuscular Disorders* 2004, **14**(10):635-649.

9. Tan D, Ge L, Fan Y, Chang X, Wang S, Wei C, Ding J, Liu A, Wang S, Li X *et al*: **Natural history and genetic study of LAMA2-related muscular dystrophy in a large Chinese cohort**. *Orphanet Journal of Rare Diseases* 2021, **16**(1):319.

10. Zambon AA, Ridout D, Main M, Mein R, Phadke R, Muntoni F, Sarkozy A: **LAMA2-related muscular dystrophy: Natural history of a large pediatric cohort**. *Ann Clin Transl Neurol* 2020, **7**(10):1870-1882.

11. Sarkozy A, Foley AR, Zambon AA, Bönnemann CG, Muntoni F: **LAMA2-Related Dystrophies: Clinical Phenotypes, Disease Biomarkers, and Clinical Trial Readiness**. *Front Mol Neurosci* 2020, **13**:123.

12. Guo L, Tang WM, Song YZ: **[Clinical features and LAMA2 mutations of patients with congenital muscular dystrophy type 1A: a case report and literature review]**. *Zhongguo Dang Dai Er Ke Za Zhi* 2020, **22**(6):608-613.

13. Farina L, Morandi L, Milanesi I, Ciceri E, Mora M, Moroni I, Pantaleoni C, Savoiardo M: **Congenital muscular dystrophy with merosin deficiency: MRI findings in five patients**. *Neuroradiology* 1998, **40**(12):807-811.

14. Philpot J, Sewry C, Pennock J, Dubowitz V: **Clinical phenotype in congenital muscular dystrophy: correlation with expression of merosin in skeletal muscle**. *Neuromuscul Disord* 1995, **5**(4):301-305.

15. Leite CC, Lucato LT, Martin MG, Ferreira LG, Resende MB, Carvalho MS, Marie SK, Jinkins JR, Reed UC: **Merosin-deficient congenital muscular dystrophy (CMD): a study of 25 Brazilian patients using MRI**. *Pediatr Radiol* 2005, **35**(6):572-579.

16. Shorer Z, Philpot J, Muntoni F, Sewry C, Dubowitz V: **Demyelinating peripheral neuropathy in merosin-deficient congenital muscular dystrophy**. *J Child Neurol* 1995, **10**(6):472-475.

17. Previtali SC, Zambon AA: **LAMA2 Neuropathies: Human Findings and Pathomechanisms From Mouse Models**. *Front Mol Neurosci* 2020, **13**:60.

18. Messina S, Bruno C, Moroni I, Pegoraro E, D'Amico A, Biancheri R, Berardinelli A, Boffi P, Cassandrini D, Farina L *et al*: **Congenital muscular dystrophies with cognitive impairment. A population study**. *Neurology* 2010, **75**(10):898-903.

19. Mercuri E, Gruter-Andrew J, Philpot J, Sewry C, Counsell S, Henderson S, Jensen A, Naom I, Bydder G, Dubowitz V *et al*: **Cognitive abilities in children with congenital muscular dystrophy: correlation with brain MRI and merosin status**. *Neuromuscul Disord* 1999, **9**(6-7):383-387.

20. Muntoni F: **Cardiomyopathy in muscular dystrophies**. *Curr Opin Neurol* 2003, **16**(5):577-583.

21. Spyrou N, Philpot J, Foale R, Camici PG, Muntoni F: **Evidence of left ventricular dysfunction in children with merosin-deficient congenital muscular dystrophy**. *Am Heart J* 1998, **136**(3):474-476.

22. Finsterer J, Ramaciotti C, Wang CH, Wahbi K, Rosenthal D, Duboc D, Melacini P: **Cardiac findings in congenital muscular dystrophies**. *Pediatrics* 2010, **126**(3):538-545.

23. Prandini P, Berardinelli A, Fanin M, Morello F, Zardini E, Pichiecchio A, Uggetti C, Lanzi G, Angelini C, Pegoraro E: **LAMA2 loss-of-function mutation in a girl with a mild congenital muscular dystrophy**. *Neurology* 2004, **63**(6):1118-1121.

24. Bonnemann CG, Wang CH, Quijano-Roy S, Deconinck N, Bertini E, Ferreiro A, Muntoni F, Sewry C, Beroud C, Mathews KD *et al*: **Diagnostic approach to the congenital muscular dystrophies**. *Neuromuscul Disord* 2014, **24**(4):289-311.

25. Geranmayeh F, Clement E, Feng LH, Sewry C, Pagan J, Mein R, Abbs S, Brueton L, Childs AM, Jungbluth H *et al*: **Genotype-phenotype correlation in a large population of muscular dystrophy patients with LAMA2 mutations**. *Neuromuscul Disord* 2010, **20**(4):241-250.

26. Wang CH, Dowling JJ, North K, Schroth MK, Sejersen T, Shapiro F, Bellini J, Weiss H, Guillet M, Amburgey K *et al*: **Consensus statement on standard of care for congenital myopathies**. *J Child Neurol* 2012, **27**(3):363-382.

27. Bowman W, Todd RB: **XXI. On the minute structure and movements of voluntary muscle**. *Philosophical Transactions of the Royal Society of London* 1840, **130**:457-501.

28. Leclech C, Natale CF, Barakat AI: **The basement membrane as a structured surface – role in vascular health and disease**. *Journal of Cell Science* 2020, **133**(18).

29. Yurchenco PD: **Basement membranes: cell scaffoldings and signaling platforms**. *Cold Spring Harb Perspect Biol* 2011, **3**(2).

30. Pöschl E, Fox JW, Block D, Mayer U, Timpl R: **Two non-contiguous regions contribute to nidogen binding to a single EGF-like motif of the laminin gamma 1 chain**. *Embo j* 1994, **13**(16):3741-3747.

31. Pöschl E, Mayer U, Stetefeld J, Baumgartner R, Holak TA, Huber R, Timpl R: **Site-directed mutagenesis and structural interpretation of the nidogen binding site of the laminin gamma1 chain**. *Embo j* 1996, **15**(19):5154-5159.

32. Pöschl E, Schlötzer-Schrehardt U, Brachvogel B, Saito K, Ninomiya Y, Mayer U: **Collagen IV is essential for basement membrane stability but dispensable for initiation of its assembly during early development**. *Development* 2004, **131**(7):1619-1628.

33. McKee KK, Capizzi S, Yurchenco PD: **Scaffold-forming and Adhesive Contributions of Synthetic Laminin-binding Proteins to Basement Membrane Assembly**. *J Biol Chem* 2009, **284**(13):8984-8994.

34. Moll J, Barzaghi P, Lin S, Bezakova G, Lochmuller H, Engvall E, Muller U, Ruegg MA: **An agrin minigene rescues dystrophic symptoms in a mouse model for congenital muscular dystrophy**. *Nature* 2001, **413**(6853):302-307.

35. Sanes JR: **The basement membrane/basal lamina of skeletal muscle**. *J Biol Chem* 2003, **278**(15):12601-12604.

36. Helbling-Leclerc A, Zhang X, Topaloglu H, Cruaud C, Tesson F, Weissenbach J, Tome FM, Schwartz K, Fardeau M, Tryggvason K *et al*: **Mutations in the laminin alpha 2-chain gene (LAMA2) cause merosin-deficient congenital muscular dystrophy**. *Nat Genet* 1995, **11**(2):216-218.

37. Zhang X, Vuolteenaho R, Tryggvason K: **Structure of the human laminin alpha2-chain gene (LAMA2), which is affected in congenital muscular dystrophy**. *J Biol Chem* 1996, **271**(44):27664-27669.

38. Vainzof M, Marie SK, Reed UC, Schwartzman JS, Pavanello RC, Passos-Bueno MR, Zatz M: **Deficiency of merosin (laminin M or alpha 2) in congenital muscular dystrophy associated with cerebral white matter alterations**. *Neuropediatrics* 1995, **26**(6):293-297.

39. Taratuto AL, Lubieniecki F, Díaz D, Schultz M, Ruggieri V, Saccoliti M, Dubrovsky A: **Merosin-deficient congenital muscular dystrophy associated with abnormal cerebral cortical gyration: an autopsy study**. *Neuromuscul Disord* 1999, **9**(2):86-94.

40. Patton BL, Miner JH, Chiu AY, Sanes JR: **Distribution and function of laminins in the neuromuscular system of developing, adult, and mutant mice**. *J Cell Biol* 1997, **139**(6):1507-1521.

41. Leivo I, Engvall E: **Merosin, a protein specific for basement membranes of Schwann cells, striated muscle, and trophoblast, is expressed late in nerve and muscle development**. *Proc Natl Acad Sci U S A* 1988, **85**(5):1544-1548.

42. Colognato H, MacCarrick M, O'Rear JJ, Yurchenco PD: **The laminin alpha2-chain short arm mediates cell adhesion through both the alpha1beta1 and alpha2beta1 integrins**. *J Biol Chem* 1997, **272**(46):29330-29336.

43. Smirnov SP, McDearmon EL, Li S, Ervasti JM, Tryggvason K, Yurchenco PD: **Contributions of the LG modules and furin processing to laminin-2 functions**. *J Biol Chem* 2002, **277**(21):18928-18937.

44. Yurchenco PD, O'Rear JJ: **Basement membrane assembly**. *Methods Enzymol* 1994, **245**:489-518.

45. Colognato H, Yurchenco PD: **The laminin alpha2 expressed by dystrophic dy(2J) mice is defective in its ability to form polymers**. *Curr Biol* 1999, **9**(22):1327-1330.

46. Talts JF, Andac Z, Gohring W, Brancaccio A, Timpl R: **Binding of the G domains of laminin alpha1 and alpha2 chains and perlecan to heparin, sulfatides, alpha-dystroglycan and several extracellular matrix proteins**. *EMBO J* 1999, **18**(4):863-870.

47. Colognato H, Winkelmann DA, Yurchenco PD: **Laminin polymerization induces a receptor-cytoskeleton network**. *J Cell Biol* 1999, **145**(3):619-631.

48. Talts JF, Timpl R: **Mutation of a basic sequence in the laminin alpha2LG3 module leads to a lack of proteolytic processing and has different effects on beta1 integrin-mediated cell adhesion and alpha-dystroglycan binding**. *FEBS Lett* 1999, **458**(3):319-323.

49. Li S, Liquari P, McKee KK, Harrison D, Patel R, Lee S, Yurchenco PD: **Laminin-sulfatide binding initiates basement membrane assembly and enables receptor signaling in Schwann cells and fibroblasts**. *J Cell Biol* 2005, **169**(1):179-189.

50. Vachon PH, Loechel F, Xu H, Wewer UM, Engvall E: **Merosin and laminin in myogenesis; specific requirement for merosin in myotube stability and survival**. *J Cell Biol* 1996, **134**(6):1483-1497.

51. Patton BL, Wang B, Tarumi YS, Seburn KL, Burgess RW: **A single point mutation in the LN domain of LAMA2 causes muscular dystrophy and peripheral amyelination**. *J Cell Sci* 2008, **121**(Pt 10):1593-1604.

52. Kuang W, Xu H, Vachon PH, Engvall E: **Disruption of the lama2 gene in embryonic stem cells: laminin alpha 2 is necessary for sustenance of mature muscle cells**. *Exp Cell Res* 1998, **241**(1):117-125.

53. Holmberg J, Durbeej M: **Laminin-211 in skeletal muscle function**. *Cell Adh Migr* 2013, **7**(1):111-121.

54. Gavassini BF, Carboni N, Nielsen JE, Danielsen ER, Thomsen C, Svenstrup K, Bello L, Maioli MA, Marrosu G, Ticca AF *et al*: **Clinical and molecular characterization of limb-girdle muscular dystrophy due to LAMA2 mutations**. *Muscle & Nerve* 2011, **44**(5):703-709.

55. Oliveira J, Santos R, Soares-Silva I, Jorge P, Vieira E, Oliveira ME, Moreira A, Coelho T, Ferreira JC, Fonseca MJ *et al*: **LAMA2 gene analysis in a cohort of 26 congenital muscular dystrophy patients**. *Clin Genet* 2008, **74**(6):502-512.

56. Gonorazky HD, Naumenko S, Ramani AK, Nelakuditi V, Mashouri P, Wang P, Kao D, Ohri K, Viththiyapaskaran S, Tarnopolsky MA *et al*: **Expanding the Boundaries of RNA Sequencing as a Diagnostic Tool for Rare Mendelian Disease**. *Am J Hum Genet* 2019, **104**(5):1007.

57. Ge L, Liu A, Gao K, Du R, Ding J, Mao B, Hua Y, Zhang X, Tan D, Yang H *et al*: **Deletion of exon 4 in LAMA2 is the most frequent mutation in Chinese patients with laminin α2-related muscular dystrophy**. *Scientific Reports* 2018, **8**(1):14989.

58. Vainzof M, Richard P, Herrmann R, Jimenez-Mallebrera C, Talim B, Yamamoto LU, Ledeuil C, Mein R, Abbs S, Brockington M *et al*: **Prenatal diagnosis in laminin alpha2 chain (merosin)-deficient congenital muscular dystrophy: a collective experience of five international centers**. *Neuromuscul Disord* 2005, **15**(9-10):588-594.

59. Oliveira J, Gruber A, Cardoso M, Taipa R, Fineza I, Goncalves A, Laner A, Winder TL, Schroeder J, Rath J *et al*: **LAMA2 gene mutation update: Toward a more comprehensive picture of the laminin-alpha2 variome and its related phenotypes**. *Hum Mutat* 2018, **39**(10):1314-1337.

60. Xiong H, Tan D, Wang S, Song S, Yang H, Gao K, Liu A, Jiao H, Mao B, Ding J *et al*: **Genotype/phenotype analysis in Chinese laminin-alpha2 deficient congenital muscular dystrophy patients**. *Clin Genet* 2015, **87**(3):233-243.

61. Pegoraro E, Marks H, Garcia CA, Crawford T, Mancias P, Connolly AM, Fanin M, Martinello F, Trevisan CP, Angelini C *et al*: **Laminin alpha2 muscular dystrophy: genotype/phenotype studies of 22 patients**. *Neurology* 1998, **51**(1):101-110.

62. Naom I, D'Alessandro M, Sewry CA, Philpot J, Manzur AY, Dubowitz V, Muntoni F: **Laminin α2-chain gene mutations in two siblings presenting with limb-girdle muscular dystrophy**. *Neuromuscular Disorders* 1998, **8**(7):495-501.

63. Ding J, Zhao D, Du R, Zhang Y, Yang H, Liu J, Yan C, Zhang F, Xiong H: **Clinical and molecular genetic analysis of a family with late-onset LAMA2-related muscular dystrophy**. *Brain and Development* 2016, **38**(2):242-249.

64. Sasaki T, Giltay R, Talts U, Timpl R, Talts JF: **Expression and distribution of laminin alpha1 and alpha2 chains in embryonic and adult mouse tissues: an immunochemical approach**. *Exp Cell Res* 2002, **275**(2):185-199.

65. Muntoni F, Sewry C, Wilson L, Angelini C, Trevisan CP, Brambati B, Dubowitz V: **Prenatal diagnosis in congenital muscular dystrophy**. *Lancet* 1995, **345**(8949):591.

66. Yurchenco PD: **Integrating Activities of Laminins that Drive Basement Membrane Assembly and Function**. *Curr Top Membr* 2015, **76**:1-30.

67. George-Weinstein M, Foster RF, Gerhart JV, Kaufman SJ: **In Vitro and in Vivo Expression α7 Integrin and Desmin Define the Primary and Secondary Myogenic Lineages**. *Developmental Biology* 1993, **156**(1):209-229.

68. Yurchenco PD, McKee KK, Reinhard JR, Ruegg MA: **Laminin-deficient muscular dystrophy: Molecular pathogenesis and structural repair strategies**. *Matrix Biol* 2018, **71-72**:174-187.

69. Gawlik KI, Durbeej M: **Skeletal muscle laminin and MDC1A: pathogenesis and treatment strategies**. *Skelet Muscle* 2011, **1**(1):9.

70. Miyagoe Y, Hanaoka K, Nonaka I, Hayasaka M, Nabeshima Y, Arahata K, Nabeshima Y, Takeda S: **Laminin alpha2 chain-null mutant mice by targeted disruption of the Lama2 gene: a new model of merosin (laminin 2)-deficient congenital muscular dystrophy**. *FEBS Lett* 1997, **415**(1):33-39.

71. Kuang W, Xu H, Vachon PH, Liu L, Loechel F, Wewer UM, Engvall E: **Merosin-deficient congenital muscular dystrophy. Partial genetic correction in two mouse models**. *J Clin Invest* 1998, **102**(4):844-852.

72. Willmann R, Gordish-Dressman H, Meinen S, Ruegg MA, Yu Q, Nagaraju K, Kumar A, Girgenrath M, Coffey CBM, Cruz V *et al*: **Improving Reproducibility of Phenotypic Assessments in the DyW Mouse Model of Laminin-alpha2 Related Congenital Muscular Dystrophy**. *J Neuromuscul Dis* 2017, **4**(2):115-126.

73. Guo LT, Zhang XU, Kuang W, Xu H, Liu LA, Vilquin JT, Miyagoe-Suzuki Y, Takeda S, Ruegg MA, Wewer UM *et al*: **Laminin alpha2 deficiency and muscular dystrophy; genotype-phenotype correlation in mutant mice**. *Neuromuscul Disord* 2003, **13**(3):207-215.

74. Meier H, Southard JL: **Muscular dystrophy in the mouse caused by an allele at the dy-locus**. *Life Sci* 1970, **9**(3):137-144.

75. Xu H, Wu XR, Wewer UM, Engvall E: **Murine muscular dystrophy caused by a mutation in the laminin alpha 2 (Lama2) gene**. *Nat Genet* 1994, **8**(3):297-302.

76. Sunada Y, Bernier SM, Utani A, Yamada Y, Campbell KP: **Identification of a novel mutant transcript of laminin alpha 2 chain gene responsible for muscular dystrophy and dysmyelination in dy2J mice**. *Hum Mol Genet* 1995, **4**(6):1055-1061.

77. Hall TE, Bryson-Richardson RJ, Berger S, Jacoby AS, Cole NJ, Hollway GE, Berger J, Currie PD: **The zebrafish candyfloss mutant implicates extracellular matrix adhesion failure in laminin alpha2-deficient congenital muscular dystrophy**. *Proc Natl Acad Sci U S A* 2007, **104**(17):7092-7097.

78. Sztal TE, Sonntag C, Hall TE, Currie PD: **Epistatic dissection of laminin-receptor interactions in dystrophic zebrafish muscle**. *Hum Mol Genet* 2012, **21**(21):4718-4731.

79. Gupta VA, Kawahara G, Myers JA, Chen AT, Hall TE, Manzini MC, Currie PD, Zhou Y, Zon LI, Kunkel LM *et al*: **A splice site mutation in laminin-α2 results in a severe muscular dystrophy and growth abnormalities in zebrafish**. *PLoS One* 2012, **7**(8):e43794.

80. Girgenrath M, Dominov JA, Kostek CA, Boone Miller J: **Inhibition of apoptosis improves outcome in a model of congenital muscular dystrophy**. *The Journal of Clinical Investigation* 2004, **114**(11):1635-1639.

81. Hara MR, Agrawal N, Kim SF, Cascio MB, Fujimuro M, Ozeki Y, Takahashi M, Cheah JH, Tankou SK, Hester LD *et al*: **S-nitrosylated GAPDH initiates apoptotic cell death by nuclear translocation following Siah1 binding**. *Nat Cell Biol* 2005, **7**(7):665-674.

82. Erb M, Meinen S, Barzaghi P, Sumanovski LT, Courdier-Fruh I, Ruegg MA, Meier T: **Omigapil ameliorates the pathology of muscle dystrophy caused by laminin-alpha2 deficiency**. *J Pharmacol Exp Ther* 2009, **331**(3):787-795.

83. Yu Q, Sali A, Van der Meulen J, Creeden BK, Gordish-Dressman H, Rutkowski A, Rayavarapu S, Uaesoontrachoon K, Huynh T, Nagaraju K *et al*: **Omigapil treatment decreases fibrosis and improves respiratory rate in dy(2J) mouse model of congenital muscular dystrophy**. *PLoS One* 2013, **8**(6):e65468.

84. Jain MS, Meilleur K, Kim E, Norato G, Waite M, Nelson L, McGuire M, Duong T, Keller K, Lott DJ *et al*: **Longitudinal changes in clinical outcome measures in COL6-related dystrophies and LAMA2-related dystrophies**. *Neurology* 2019, **93**(21):e1932-e1943.

85. **Omigapil community statement** [https://www.curecmd.org/omigapil-statement-2021-09]

86. LAMA2-EUROPE: **LAMA2 Muscular Dystrophy (LAMA2-MD): Paving the road to therapy**. 2023.

87. Carmignac V, Quéré R, Durbeej M: **Proteasome inhibition improves the muscle of laminin α2 chain-deficient mice**. *Human Molecular Genetics* 2010, **20**(3):541-552.

88. Carmignac V, Svensson M, Körner Z, Elowsson L, Matsumura C, Gawlik KI, Allamand V, Durbeej M: **Autophagy is increased in laminin α2 chain-deficient muscle and its inhibition improves muscle morphology in a mouse model of MDC1A**. *Human Molecular Genetics* 2011, **20**(24):4891-4902.

89. Körner Z, Fontes-Oliveira CC, Holmberg J, Carmignac V, Durbeej M: **Bortezomib partially improves laminin α2 chain-deficient muscular dystrophy**. *Am J Pathol* 2014, **184**(5):1518-1528.

90. Nevo Y, Halevy O, Genin O, Moshe I, Turgeman T, Harel M, Biton E, Reif S, Pines M: **Fibrosis inhibition and muscle histopathology improvement in laminin-alpha2-deficient mice**. *Muscle Nerve* 2010, **42**(2):218-229.

91. Elbaz M, Yanay N, Aga-Mizrachi S, Brunschwig Z, Kassis I, Ettinger K, Barak V, Nevo Y: **Losartan, a therapeutic candidate in congenital muscular dystrophy: studies in the dy(2J) /dy(2J) mouse**. *Ann Neurol* 2012, **71**(5):699-708.

92. Dong JY, Fan PD, Frizzell RA: **Quantitative analysis of the packaging capacity of recombinant adeno-associated virus**. *Hum Gene Ther* 1996, **7**(17):2101-2112.

93. Wu Z, Yang H, Colosi P: **Effect of genome size on AAV vector packaging**. *Mol Ther* 2010, **18**(1):80-86.

94. Packer D, Martin PT: **Micro-laminin gene therapy can function as an inhibitor of muscle disease in the dy(W) mouse model of MDC1A**. *Mol Ther Methods Clin Dev* 2021, **21**:274-287.

95. Bentzinger CF, Barzaghi P, Lin S, Ruegg MA: **Overexpression of mini-agrin in skeletal muscle increases muscle integrity and regenerative capacity in laminin-alpha2-deficient mice**. *FASEB J* 2005, **19**(8):934-942.

96. McKee KK, Crosson SC, Meinen S, Reinhard JR, Ruegg MA, Yurchenco PD: **Chimeric protein repair of laminin polymerization ameliorates muscular dystrophy phenotype**. *J Clin Invest* 2017, **127**(3):1075-1089.

97. Reinhard JR, Lin S, McKee KK, Meinen S, Crosson SC, Sury M, Hobbs S, Maier G, Yurchenco PD, Rüegg MA: **Linker proteins restore basement membrane and correct LAMA2-related muscular dystrophy in mice**. *Sci Transl Med* 2017, **9**(396).

98. Kemaladewi DU, Maino E, Hyatt E, Hou H, Ding M, Place KM, Zhu X, Bassi P, Baghestani Z, Deshwar AG *et al*: **Correction of a splicing defect in a mouse model of congenital muscular dystrophy type 1A using a homology-directed-repair-independent mechanism**. *Nat Med* 2017, **23**(8):984-989.

99. Guicheney P, Vignier N, Helbling-Leclerc A, Nissinen M, Zhang X, Cruaud C, Lambert JC, Richelme C, Topaloglu H, Merlini L *et al*: **Genetics of laminin alpha 2 chain (or merosin) deficient congenital muscular dystrophy: from identification of mutations to prenatal diagnosis**. *Neuromuscul Disord* 1997, **7**(3):180-186.

100. Allamand V, Guicheney P: **Merosin-deficient congenital muscular dystrophy, autosomal recessive (MDC1A, MIM#156225, LAMA2 gene coding for alpha2 chain of laminin)**. *Eur J Hum Genet* 2002, **10**(2):91-94.

101. Millino C, Bellin M, Fanin M, Romualdi C, Pegoraro E, Angelini C, Lanfranchi G: **Expression profiling characterization of laminin alpha-2 positive MDC**. *Biochem Biophys Res Commun* 2006, **350**(2):345-351.

102. Di Blasi C, Bellafiore E, Salih MA, Manzini MC, Moore SA, Seidahmed MZ, Mukhtar MM, Karrar ZA, Walsh CA, Campbell KP *et al*: **Variable disease severity in Saudi Arabian and Sudanese families with c.3924 + 2 T > C mutation of LAMA2**. *BMC Res Notes* 2011, **4**:534.

103. Rajakulendran S, Parton M, Holton JL, Hanna MG: **Clinical and pathological heterogeneity in late-onset partial merosin deficiency**. *Muscle Nerve* 2011, **44**(4):590-593.

104. Çavdarlı B, Köken ÖY, Satılmış SBA, Bilen Ş, Ardıçlı D, Ceylan AC, Gündüz CNS, Topaloğlu H: **High diagnostic yield of targeted next-generation sequencing panel as a first-tier molecular test for the patients with myopathy or muscular dystrophy**. *Annals of Human Genetics* 2022, **n/a**(n/a).

105. Gawlik K, Miyagoe-Suzuki Y, Ekblom P, Takeda S, Durbeej M: **Laminin alpha1 chain reduces muscular dystrophy in laminin alpha2 chain deficient mice**. *Hum Mol Genet* 2004, **13**(16):1775-1784.

106. Gawlik KI, Li JY, Petersen A, Durbeej M: **Laminin alpha1 chain improves laminin alpha2 chain deficient peripheral neuropathy**. *Hum Mol Genet* 2006, **15**(18):2690-2700.

107. Gawlik KI, Mayer U, Blomberg K, Sonnenberg A, Ekblom P, Durbeej M: **Laminin alpha1 chain mediated reduction of laminin alpha2 chain deficient muscular dystrophy involves integrin alpha7beta1 and dystroglycan**. *FEBS Lett* 2006, **580**(7):1759-1765.

108. Gawlik KI, Akerlund M, Carmignac V, Elamaa H, Durbeej M: **Distinct roles for laminin globular domains in laminin alpha1 chain mediated rescue of murine laminin alpha2 chain deficiency**. *PLoS One* 2010, **5**(7):e11549.

109. Gawlik KI, Harandi VM, Cheong RY, Petersen A, Durbeej M: **Laminin alpha1 reduces muscular dystrophy in dy(2J) mice**. *Matrix Biol* 2018, **70**:36-49.

110. Kemaladewi DU, Bassi PS, Erwood S, Al-Basha D, Gawlik KI, Lindsay K, Hyatt E, Kember R, Place KM, Marks RM *et al*: **A mutation-independent approach for muscular dystrophy via upregulation of a modifier gene**. *Nature* 2019, **572**(7767):125-130.

111. Barrangou R, Fremaux C, Deveau H, Richards M, Boyaval P, Moineau S, Romero DA, Horvath P: **CRISPR provides acquired resistance against viruses in prokaryotes**. *Science* 2007, **315**(5819):1709-1712.

112. Garneau JE, Dupuis ME, Villion M, Romero DA, Barrangou R, Boyaval P, Fremaux C, Horvath P, Magadan AH, Moineau S: **The CRISPR/Cas bacterial immune system cleaves bacteriophage and plasmid DNA**. *Nature* 2010, **468**(7320):67-71.

113. Jinek M, Chylinski K, Fonfara I, Hauer M, Doudna JA, Charpentier E: **A programmable dual-RNA-guided DNA endonuclease in adaptive bacterial immunity**. *Science* 2012, **337**(6096):816-821.

114. Ran FA, Cong L, Yan WX, Scott DA, Gootenberg JS, Kriz AJ, Zetsche B, Shalem O, Wu X, Makarova KS *et al*: **In vivo genome editing using Staphylococcus aureus Cas9**. *Nature* 2015, **520**(7546):186-191.

115. Friedland AE, Baral R, Singhal P, Loveluck K, Shen S, Sanchez M, Marco E, Gotta GM, Maeder ML, Kennedy EM *et al*: **Characterization of Staphylococcus aureus Cas9: a**

smaller Cas9 for all-in-one adeno-associated virus delivery and paired nickase applications. *Genome Biology* 2015, **16**(1):257.

116. Danner E, Lebedin M, de la Rosa K, Kühn R: **A homology independent sequence replacement strategy in human cells using a CRISPR nuclease**. *Open Biology* 2021, **11**(1):200283.

117. Auer TO, Duroure K, De Cian A, Concordet JP, Del Bene F: **Highly efficient CRISPR/Cas9-mediated knock-in in zebrafish by homology-independent DNA repair**. *Genome Res* 2014, **24**(1):142-153.

118. Cristea S, Freyvert Y, Santiago Y, Holmes MC, Urnov FD, Gregory PD, Cost GJ: **In vivo cleavage of transgene donors promotes nuclease-mediated targeted integration**. *Biotechnology and Bioengineering* 2013, **110**(3):871-880.

119. He X, Tan C, Wang F, Wang Y, Zhou R, Cui D, You W, Zhao H, Ren J, Feng B: **Knock-in of large reporter genes in human cells via CRISPR/Cas9-induced homology-dependent and independent DNA repair**. *Nucleic Acids Research* 2016, **44**(9):e85-e85.

120. Cong L, Ran FA, Cox D, Lin S, Barretto R, Habib N, Hsu PD, Wu X, Jiang W, Marraffini LA *et al*: **Multiplex Genome Engineering Using CRISPR/Cas Systems**. *Science* 2013, **339**(6121):819-823.

121. Mali P, Yang L, Esvelt KM, Aach J, Guell M, DiCarlo JE, Norville JE, Church GM: **RNA-guided human genome engineering via Cas9**. *Science* 2013, **339**(6121):823-826.

122. Xue C, Greene EC: **DNA Repair Pathway Choices in CRISPR-Cas9-Mediated Genome Editing**. *Trends Genet* 2021, **37**(7):639-656.

123. Anzalone AV, Koblan LW, Liu DR: **Genome editing with CRISPR–Cas nucleases, base editors, transposases and prime editors**. *Nature Biotechnology* 2020, **38**(7):824-844.

124. Komor AC, Kim YB, Packer MS, Zuris JA, Liu DR: **Programmable editing of a target base in genomic DNA without double-stranded DNA cleavage**. *Nature* 2016, **533**(7603):420-424.

125. Gaudelli NM, Komor AC, Rees HA, Packer MS, Badran AH, Bryson DI, Liu DR: **Programmable base editing of A*T to G*C in genomic DNA without DNA cleavage**. *Nature* 2017, **551**(7681):464-471.

126. Newby GA, Yen JS, Woodard KJ, Mayuranathan T, Lazzarotto CR, Li Y, Sheppard-Tillman H, Porter SN, Yao Y, Mayberry K *et al*: **Base editing of haematopoietic stem cells rescues sickle cell disease in mice**. *Nature* 2021, **595**(7866):295-302.

127. Anzalone AV, Randolph PB, Davis JR, Sousa AA, Koblan LW, Levy JM, Chen PJ, Wilson C, Newby GA, Raguram A *et al*: **Search-and-replace genome editing without double-strand breaks or donor DNA**. *Nature* 2019, **576**(7785):149-157.

128. Zhi S, Chen Y, Wu G, Wen J, Wu J, Liu Q, Li Y, Kang R, Hu S, Wang J *et al*: **Dual-AAV delivering split prime editor system for in vivo genome editing**. *Mol Ther* 2022, **30**(1):283-294.

129. Qi LS, Larson MH, Gilbert LA, Doudna JA, Weissman JS, Arkin AP, Lim WA: **Repurposing CRISPR as an RNA-guided platform for sequence-specific control of gene expression**. *Cell* 2013, **152**(5):1173-1183.

130. Chavez A, Scheiman J, Vora S, Pruitt BW, Tuttle M, E PRI, Lin S, Kiani S, Guzman CD, Wiegand DJ *et al*: **Highly efficient Cas9-mediated transcriptional programming**. *Nat Methods* 2015, **12**(4):326-328.

131. Maeder ML, Linder SJ, Cascio VM, Fu Y, Ho QH, Joung JK: **CRISPR RNA-guided activation of endogenous human genes**. *Nat Methods* 2013, **10**(10):977-979.

132. Perez-Pinera P, Kocak DD, Vockley CM, Adler AF, Kabadi AM, Polstein LR, Thakore PI, Glass KA, Ousterout DG, Leong KW *et al*: **RNA-guided gene activation by CRISPR-Cas9-based transcription factors**. *Nat Methods* 2013, **10**(10):973-976.

133. Konermann S, Brigham MD, Trevino AE, Joung J, Abudayyeh OO, Barcena C, Hsu PD, Habib N, Gootenberg JS, Nishimasu H *et al*: **Genome-scale transcriptional activation by an engineered CRISPR-Cas9 complex**. *Nature* 2015, **517**(7536):583-588.

134. Tanenbaum ME, Gilbert LA, Qi LS, Weissman JS, Vale RD: **A protein-tagging system for signal amplification in gene expression and fluorescence imaging**. *Cell* 2014, **159**(3):635-646.

135. Chavez A, Tuttle M, Pruitt BW, Ewen-Campen B, Chari R, Ter-Ovanesyan D, Haque SJ, Cecchi RJ, Kowal EJK, Buchthal J *et al*: **Comparison of Cas9 activators in multiple species**. *Nat Methods* 2016, **13**(7):563-567.

136. Gilbert LA, Larson MH, Morsut L, Liu Z, Brar GA, Torres SE, Stern-Ginossar N, Brandman O, Whitehead EH, Doudna JA *et al*: **CRISPR-mediated modular RNA-guided regulation of transcription in eukaryotes**. *Cell* 2013, **154**(2):442-451.

137. Cox JJ, Reimann F, Nicholas AK, Thornton G, Roberts E, Springell K, Karbani G, Jafri H, Mannan J, Raashid Y *et al*: **An SCN9A channelopathy causes congenital inability to experience pain**. *Nature* 2006, **444**(7121):894-898.

138. Moreno AM, Alemán F, Catroli GF, Hunt M, Hu M, Dailamy A, Pla A, Woller SA, Palmer N, Parekh U *et al*: **Long-lasting analgesia via targeted in situ repression of Na(V)1.7 in mice**. *Sci Transl Med* 2021, **13**(584).

139. Liu XS, Wu H, Ji X, Stelzer Y, Wu X, Czauderna S, Shu J, Dadon D, Young RA, Jaenisch R: **Editing DNA Methylation in the Mammalian Genome**. *Cell* 2016, **167**(1):233-247.e217.

140. Vojta A, Dobrinić P, Tadić V, Bočkor L, Korać P, Julg B, Klasić M, Zoldoš V: **Repurposing the CRISPR-Cas9 system for targeted DNA methylation**. *Nucleic Acids Res* 2016, **44**(12):5615-5628.

141. McDonald JI, Celik H, Rois LE, Fishberger G, Fowler T, Rees R, Kramer A, Martens A, Edwards JR, Challen GA: **Reprogrammable CRISPR/Cas9-based system for inducing site-specific DNA methylation**. *Biol Open* 2016, **5**(6):866-874.

142. Liu XS, Wu H, Krzisch M, Wu X, Graef J, Muffat J, Hnisz D, Li CH, Yuan B, Xu C *et al*: **Rescue of Fragile X Syndrome Neurons by DNA Methylation Editing of the FMR1 Gene**. *Cell* 2018, **172**(5):979-992.e976.

143. Hilton IB, D'Ippolito AM, Vockley CM, Thakore PI, Crawford GE, Reddy TE, Gersbach CA: **Epigenome editing by a CRISPR-Cas9-based acetyltransferase activates genes from promoters and enhancers**. *Nat Biotechnol* 2015, **33**(5):510-517.

144. Kwon DY, Zhao YT, Lamonica JM, Zhou Z: **Locus-specific histone deacetylation using a synthetic CRISPR-Cas9-based HDAC**. *Nat Commun* 2017, **8**:15315.

145. Liu J, Sun M, Cho KB, Gao X, Guo B: **A CRISPR-Cas9 repressor for epigenetic silencing of KRAS**. *Pharmacol Res* 2021, **164**:105304.

146. Kiani S, Chavez A, Tuttle M, Hall RN, Chari R, Ter-Ovanesyan D, Qian J, Pruitt BW, Beal J, Vora S *et al*: **Cas9 gRNA engineering for genome editing, activation and repression**. *Nat Methods* 2015, **12**(11):1051-1054.

147. Kempton HR, Goudy LE, Love KS, Qi LS: **Multiple Input Sensing and Signal Integration Using a Split Cas12a System**. *Mol Cell* 2020, **78**(1):184-191.e183.

148. Adli M: **The CRISPR tool kit for genome editing and beyond**. *Nature Communications* 2018, **9**(1):1911.

149. Chavez M, Chen X, Finn PB, Qi LS: **Advances in CRISPR therapeutics**. *Nature Reviews Nephrology* 2023, **19**(1):9-22.

150. Nelson CE, Hakim CH, Ousterout DG, Thakore PI, Moreb EA, Castellanos Rivera RM, Madhavan S, Pan X, Ran FA, Yan WX *et al*: **In vivo genome editing improves muscle function in a mouse model of Duchenne muscular dystrophy**. *Science* 2016, **351**(6271):403-407.

151. Hakim CH, Wasala NB, Nelson CE, Wasala LP, Yue Y, Louderman JA, Lessa TB, Dai A, Zhang K, Jenkins GJ *et al*: **AAV CRISPR editing rescues cardiac and muscle function for 18 months in dystrophic mice**. *JCI Insight* 2018, **3**(23).

152. Tabebordbar M, Zhu K, Cheng JKW, Chew WL, Widrick JJ, Yan WX, Maesner C, Wu EY, Xiao R, Ran FA *et al*: **In vivo gene editing in dystrophic mouse muscle and muscle stem cells**. *Science* 2016, **351**(6271):407-411.

153. Zhang Y, Long C, Li H, McAnally JR, Baskin KK, Shelton JM, Bassel-Duby R, Olson EN: **CRISPR-Cpf1 correction of muscular dystrophy mutations in human cardiomyocytes and mice**. *Sci Adv* 2017, **3**(4):e1602814.

154. Amoasii L, Hildyard JCW, Li H, Sanchez-Ortiz E, Mireault A, Caballero D, Harron R, Stathopoulou TR, Massey C, Shelton JM *et al*: **Gene editing restores dystrophin expression in a canine model of Duchenne muscular dystrophy**. *Science* 2018, **362**(6410):86-91.

155. Xu L, Park KH, Zhao L, Xu J, El Refaey M, Gao Y, Zhu H, Ma J, Han R: **CRISPR-mediated Genome Editing Restores Dystrophin Expression and Function in mdx Mice**. *Mol Ther* 2016, **24**(3):564-569.

156. El Refaey M, Xu L, Gao Y, Canan BD, Adesanya TMA, Warner SC, Akagi K, Symer DE, Mohler PJ, Ma J *et al*: **In Vivo Genome Editing Restores Dystrophin Expression and Cardiac Function in Dystrophic Mice**. *Circ Res* 2017, **121**(8):923-929.

157. Ryu SM, Koo T, Kim K, Lim K, Baek G, Kim ST, Kim HS, Kim DE, Lee H, Chung E *et al*: **Adenine base editing in mouse embryos and an adult mouse model of Duchenne muscular dystrophy**. *Nat Biotechnol* 2018, **36**(6):536-539.

158. Kwon JB, Ettyreddy AR, Vankara A, Bohning JD, Devlin G, Hauschka SD, Asokan A, Gersbach CA: **In Vivo Gene Editing of Muscle Stem Cells with Adeno-Associated Viral Vectors in a Mouse Model of Duchenne Muscular Dystrophy**. *Mol Ther Methods Clin Dev* 2020, **19**:320-329.

159. Wojtal D, Kemaladewi DU, Malam Z, Abdullah S, Wong TW, Hyatt E, Baghestani Z, Pereira S, Stavropoulos J, Mouly V *et al*: **Spell Checking Nature: Versatility of CRISPR/Cas9 for Developing Treatments for Inherited Disorders**. *Am J Hum Genet* 2016, **98**(1):90-101.

160. Maino E, Wojtal D, Evagelou SL, Farheen A, Wong TWY, Lindsay K, Scott O, Rizvi SZ, Hyatt E, Rok M *et al*: **Targeted genome editing in vivo corrects a Dmd duplication restoring wild-type dystrophin expression**. *EMBO Mol Med* 2021, **13**(5):e13228.

161. Young CS, Hicks MR, Ermolova NV, Nakano H, Jan M, Younesi S, Karumbayaram S, Kumagai-Cresse C, Wang D, Zack JA *et al*: **A Single CRISPR-Cas9 Deletion Strategy**

that Targets the Majority of DMD Patients Restores Dystrophin Function in hiPSC-Derived Muscle Cells. *Cell Stem Cell* 2016, **18**(4):533-540.

162. Pickar-Oliver A, Gough V, Bohning JD, Liu S, Robinson-Hamm JN, Daniels H, Majoros WH, Devlin G, Asokan A, Gersbach CA: **Full-length dystrophin restoration via targeted exon integration by AAV-CRISPR in a humanized mouse model of Duchenne muscular dystrophy**. *Mol Ther* 2021, **29**(11):3243-3257.

163. Bengtsson NE, Hall JK, Odom GL, Phelps MP, Andrus CR, Hawkins RD, Hauschka SD, Chamberlain JR, Chamberlain JS: **Muscle-specific CRISPR/Cas9 dystrophin gene editing ameliorates pathophysiology in a mouse model for Duchenne muscular dystrophy**. *Nature Communications* 2017, **8**(1):14454.

164. Chemello F, Chai AC, Li H, Rodriguez-Caycedo C, Sanchez-Ortiz E, Atmanli A, Mireault AA, Liu N, Bassel-Duby R, Olson EN: **Precise correction of Duchenne muscular dystrophy exon deletion mutations by base and prime editing**. *Sci Adv* 2021, **7**(18).

165. Sengupta K, Mishra MK, Loro E, Spencer MJ, Pyle AD, Khurana TS: **Genome Editing-Mediated Utrophin Upregulation in Duchenne Muscular Dystrophy Stem Cells**. *Mol Ther Nucleic Acids* 2020, **22**:500-509.

166. Suominen T, Bachinski LL, Auvinen S, Hackman P, Baggerly KA, Angelini C, Peltonen L, Krahe R, Udd B: **Population frequency of myotonic dystrophy: higher than expected frequency of myotonic dystrophy type 2 (DM2) mutation in Finland**. *Eur J Hum Genet* 2011, **19**(7):776-782.

167. Wang Y, Hao L, Wang H, Santostefano K, Thapa A, Cleary J, Li H, Guo X, Terada N, Ashizawa T *et al*: **Therapeutic Genome Editing for Myotonic Dystrophy Type 1 Using CRISPR/Cas9**. *Mol Ther* 2018, **26**(11):2617-2630.

168. Lo Scrudato M, Poulard K, Sourd C, Tomé S, Klein AF, Corre G, Huguet A, Furling D, Gourdon G, Buj-Bello A: **Genome Editing of Expanded CTG Repeats within the Human DMPK Gene Reduces Nuclear RNA Foci in the Muscle of DM1 Mice**. *Mol Ther* 2019, **27**(8):1372-1388.

169. Batra R, Nelles DA, Pirie E, Blue SM, Marina RJ, Wang H, Chaim IA, Thomas JD, Zhang N, Nguyen V *et al*: **Elimination of Toxic Microsatellite Repeat Expansion RNA by RNA-Targeting Cas9**. *Cell* 2017, **170**(5):899-912.e810.

170. Batra R, Nelles DA, Roth DM, Krach F, Nutter CA, Tadokoro T, Thomas JD, Sznajder ŁJ, Blue SM, Gutierrez HL *et al*: **The sustained expression of Cas9 targeting toxic RNAs reverses disease phenotypes in mouse models of myotonic dystrophy type 1**. *Nature biomedical engineering* 2021, **5**(2):157-168.

171. Cardinali B, Provenzano C, Izzo M, Voellenkle C, Battistini J, Strimpakos G, Golini E, Mandillo S, Scavizzi F, Raspa M *et al*: **Time-controlled and muscle-specific**

CRISPR/Cas9-mediated deletion of CTG-repeat expansion in the DMPK gene. *Mol Ther Nucleic Acids* 2022, **27**:184-199.

172. Himeda CL, Jones TI, Jones PL: **CRISPR/dCas9-mediated Transcriptional Inhibition Ameliorates the Epigenetic Dysregulation at D4Z4 and Represses DUX4-fl in FSH Muscular Dystrophy**. *Mol Ther* 2016, **24**(3):527-535.

173. Himeda CL, Jones TI, Jones PL: **Targeted epigenetic repression by CRISPR/dSaCas9 suppresses pathogenic DUX4-fl expression in FSHD**. *Mol Ther Methods Clin Dev* 2021, **20**:298-311.

174. Allamand V, Brinas L, Richard P, Stojkovic T, Quijano-Roy S, Bonne G: **ColVI myopathies: where do we stand, where do we go?** *Skelet Muscle* 2011, **1**:30.

175. Bonnemann CG: **The collagen VI-related myopathies: muscle meets its matrix**. *Nat Rev Neurol* 2011, **7**(7):379-390.

176. Brinas L, Richard P, Quijano-Roy S, Gartioux C, Ledeuil C, Lacene E, Makri S, Ferreiro A, Maugenre S, Topaloglu H *et al*: **Early onset collagen VI myopathies: Genetic and clinical correlations**. *Ann Neurol* 2010, **68**(4):511-520.

177. Bolduc V, Foley AR, Solomon-Degefa H, Sarathy A, Donkervoort S, Hu Y, Chen GS, Sizov K, Nalls M, Zhou H *et al*: **A recurrent COL6A1 pseudoexon insertion causes muscular dystrophy and is effectively targeted by splice-correction therapies**. *JCI Insight* 2019, **4**(6).

178. Amoasii L, Long C, Li H, Mireault AA, Shelton JM, Sanchez-Ortiz E, McAnally JR, Bhattacharyya S, Schmidt F, Grimm D *et al*: **Single-cut genome editing restores dystrophin expression in a new mouse model of muscular dystrophy**. *Sci Transl Med* 2017, **9**(418).

179. Wong TWY, Ahmed A, Yang G, Maino E, Steiman S, Hyatt E, Chan P, Lindsay K, Wong N, Golebiowski D *et al*: **A novel mouse model of Duchenne muscular dystrophy carrying a multi-exonic Dmd deletion exhibits progressive muscular dystrophy and early-onset cardiomyopathy**. *Dis Model Mech* 2020, **13**(9).

180. Nakamura K, Fujii W, Tsuboi M, Tanihata J, Teramoto N, Takeuchi S, Naito K, Yamanouchi K, Nishihara M: **Generation of muscular dystrophy model rats with a CRISPR/Cas system**. *Sci Rep* 2014, **4**:5635.

181. Yu HH, Zhao H, Qing YB, Pan WR, Jia BY, Zhao HY, Huang XX, Wei HJ: **Porcine Zygote Injection with Cas9/sgRNA Results in DMD-Modified Pig with Muscle Dystrophy**. *Int J Mol Sci* 2016, **17**(10).

182. Sui T, Lau YS, Liu D, Liu T, Xu L, Gao Y, Lai L, Li Z, Han R: **A novel rabbit model of Duchenne muscular dystrophy generated by CRISPR/Cas9**. *Dis Model Mech* 2018, **11**(6).

183. Yip BH: **Recent Advances in CRISPR/Cas9 Delivery Strategies**. *Biomolecules* 2020, **10**(6):839.

184. Lino CA, Harper JC, Carney JP, Timlin JA: **Delivering CRISPR: a review of the challenges and approaches**. *Drug Deliv* 2018, **25**(1):1234-1257.

185. Kotterman MA, Chalberg TW, Schaffer DV: **Viral Vectors for Gene Therapy: Translational and Clinical Outlook**. *Annu Rev Biomed Eng* 2015, **17**:63-89.

186. Popescu NC, Zimonjic D, DiPaolo JA: **Viral integration, fragile sites, and proto-oncogenes in human neoplasia**. *Human Genetics* 1990, **84**(5):383-386.

187. Horii T, Arai Y, Yamazaki M, Morita S, Kimura M, Itoh M, Abe Y, Hatada I: **Validation of microinjection methods for generating knockout mice by CRISPR/Cas-mediated genome engineering**. *Scientific Reports* 2014, **4**(1):4513.

188. Dever DP, Bak RO, Reinisch A, Camarena J, Washington G, Nicolas CE, Pavel-Dinu M, Saxena N, Wilkens AB, Mantri S *et al*: **CRISPR/Cas9 β-globin gene targeting in human haematopoietic stem cells**. *Nature* 2016, **539**(7629):384-389.

189. Lee CS, Bishop ES, Zhang R, Yu X, Farina EM, Yan S, Zhao C, Zeng Z, Shu Y, Wu X *et al*: **Adenovirus-mediated gene delivery: Potential applications for gene and cell-based therapies in the new era of personalized medicine**. *Genes & Diseases* 2017, **4**(2):43-63.

190. Yang Y, Wang L, Bell P, McMenamin D, He Z, White J, Yu H, Xu C, Morizono H, Musunuru K *et al*: **A dual AAV system enables the Cas9-mediated correction of a metabolic liver disease in newborn mice**. *Nature Biotechnology* 2016, **34**(3):334-338.

191. Truong DJ, Kühner K, Kühn R, Werfel S, Engelhardt S, Wurst W, Ortiz O: **Development of an intein-mediated split-Cas9 system for gene therapy**. *Nucleic Acids Res* 2015, **43**(13):6450-6458.

192. Chew WL, Tabebordbar M, Cheng JK, Mali P, Wu EY, Ng AH, Zhu K, Wagers AJ, Church GM: **A multifunctional AAV-CRISPR-Cas9 and its host response**. *Nat Methods* 2016, **13**(10):868-874.

193. Rosenblum D, Gutkin A, Kedmi R, Ramishetti S, Veiga N, Jacobi AM, Schubert MS, Friedmann-Morvinski D, Cohen ZR, Behlke MA *et al*: **CRISPR-Cas9 genome editing using targeted lipid nanoparticles for cancer therapy**. *Science Advances* 2020, **6**(47):eabc9450.

194. Lee K, Conboy M, Park HM, Jiang F, Kim HJ, Dewitt MA, Mackley VA, Chang K, Rao A, Skinner C *et al*: **Nanoparticle delivery of Cas9 ribonucleoprotein and donor DNA in vivo induces homology-directed DNA repair**. *Nature Biomedical Engineering* 2017, **1**(11):889-901.

195. Mangeot PE, Risson V, Fusil F, Marnef A, Laurent E, Blin J, Mournetas V, Massouridès E, Sohier TJM, Corbin A *et al*: **Genome editing in primary cells and in vivo using viral-derived Nanoblades loaded with Cas9-sgRNA ribonucleoproteins**. *Nature Communications* 2019, **10**(1):45.

196. Hamilton JR, Tsuchida CA, Nguyen DN, Shy BR, McGarrigle ER, Sandoval Espinoza CR, Carr D, Blaeschke F, Marson A, Doudna JA: **Targeted delivery of CRISPR-Cas9 and transgenes enables complex immune cell engineering**. *Cell Rep* 2021, **35**(9):109207.

197. Banskota S, Raguram A, Suh S, Du SW, Davis JR, Choi EH, Wang X, Nielsen SC, Newby GA, Randolph PB *et al*: **Engineered virus-like particles for efficient in vivo delivery of therapeutic proteins**. *Cell* 2022, **185**(2):250-265.e216.

198. Raguram A, Banskota S, Liu DR: **Therapeutic in vivo delivery of gene editing agents**. *Cell* 2022, **185**(15):2806-2827.

199. Segel M, Lash B, Song J, Ladha A, Liu CC, Jin X, Mekhedov SL, Macrae RK, Koonin EV, Zhang F: **Mammalian retrovirus-like protein PEG10 packages its own mRNA and can be pseudotyped for mRNA delivery**. *Science* 2021, **373**(6557):882-889.

200. Colasante G, Lignani G, Brusco S, Di Berardino C, Carpenter J, Giannelli S, Valassina N, Bido S, Ricci R, Castoldi V *et al*: **dCas9-Based Scn1a Gene Activation Restores Inhibitory Interneuron Excitability and Attenuates Seizures in Dravet Syndrome Mice**. *Mol Ther* 2020, **28**(1):235-253.

201. Toma L, Barbălată T, Sanda GM, Niculescu LS, Sima AV, Stancu CS: **CRISPR/dCas9 Transcriptional Activation of Endogenous Apolipoprotein AI and Paraoxonase 1 in Enterocytes Alleviates Endothelial Cell Dysfunction**. *Biomolecules* 2021, **11**(12).

202. Ran FA, Hsu PD, Wright J, Agarwala V, Scott DA, Zhang F: **Genome engineering using the CRISPR-Cas9 system**. *Nature Protocols* 2013, **8**(11):2281-2308.

203. Pan TC, Zhang RZ, Markova D, Arita M, Zhang Y, Bogdanovich S, Khurana TS, Bonnemann CG, Birk DE, Chu ML: **COL6A3 protein deficiency in mice leads to muscle and tendon defects similar to human collagen VI congenital muscular dystrophy**. *J Biol Chem* 2013, **288**(20):14320-14331.

204. Han YM, Lee NR, Bae MH, Park KH, Shin JH, Kim DS, Byun SY: **Merosin-Deficient Congenital Muscular Dystrophy with Polymicrogyria and Subcortical Heterotopia: A Case Report**. *Neonatal Med* 2016, **23**(3):173-177.

205. Lin Y, Cradick TJ, Brown MT, Deshmukh H, Ranjan P, Sarode N, Wile BM, Vertino PM, Stewart FJ, Bao G: **CRISPR/Cas9 systems have off-target activity with insertions or deletions between target DNA and guide RNA sequences**. *Nucleic Acids Res* 2014, **42**(11):7473-7485.

206. Sledzinski P, Nowaczyk M, Olejniczak M: **Computational Tools and Resources Supporting CRISPR-Cas Experiments**. *Cells* 2020, **9**(5):1288.

207. Cancellieri S, Zeng J, Lin LY, Tognon M, Nguyen MA, Lin J, Bombieri N, Maitland SA, Ciuculescu M-F, Katta V *et al*: **Human genetic diversity alters off-target outcomes of therapeutic gene editing**. *Nature Genetics* 2023, **55**(1):34-43.

208. Durbeej M: **Laminin-alpha2 Chain-Deficient Congenital Muscular Dystrophy: Pathophysiology and Development of Treatment**. *Curr Top Membr* 2015, **76**:31-60.

209. Yépez VA, Gusic M, Kopajtich R, Mertes C, Smith NH, Alston CL, Ban R, Beblo S, Berutti R, Blessing H *et al*: **Clinical implementation of RNA sequencing for Mendelian disease diagnostics**. *Genome Medicine* 2022, **14**(1):38.

210. Kukurba KR, Montgomery SB: **RNA Sequencing and Analysis**. *Cold Spring Harb Protoc* 2015, **2015**(11):951-969.

211. Yanay N, Elbaz M, Konikov-Rozenman J, Elgavish S, Nevo Y, Fellig Y, Rabie M, Mitrani-Rosenbaum S, Nevo Y: **Pax7, Pax3 and Mamstr genes are involved in skeletal muscle impaired regeneration of dy2J/dy2J mouse model of Lama2-CMD**. *Human Molecular Genetics* 2019, **28**(20):3369-3390.

212. Fontes-Oliveira CC, Steinz M, Schneiderat P, Mulder H, Durbeej M: **Bioenergetic Impairment in Congenital Muscular Dystrophy Type 1A and Leigh Syndrome Muscle Cells**. *Sci Rep* 2017, **7**:45272.

213. Livak KJ, Schmittgen TD: **Analysis of relative gene expression data using real-time quantitative PCR and the 2(-Delta Delta C(T)) Method**. *Methods* 2001, **25**(4):402-408.

214. Liu C-H, Di YP: **Analysis of RNA Sequencing Data Using CLC Genomics Workbench**. In: *Molecular Toxicology Protocols.* Edited by Keohavong P, Singh KP, Gao W. New York, NY: Springer US; 2020: 61-113.

215. Capitanio D, Moriggi M, Barbacini P, Torretta E, Moroni I, Blasevich F, Morandi L, Mora M, Gelfi C: **Molecular Fingerprint of BMD Patients Lacking a Portion in the Rod Domain of Dystrophin**. *International Journal of Molecular Sciences* 2022, **23**(5):2624.

216. Chen C, Cui S, Li W, Jin H, Fan J, Sun Y, Cui Z: **Ingenuity pathway analysis of human facet joint tissues: Insight into facet joint osteoarthritis**. *Exp Ther Med* 2020, **19**(4):2997-3008.

217. Wang Y, Song Q, Huang W, Lin Y, Wang X, Wang C, Willard B, Zhao C, Nan J, Holvey-Bates E *et al*: **A virus-induced conformational switch of STAT1-STAT2 dimers boosts antiviral defenses**. *Cell Research* 2021, **31**(2):206-218.

218. Jefferies CA: **Regulating IRFs in IFN Driven Disease**. *Frontiers in Immunology* 2019, **10**.

219. Hakim CH, Kumar SRP, Pérez-López DO, Wasala NB, Zhang D, Yue Y, Teixeira J, Pan X, Zhang K, Million ED *et al*: **Cas9-specific immune responses compromise local and systemic AAV CRISPR therapy in multiple dystrophic canine models**. *Nature Communications* 2021, **12**(1):6769.

220. Vaidyanathan S, Azizian KT, Haque A, Henderson JM, Hendel A, Shore S, Antony JS, Hogrefe RI, Kormann MSD, Porteus MH *et al*: **Uridine Depletion and Chemical Modification Increase Cas9 mRNA Activity and Reduce Immunogenicity without HPLC Purification**. *Mol Ther Nucleic Acids* 2018, **12**:530-542.

221. Pichlmair A, Schulz O, Tan CP, Rehwinkel J, Kato H, Takeuchi O, Akira S, Way M, Schiavo G, Reis e Sousa C: **Activation of MDA5 requires higher-order RNA structures generated during virus infection**. *J Virol* 2009, **83**(20):10761-10769.

222. Schlee M, Roth A, Hornung V, Hagmann CA, Wimmenauer V, Barchet W, Coch C, Janke M, Mihailovic A, Wardle G *et al*: **Recognition of 5' triphosphate by RIG-I helicase requires short blunt double-stranded RNA as contained in panhandle of negative-strand virus**. *Immunity* 2009, **31**(1):25-34.

223. Sun M, Rethi B, krishnamurthy A, Joshua V, Wähämaa H, Catrina S-B, Catrina A: **An Image-based Dynamic High-throughput Analysis of Adherent Cell Migration**. *Bio-protocol* 2021, **11**(6):e3957.

224. Wang K, Hu F, Xu K, Cheng H, Jiang M, Feng R, Li J, Wen T: **CASCADE_SCAN: mining signal transduction network from high-throughput data based on steepest descent method**. *BMC Bioinformatics* 2011, **12**(1):164.

225. Takahashi A, Ohtani N, Hara E: **Irreversibility of cellular senescence: dual roles of p16INK4a/Rb-pathway in cell cycle control**. *Cell division* 2007, **2**(1):1-5.

226. Kabir MH, Patrick R, Ho JWK, O'Connor MD: **Identification of active signaling pathways by integrating gene expression and protein interaction data**. *BMC Systems Biology* 2018, **12**(9):120.

227. de Oliveira BM, Matsumura CY, Fontes-Oliveira CC, Gawlik KI, Acosta H, Wernhoff P, Durbeej M: **Quantitative proteomic analysis reveals metabolic alterations, calcium dysregulation, and increased expression of extracellular matrix proteins in laminin α2 chain-deficient muscle**. *Mol Cell Proteomics* 2014, **13**(11):3001-3013.

228. Kanda T, Funato N, Baba Y, Kuroda T: **Evidence for fibroblast growth factor receptors in myofibroblasts during palatal mucoperiosteal repair**. *Arch Oral Biol* 2003, **48**(3):213-221.

229. Margadant C, Sonnenberg A: **Integrin-TGF-beta crosstalk in fibrosis, cancer and wound healing**. *EMBO Rep* 2010, **11**(2):97-105.

230. Meyer M, Müller AK, Yang J, Moik D, Ponzio G, Ornitz DM, Grose R, Werner S: **FGF receptors 1 and 2 are key regulators of keratinocyte migration in vitro and in wounded skin**. *J Cell Sci* 2012, **125**(Pt 23):5690-5701.

231. Mehuron T, Kumar A, Duarte L, Yamauchi J, Accorsi A, Girgenrath M: **Dysregulation of matricellular proteins is an early signature of pathology in laminin-deficient muscular dystrophy**. *Skelet Muscle* 2014, **4**:14.

232. Liang J, Li H, Han J, Jiang J, Wang J, Li Y, Feng Z, Zhao R, Sun Z, Lv B *et al*: **Mex3a interacts with LAMA2 to promote lung adenocarcinoma metastasis via PI3K/AKT pathway**. *Cell Death & Disease* 2020, **11**(8):614.

233. Wang R-Q, Lan Y-L, Lou J-C, Lyu Y-Z, Hao Y-C, Su Q-F, Ma B-B, Yuan Z-B, Yu Z-K, Zhang H-Q *et al*: **Expression and methylation status of LAMA2 are associated with the invasiveness of nonfunctioning PitNET**. *Therapeutic Advances in Endocrinology and Metabolism* 2019, **10**:2042018818821296.

234. McPherson JR, Ong C-K, Ng CC-Y, Rajasegaran V, Heng H-L, Yu WS-S, Tan BK-T, Madhukumar P, Teo MC-C, Ngeow J *et al*: **Whole-exome sequencing of breast cancer, malignant peripheral nerve sheath tumor and neurofibroma from a patient with neurofibromatosis type 1**. *Cancer Medicine* 2015, **4**(12):1871-1878.

235. Lee S, Oh T, Chung H, Rha S, Kim C, Moon Y, Hoehn BD, Jeong D, Lee S, Kim N *et al*: **Identification of GABRA1 and LAMA2 as new DNA methylation markers in colorectal cancer**. *Int J Oncol* 2012, **40**(3):889-898.

236. Ni RS, Shen X, Qian X, Yu C, Wu H, Gao X: **Detection of differentially expressed genes and association with clinicopathological features in laryngeal squamous cell carcinoma**. *Oncol Lett* 2012, **4**(6):1354-1360.

237. Jhunjhunwala S, Jiang Z, Stawiski EW, Gnad F, Liu J, Mayba O, Du P, Diao J, Johnson S, Wong KF *et al*: **Diverse modes of genomic alteration in hepatocellular carcinoma**. *Genome Biol* 2014, **15**(8):436.

238. Januchowski R, Zawierucha P, Rucinski M, Nowicki M, Zabel M: **Extracellular matrix proteins expression profiling in chemoresistant variants of the A2780 ovarian cancer cell line**. *Biomed Res Int* 2014, **2014**:365867.

239. Gallia GL, Zhang M, Ning Y, Haffner MC, Batista D, Binder ZA, Bishop JA, Hann CL, Hruban RH, Ishii M *et al*: **Genomic analysis identifies frequent deletions of Dystrophin in olfactory neuroblastoma**. *Nature Communications* 2018, **9**(1):5410.

240. Chermuła B, Brązert M, Jeseta M, Ożegowska K, Sujka-Kordowska P, Konwerska A, Bryja A, Kranc W, Jankowski M, Nawrocki MJ *et al*: **The Unique Mechanisms of Cellular Proliferation, Migration and Apoptosis are Regulated through Oocyte Maturational Development—A Complete Transcriptomic and Histochemical Study**. *International Journal of Molecular Sciences* 2019, **20**(1):84.

241. Colognato H, Yurchenco PD: **Form and function: the laminin family of heterotrimers**. *Dev Dyn* 2000, **218**(2):213-234.

242. Gilbert LA, Horlbeck MA, Adamson B, Villalta JE, Chen Y, Whitehead EH, Guimaraes C, Panning B, Ploegh HL, Bassik MC *et al*: **Genome-Scale CRISPR-Mediated Control of Gene Repression and Activation**. *Cell* 2014, **159**(3):647-661.

243. Doench JG, Hartenian E, Graham DB, Tothova Z, Hegde M, Smith I, Sullender M, Ebert BL, Xavier RJ, Root DE: **Rational design of highly active sgRNAs for CRISPR-Cas9-mediated gene inactivation**. *Nat Biotechnol* 2014, **32**(12):1262-1267.

244. Moreno-Mateos MA, Vejnar CE, Beaudoin JD, Fernandez JP, Mis EK, Khokha MK, Giraldez AJ: **CRISPRscan: designing highly efficient sgRNAs for CRISPR-Cas9 targeting in vivo**. *Nat Methods* 2015, **12**(10):982-988.

245. Hsu PD, Scott DA, Weinstein JA, Ran FA, Konermann S, Agarwala V, Li Y, Fine EJ, Wu X, Shalem O *et al*: **DNA targeting specificity of RNA-guided Cas9 nucleases**. *Nat Biotechnol* 2013, **31**(9):827-832.

246. Xu H, Xiao T, Chen CH, Li W, Meyer CA, Wu Q, Wu D, Cong L, Zhang F, Liu JS *et al*: **Sequence determinants of improved CRISPR sgRNA design**. *Genome Res* 2015, **25**(8):1147-1157.

247. Jinek M, East A, Cheng A, Lin S, Ma E, Doudna J: **RNA-programmed genome editing in human cells**. *Elife* 2013, **2**:e00471.

248. Fu Y, Foden JA, Khayter C, Maeder ML, Reyon D, Joung JK, Sander JD: **High-frequency off-target mutagenesis induced by CRISPR-Cas nucleases in human cells**. *Nat Biotechnol* 2013, **31**(9):822-826.

249. Kim S, Kim D, Cho SW, Kim J, Kim JS: **Highly efficient RNA-guided genome editing in human cells via delivery of purified Cas9 ribonucleoproteins**. *Genome Res* 2014, **24**(6):1012-1019.

250. Allen TM, Brehm MA, Bridges S, Ferguson S, Kumar P, Mirochnitchenko O, Palucka K, Pelanda R, Sanders-Beer B, Shultz LD *et al*: **Humanized immune system mouse models: progress, challenges and opportunities**. *Nat Immunol* 2019, **20**(7):770-774.

251. Colque-Navarro P, Jacobsson G, Andersson R, Flock JI, Möllby R: **Levels of antibody against 11 Staphylococcus aureus antigens in a healthy population**. *Clin Vaccine Immunol* 2010, **17**(7):1117-1123.

252. Dryla A, Prustomersky S, Gelbmann D, Hanner M, Bettinger E, Kocsis B, Kustos T, Henics T, Meinke A, Nagy E: **Comparison of antibody repertoires against Staphylococcus aureus in healthy individuals and in acutely infected patients**. *Clin Diagn Lab Immunol* 2005, **12**(3):387-398.

253. Charlesworth CT, Deshpande PS, Dever DP, Camarena J, Lemgart VT, Cromer MK, Vakulskas CA, Collingwood MA, Zhang L, Bode NM *et al*: **Identification of preexisting adaptive immunity to Cas9 proteins in humans**. *Nature Medicine* 2019, **25**(2):249-254.

254. Simhadri VL, McGill J, McMahon S, Wang J, Jiang H, Sauna ZE: **Prevalence of Pre-existing Antibodies to CRISPR-Associated Nuclease Cas9 in the USA Population**. *Molecular Therapy - Methods & Clinical Development* 2018, **10**:105-112.

255. Hewitt EW: **The MHC class I antigen presentation pathway: strategies for viral immune evasion**. *Immunology* 2003, **110**(2):163-169.

256. Crudele JM, Chamberlain JS: **Cas9 immunity creates challenges for CRISPR gene editing therapies**. *Nature Communications* 2018, **9**(1):3497.

257. Boutin S, Monteilhet V, Veron P, Leborgne C, Benveniste O, Montus MF, Masurier C: **Prevalence of serum IgG and neutralizing factors against adeno-associated virus (AAV) types 1, 2, 5, 6, 8, and 9 in the healthy population: implications for gene therapy using AAV vectors**. *Hum Gene Ther* 2010, **21**(6):704-712.

258. Louis Jeune V, Joergensen JA, Hajjar RJ, Weber T: **Pre-existing anti-adeno-associated virus antibodies as a challenge in AAV gene therapy**. *Hum Gene Ther Methods* 2013, **24**(2):59-67.

259. Barnes C, Scheideler O, Schaffer D: **Engineering the AAV capsid to evade immune responses**. *Current Opinion in Biotechnology* 2019, **60**:99-103.

260. Monteilhet V, Saheb S, Boutin S, Leborgne C, Veron P, Montus M-F, Moullier P, Benveniste O, Masurier C: **A 10 Patient Case Report on the Impact of Plasmapheresis Upon Neutralizing Factors Against Adeno-associated Virus (AAV) Types 1, 2, 6, and 8**. *Molecular Therapy* 2011, **19**(11):2084-2091.

261. Chicoine LG, Montgomery CL, Bremer WG, Shontz KM, Griffin DA, Heller KN, Lewis S, Malik V, Grose WE, Shilling CJ *et al*: **Plasmapheresis Eliminates the Negative**

Impact of AAV Antibodies on Microdystrophin Gene Expression Following Vascular Delivery. *Molecular Therapy* 2014, **22**(2):338-347.

262. Liao HK, Hatanaka F, Araoka T, Reddy P, Wu MZ, Sui Y, Yamauchi T, Sakurai M, O'Keefe DD, Nunez-Delicado E *et al*: **In Vivo Target Gene Activation via CRISPR/Cas9-Mediated Trans-epigenetic Modulation**. *Cell* 2017, **171**(7):1495-1507 e1415.

263. Yamagata T, Raveau M, Kobayashi K, Miyamoto H, Tatsukawa T, Ogiwara I, Itohara S, Hensch TK, Yamakawa K: **CRISPR/dCas9-based Scn1a gene activation in inhibitory neurons ameliorates epileptic and behavioral phenotypes of Dravet syndrome model mice**. *Neurobiol Dis* 2020, **141**:104954.

264. Matharu N, Rattanasopha S, Tamura S, Maliskova L, Wang Y, Bernard A, Hardin A, Eckalbar WL, Vaisse C, Ahituv N: **CRISPR-mediated activation of a promoter or enhancer rescues obesity caused by haploinsufficiency**. *Science* 2019, **363**(6424).